Available online at www.sciencedirect.com
ScienceDirect
Dynamics of Atmospheres and Oceans
42 (2006) 152–215
dynamics of atmospheres and oceans
www.elsevier.com/locate/dynatmoce

Modulating synoptic scale convective activity and boundary layer dissipation in the IPESD models of the Madden–Julian oscillation

Joseph A. Biello*, Andrew J. Majda

Courant Institute of Mathematical Sciences, New York University, 251 Mercer Street, New York, NY 10012, United States

Available online 6 September 2006

Abstract

A self-contained derivation of the IPESD models [Majda, A.J., Klein, R., 2003. Systematic multi-scale models for the tropics. J. Atmos. Sci. 60, 393–408] governing synoptic and planetary scale tropical flows is provided. This derivation demonstrates the analytic tractability of the model and the effect of zonally and meridionally tilted synoptic scale heating on the forcing of planetary scale flows through upscale momentum and temperature fluxes. Exploiting the analytic tractability of the models, different aspects of the planetary scale forcing are traced to meridional and vertical tilts in the synoptic scale heating profile. Variants of the archetypal IPESD models for the Madden–Julian oscillation (MJO) presented in Majda and Biello [Majda, A.J., Biello, J.A., 2004. A multi-scale model for tropical intraseasonal oscillations. Proc. Natl. Acad. Sci. 101, 4736–4741; Biello, J.A., Majda, A.J., 2005. A new multi-scale model for the Madden–Julian oscillation. J. Atmos. Sci. 62, 1694–1721] are studied. In addition to vertically tilted synoptic scale heating, the models discussed herein incorporate upscale zonal momentum flux due to meridional flux convergence arising from meridionally tilted heating. The effect of a boundary layer momentum drag at the base of the free troposphere is also systematically incorporated into the IPESD models. Both meridional tilts and lower boundary layer drag are shown to meridionally confine the MJO westerly wind burst and drive a planetary scale barotropic flow. Meridionally tilted heating can also greatly strengthen the wind burst at the base of the troposphere and modify its vertical profile. The competing effects of meridionally tilted, and off-equatorial heating can also significantly weaken the MJO winds. Appendices are provided which discuss generalizations and a solution algorithm for the IPESD models.

Keywords: Tropical intraseasonal oscillations; Madden–Julian oscillation; Multi-scale asymptotics

* Corresponding author at: Department of Mathematics, University of California, Davis, CA 95616, United States.
E-mail address: biello@cims.nyu.edu (J.A. Biello).

0377-0265/$ – see front matter © 2006 Elsevier B.V. All rights reserved.
doi:10.1016/j.dynatmoce.2005.10.005

1. Introduction

Convection in the tropics has a profound impact on short-term climate. Observational data indicate that tropical deep convection is organized on a hierarchy of scales ranging from cumulus clouds over a few kilometers to intraseasonal oscillations over planetary scales of order 40,000 km (Nakazawa, 1988; Hendon and Leibmann, 1994; Wheeler and Kiladis, 1999). The mechanisms for this behavior present a major unsolved problem, despite the fact that there has been extensive research over the last few decades on these topics through parameterization of convection in general circulation models (Emanuel and Raymond, 1993) as well as theory (see Majda and Shefter, 2001; Majda et al., 2004, and references therein).

The dominant component of intraseasonal variability in the tropics is the 40–50 day tropical intraseasonal oscillation, often called the Madden–Julian oscillation (MJO) after its discoverers (Madden and Julian, 1972). In the troposphere, the MJO is an equatorial planetary scale wave envelope of complex multi-scale convective processes which propagates across the Indian Ocean and Western Pacific at a speed of roughly 5 m/s (Nakazawa, 1988; Hendon and Salby, 1994; Hendon and Leibmann, 1994; Maloney and Hartmann, 1998). The planetary scale circulation anomalies associated with the MJO significantly affect monsoon development, intraseasonal predictability in mid-latitudes, and impact the development of the El Nino Southern Oscillation (ENSO) in the Pacific Ocean (Madden and Julian, 1994; Vecchi and Harrison, 2000; Zhang and Anderson, 2003). Present day computer general circulation models (GCM) typically poorly represent the MJO (Sperber et al., 1997). One conjecture for the reason for this poor performance of GCMs is the inadequate treatment across multiple spatial scales of the interaction of the hierarchy of organized structures which generate the MJO as their envelope.

There have been a large number of theories attempting to explain the MJO, for example, through evaporation wind feedback (Emanuel, 1987; Neelin et al., 1987), boundary layer frictional convective instability (Wang and Rui, 1990), stochastic linearized convection (Salby et al., 1994), radiation instability (Raymond, 2001) and the planetary scale linear response to moving heat sources (Chao, 1987). Recent models have recognized the importance of the interaction across spatial scales through either a phenomenological picture (Moncrieff, 2004), or numerical simulations which invoke "super-parametrization" to implement the interaction with smaller scales (Grabowski, 2001, 2003). Though super-parametrization does model the interaction of planetary scales with mesoscales, it is computationally feasible because it simplifies the mesoscale dynamics using two dimensional models and leaves a gap between length scales of 200–1200 km.

In two recent studies Majda and Biello (2004) and Biello and Majda (2005), the present authors have proposed a new way to look at the MJO as a multi-scale process in space on intraseasonal time scales. Through the systematic, asymptotic inclusion of upscale flux convergences from the synoptic scales, these models generalize and enlarge the linear, shallow water Matsuno–Gill heating models (Matsuno, 1966; Gill, 1980), and the linear equatorial long wave theory (Stevens et al., 1990). The multi-scale model developed by the authors clearly demonstrates the fashion in which planetary-scale circulations which share several features in common with the MJO are generated on intraseasonal time scales through the upscale transfer of kinetic and thermal energy from organized synoptic scale circulations. The theoretical framework utilized there and in the present study is the intraseasonal planetary equatorial synoptic dynamics (IPESD) model derived recently by Majda and Klein (2003). The IPESD model is a multi-scale balanced model, systematically derived from the compressible Euler equations in a rotating frame of reference through systematic asymptotics and provides simplified equations for the upscale transfer of energy from a wave train of equatorial synoptic-scale circulations to the planetary scale as well as

the response on planetary scales to the large scale envelope of heating. The IPESD models have firm mathematical underpinnings, conceptual simplicity and analytic tractability while representing some of the crucial multi-scale interactions for the planetary scale response.

Observations suggest that the synoptic scale organization within the MJO is manifested as westward titled convective supercluster systems in the Rossby-gyre region of the MJO (Wheeler et al., 2000; Moncrieff and Klinker, 1997) while it is more akin to lower troposphere congestus heating in the eastern region leading the "westerly onset" in the MJO (Lin and Johnson, 1996; Johnson and Lin, 1997; Houze et al., 2000; Kiladis et al., 2004). The synoptic scale model described in Biello and Majda (2005) considered convective activity which is localized in a eastward moving envelope and which resembles a heating profile arising from lower troposphere congestus clouds in its eastern portion and deep, upward/westward tilted superclusters in its western portion.

The planetary scale flows calculated in Biello and Majda (2005) using the IPESD model and arising from the envelope of congestus/supercluster heating described above have several features in common with the observed structure of the MJO (Kiladis et al., 2004; Lin and Johnson, 1996; Hendon and Salby, 1994). Among these results are that easterlies precede a westerly wind burst in the lower troposphere, that the maximum of the westerly wind burst occurs at heights of 4–6 km, that the westerly wind burst has a distinct upward/westward tilt, and that the MJO envelope has a quadrupolar structure in the horizontal plane, with a leading pair of anticyclones and a trailing pair of cyclones in the strong westerly region. Each of these features were traced to specific aspects of the upscale momentum and temperature transport and the mean planetary scale heating.

The present work generalizes the synoptic scale heating models and planetary scale response considered in Majda and Biello (2004) and Biello and Majda (2005) and has three main goals. The first is to derive the IPESD models starting with the hydrostatic, anelastic equations on an equatorial β-plane as the primitive equations rather than the compressible Euler equation in Majda and Klein (2003). This simplified derivation will clearly spell out the assumptions of the IPESD model and allow us to systematically add the effects of an Ekman boundary layer at the base of the free troposphere. Furthermore, the derivation will highlight the relationship between synoptic scale convective activity and the resultant planetary scale momentum and temperature flux convergence. In particular, the analytic form of the flux convergences allows us to relate different aspects of the synoptic scale heating fluctuations, due to convective activity, to features of the planetary scale flows in a quantitative fashion.

The second goal is to explore the effect of meridional momentum flux convergence on the planetary scale flows. In the models considered by Biello and Majda (2005), it was shown that the ubiquitous term in the upscale flux convergence from a vertically tilted convective heating profile is the vertical flux of zonal momentum. The meridional flux of zonal momentum was identically zero in those models, and the temperature flux convergence was shown to be much smaller than the momentum flux convergence for flows near the equator. Meridional tilt in the synoptic scale heating fluctuations generates a meridional component of zonal momentum flux convergence driving planetary scale flows, and it is the only mechanism which can force a planetary scale barotropic response in this model in the absence of boundary layer friction.

The third goal is to systematically derive and understand the effects of lower boundary layer Ekman drag on planetary scale flows. The inclusion of a barotropic boundary layer below the free troposphere drives a vertical velocity at the base of the free troposphere in regions of non-zero zonal velocity. This Ekman pump dissipates energy near the base of free troposphere and preferentially at different latitudes. Below, we examine the effect of Ekman drag on the lower troposphere westerly wind burst.

This paper begins by introducing the primitive equations, their nondimensionalization and strength of the heating rate and flow response in Section 1.1. In Section 2 the IPESD model is derived asymptotically using the primitive equations. Of particular importance are the derivations of the synoptic scale balanced equations in Section 2.2 and the coupled planetary scale dynamics in Section 2.3. In Section 2.4, we systematically derive the effects of boundary layer dissipation both in a linear and non-linear Ekman model. The models utilized in the remainder of the paper focus on the Boussinesq version of the IPESD model where synoptic scale heating fluctuations are much stronger than planetary scale mean heating (Section 2.5), which is consistent with observational evidence in the tropics (Lin and Johnson, 1996; Yanai et al., 2000).

The general expression for the upscale momentum flux arising from synoptic scale heating fluctuations are calculated in Section 3. In particular, this calculation highlights the effects of different synoptic scale heating profiles on the upscale flux convergence. In Section 4 the canonical MJO models presented in Biello and Majda (2005) are recapitulated. These are compared with the planetary scale flows arising from synoptic scale structures where the meridional flux of zonal momentum is non-zero. The effect of lower boundary layer Ekman dissipation on planetary scale flows is explored through several examples presented in Section 5. The paper concludes with a discussion of the theory and the results.

In Appendix A the more general IPESD model is derived, in the presence of a planetary scale mean heating which is about the same strength as the synoptic scale heating fluctuations. Recorded in Appendix B is an interesting transformation which relates the anelastic and Boussinesq IPESD theories. Appendix C describes the analytic solution of the boundary layer equations with nonlinear friction and our numerical algorithm for calculating planetary scale flows. These appendices are included online in the electronic version of the paper.

1.1. The equatorial anelastic equations with a barotropic boundary layer

The derivation of the intraseasonal planetary equatorial synoptic dynamics (IPESD) model first presented in Majda and Klein (2003) begins with the fully compressible Euler equations in a rotating frame of reference as the primitive equations. This derivation has the advantage of clearly relating the IPESD model to other dynamical models which arise on different length and time scales in the tropics. In the next section, we shall present a derivation of the IPESD model which takes as its starting point the anelastic, hydrostatic Euler equations on a β-plane. These equations are appropriate at least for synoptic scales and larger in the tropics and, since the derivation is more concise than that given in Majda and Klein (2003), we feel that it may be more accessible. Furthermore, by listing the assumptions of the model, demonstrating an analytic solution for synoptic scale flows, and detailing a solution algorithm (see Appendix C), we intend this paper to serve as a tool for other researchers who want to utilize the IPESD models in future applications.

Our discussion begins with the hydrostatic, anelastic Euler equations on a equatorial β-plane:

$$\begin{aligned}
\frac{D}{D\tau}u - yv &= -p_x + \epsilon S_u,\\
\frac{D}{D\tau}v + yu &= -p_y + \epsilon S_v,\\
\frac{D}{D\tau}\theta + N^2 w &= \epsilon S_\theta,\\
p_z &= \theta,\\
(\rho u)_x + (\rho v)_y + (\rho w)_z &= 0
\end{aligned} \tag{1}$$

where $\rho = \rho(z)$ and $N^2 = N^2(z)$ are the density and buoyancy frequency, respectively, and depend on the height in the troposphere alone. The time scales, τ, are nondimensionalized with the unit of the equatorial time scale, $T_E = (c\beta)^{-1/2} \approx 8.3$ h, the horizontal length scales to the equatorial deformation radius, $L_E = (c/\beta)^{1/2} = 1500$ km and the vertical length scale to the troposphere height divided by π, $H_T/\pi \approx 5$ km. The horizontal velocities are scaled to the dry Kelvin/gravity wave speed, $c = 50$ m/s whereas the vertical velocity is scaled to the vertical/horizontal aspect ratio times this speed, $= 5/1500c \approx 0.16$ m/s. The temperature scale is equal to the thermal lapse rate in the atmosphere measured over one unit of the vertical scale, $[\theta] \approx 33$ K. In these units, the density is scaled to that at the base of the free troposphere, $\rho(z = 0) = 1$ (and is elsewhere less than or equal to one) and the buoyancy frequency (whose average in the troposphere is about 10^{-2} s) is equal to one plus a small variation as a function of height, $N^2(z) = 1 + \mu(z)$. In this nondimensionalization, the free troposphere occupies the domain $0 \le z \le \pi$, $-40/3 \le x \le 40/3$ and $-10/3 \le y \le 10/3$. All examples we discuss will use constant density and buoyancy frequency and a rigid lid at the top of the troposphere, that is to say that the vertical velocity vanishes there. The scales of the nondimensionalization along with parameter values and the allowed strengths of the forcing are summarized in Table 1.

The forcing terms have already been scaled as small, order ϵ. For $\epsilon = 0.1$ order one forcing implies dimensional strengths of $\sim \epsilon 33\,\mathrm{K}/(1/3\,\mathrm{day}) \sim 10$ K/day for the heating and $\sim \epsilon 50$ m/s$/(1/3$ day$) \sim 15$ m/s/day for the horizontal momentum. This scale for the forcing is consistent with observed values in the equatorial troposphere (Lin and Johnson, 1996; Yanai et al., 2000).

At the base of the free troposphere there is a constant density barotropic boundary layer of thickness:

$$z_B = 0.5\,\mathrm{km} \tag{2}$$

Table 1
The scales and nondimensional parameters of the IPESD model

Physical quantity	Name	Value or unit scale
Froude number	ϵ	0.1
Gravity wave speed	c	50 m/s
Equatorial time scale	T_E	$(c\beta)^{-1/2} = 8.3$ h
Equatorial deformation radius	l_s	$(c/\beta)^{1/2} = 1500$ km
Troposphere height	H_T	16 km
Synoptic scale dimensions	$[x, y]$	$l_s = 1500$ km
Vertical dimension	$[z]$	$H_T/\pi \approx 5$ km
Zonal planetary scale	$[X]$	$l_s/\epsilon = 15,000$ km
Planetary advection time	$[t]$	$T_I \equiv T_E/\epsilon \approx 3$ days
Horizontal velocity scale	$[u', v', \bar{U}]$	$\epsilon c = 5$ m/s
Vertical velocity scale	$[w']$	$\epsilon c H/l_s = 2.5$ cm/s
Temperature scale	$[\theta', \bar{\Theta}]$	3 K
Pressure scale	$[p', \bar{P}]$	$\epsilon c^2 = 250$ (m/s)^2
Synoptic scale heating rate	$[S^{\theta'}]$	10 K/day
Planetary scale heating rate	$[\bar{S}^{\theta}]$	1 K/day
Momentum drag rate	d_0	$T_I\,(5\,\mathrm{days})^{-1} \approx 0.55$
Thermal dissipation rate	d_θ	$T_I\,(15\,\mathrm{days})^{-1} \approx 0.18$
Boundary layer thickness	z_B	0.5 km
Boundary layer ratio	Δ_B	$z_B/H \approx 0.03$
Scaled boundary layer ratio	Δ	$\Delta_B/\epsilon \approx 0.3$
Boundary layer drag timescale	d	$T_E\,(1\,\mathrm{day})^{-1} \approx 0.35$
Turbulent boundary layer velocity	V_*	$(5\,m/s)/(\epsilon c) \approx 1$

Square brackets indicate that the value of one unit of the nondimensional variable corresponds to given scale.

which, in the theory, occupies the region $-\pi\Delta_B \le z \le 0$, $\Delta_B \equiv z_B/H_T \approx 0.5/16$. The horizontal velocity is independent of height in this layer and the dissipation is due to a drag law which depends on the velocity:

$$\frac{D^B}{D\tau}\vec{u}^B + y(\vec{u}^B)^\perp = -\nabla p^B - \tilde{d}(|\vec{u}^B|)\vec{u}^B + \text{n.l.t's}, \qquad u_x^B + v_y^B + w_z^B = 0 \tag{3}$$

where the density equals that of the base of the free troposphere, $\rho = 1$. The advective derivative is taken with respect to the velocity in the boundary layer:

$$\frac{D^B}{D\tau} = \frac{\partial}{\partial\tau} + u^B\frac{\partial}{\partial x} + v^B\frac{\partial}{\partial y} \tag{4}$$

and the expression "n.l.t's" accounts for quadratic advective nonlinearities which, in the absence of dissipation, correct for total energy conservation between the free troposphere and the boundary layer. The drag dissipation in the boundary layer is assumed to have the nonlinear form arising from standard turbulent drag parametrization:

$$\tilde{d}(|\vec{u}^B|) = d\sqrt{1 + \left(\frac{|\vec{u}^B|}{\epsilon V_*}\right)^2} \tag{5}$$

where a dimensional dissipation time of 1 day corresponds to $d = 0.35$. The dimensional value of the turbulent velocity scale, ϵV_*, is typically of order several meters per second.

Since the horizontal velocity in the boundary layer is independent of the height, the divergence condition for the vertical velocity can be solved for w^B. Since the vertical velocity must vanish at the ground ($z = -\pi\Delta_B$) the vertical velocity is simply a linear function of height in the boundary layer:

$$w^B = -(z + \pi\Delta_B)[u_x^B + v_y^B] \tag{6}$$

In order for the boundary layer to communicate its presence to the free troposphere, the two must be coupled. The natural boundary condition involves the continuity of pressure:

$$p^B = p|_{z=0} \tag{7}$$

and of vertical velocity:

$$w|_{z=0} = w^B = -\pi\Delta_B[u_x^B + v_y^B] \tag{8}$$

across the interface $z = 0$. The expression for the vertical velocity in Eq. (6) has been used for the second equality in (8). Notice that a vertical velocity at $z = 0$ would imply that the interface between the boundary layer and free troposphere is not constant in time and this would affect the boundary conditions and the energy conservation equation. However, this effect is higher order and will be neglected in the following discussion (see Biello and Majda, 2004, for further elaboration).

2. The IPESD model: low Froude number, multiple zonal length- and time-scale asymptotics

Consistent with an order ϵ forcing strength is an order ϵ response in the velocity, pressure and temperature which justifies a low Froude number expansion:

$$Fr \equiv \frac{|\vec{u}|}{c} = \epsilon \approx 0.1 \tag{9}$$

Therefore, the theory describes zonal/meridional velocities of order 5 m/s and vertical velocities 0.016 m/s. Furthermore, the IPESD models consider a multiple time- and zonal length-scale expansion which implies that all variables vary as

$$f(x, y, z, \tau, \epsilon x, \epsilon\tau) \tag{10}$$

All variables undergo order one variations when any of their arguments undergo order one changes. This motivates the definition of the long, intraseasonal, time scale:

$$t = \epsilon\tau \tag{11}$$

which is measured in units of 3.3 days and the planetary zonal length scale:

$$X = \epsilon x \tag{12}$$

which is measured in units of about 15,000 km. Upon substituting the low Froude number, multiple time and zonal length scale approximation into the anelastic equations for the free troposphere and redefining the variables as their ϵ-scaled counterparts:

$$u \longrightarrow \epsilon u, \qquad v \longrightarrow \epsilon v, \qquad w \longrightarrow \epsilon w, \qquad p \longrightarrow \epsilon p, \qquad \theta \longrightarrow \epsilon\theta \tag{13}$$

the equations for the free troposphere become:

$$\begin{aligned}
\left[\frac{\partial}{\partial\tau} + \epsilon\frac{\partial}{\partial t} + \epsilon\left(u\frac{\partial}{\partial x} + v\frac{\partial}{\partial y} + w\frac{\partial}{\partial z}\right) + \epsilon^2 u\frac{\partial}{\partial X}\right] u - yv &= -p_x - \epsilon p_X + S_u,\\
\left[\frac{\partial}{\partial\tau} + \epsilon\frac{\partial}{\partial t} + \epsilon\left(u\frac{\partial}{\partial x} + v\frac{\partial}{\partial y} + w\frac{\partial}{\partial z}\right) + \epsilon^2 u\frac{\partial}{\partial X}\right] v + yu &= -p_y + S_v,\\
\left[\frac{\partial}{\partial\tau} + \epsilon\frac{\partial}{\partial t} + \epsilon\left(u\frac{\partial}{\partial x} + v\frac{\partial}{\partial y} + w\frac{\partial}{\partial z}\right) + \epsilon^2 u\frac{\partial}{\partial X}\right] \theta + N^2 w &= S_\theta,\\
p_z &= \theta,\\
u_x + v_y + \frac{(\rho w)_z}{\rho} + \epsilon u_X &= 0
\end{aligned} \tag{14}$$

Again, all of the values and scales are summarized in Table 1.

The flow in the boundary layer is also assumed to be of low Froude number and the horizontal velocity there is replaced by its ϵ-scaled counterpart:

$$\epsilon u^{\mathrm{B}} \longrightarrow u^{\mathrm{B}}, \qquad \epsilon v^{\mathrm{B}} \longrightarrow v^{\mathrm{B}} \tag{15}$$

Using this approximation along with the assumption of multiple scales, the boundary layer equations become:

$$\begin{aligned}
\left[\frac{\partial}{\partial\tau} + \epsilon\left(\frac{\tilde{D}}{Dt} + \epsilon u^{\mathrm{B}}\frac{\partial}{\partial X}\right)\right] u^{\mathrm{B}} - yv^{\mathrm{B}} &= -p_x^{\mathrm{B}} - \epsilon p_X^{\mathrm{B}} - \tilde{d}u^{\mathrm{B}},\\
\left[\frac{\partial}{\partial\tau} + \epsilon\left(\frac{\tilde{D}}{Dt} + \epsilon u^{\mathrm{B}}\frac{\partial}{\partial X}\right)\right] v^{\mathrm{B}} + yu^{\mathrm{B}} &= -p_y^{\mathrm{B}} - \tilde{d}v^{\mathrm{B}}
\end{aligned} \tag{16}$$

where

$$\frac{\tilde{D}}{Dt} = \frac{\partial}{\partial t} + u^{\mathrm{B}}\frac{\partial}{\partial x} + v^{\mathrm{B}}\frac{\partial}{\partial y} \tag{17}$$

The ϵ-scale in the expression for the nonlinear dissipation, Eq. (5) was chosen with the knowledge that the turbulent velocity V_* is small compared to the Kelvin wave speed but of the same order of magnitude as typical large scale flows. In fact:

$$\epsilon V_* \sim \mathrm{O}(5\ \mathrm{m/s}) \tag{18}$$

in dimensional units, making V_* order one in the rescaling. Thus, the expression for the nonlinear dissipation becomes:

$$\tilde{d}(|\vec{u}^{\mathrm{B}}|) = d\sqrt{1 + \left(\frac{|\vec{u}^{\mathrm{B}}|}{V_*}\right)^2} \tag{19}$$

Since both the free troposphere variables and the boundary layer variables are replaced by their ϵ-scaled counterparts, the matching conditions across $z = 0$ remain essentially unchanged except for the multiple scales ansatz which adds a derivative with respect to the planetary zonal scale in the continuity of vertical velocity:

$$w|_{z=0} = -\pi \Delta_{\mathrm{B}}[u_x^{\mathrm{B}} + v_y^{\mathrm{B}} + \epsilon u_X^{\mathrm{B}}] \tag{20}$$

whereas the expression of pressure continuity remains unchanged:

$$p^{\mathrm{B}} = p|_{z=0} \tag{21}$$

The linearized version of the equations obtained by setting $\epsilon = 0$ in (14) contain all of the equatorial linear waves on the synoptic length and timescales (Kelvin, Rossby, gravity and mixed Rossby-gravity waves). Furthermore, on the longer time and length scales, there exists a balanced dynamics which describes planetary scale flows of Rossby and Kelvin waves; these correspond to unforced solutions of the linear theory which do not vary on the fast time scale. Both Kelvin waves and long Rossby waves have the property that, in the limit of long zonal wavelengths, the waves have meridional and vertical velocities which also tend to zero, whereas zonal velocity, pressure and temperature perturbations remain finite. Having assumed a separation of zonal length scales and corresponding wave time scales, we seek solutions of Eq. (14) which allow for unbalanced dynamics on the fast time and zonal synoptic scale, yet contain balanced dynamics on the planetary length and intraseasonal time scale. We therefore consider solutions of the form:

$$\begin{aligned}
\theta &= \theta'(\epsilon x, x, y, z, \epsilon\tau, \tau) + \bar{\Theta}(\epsilon x, y, z, \epsilon\tau) + \mathrm{O}(\epsilon),\\
p &= p'(\epsilon x, x, y, z, \epsilon\tau, \tau) + \bar{P}(\epsilon x, y, z, \epsilon\tau) + \mathrm{O}(\epsilon),\\
u &= u'(\epsilon x, x, y, z, \epsilon\tau, \tau) + \bar{U}(\epsilon x, y, z, \epsilon\tau) + \mathrm{O}(\epsilon),\\
v &= v'(\epsilon x, x, y, z, \epsilon\tau, \tau) + \epsilon\bar{V}(\epsilon x, y, z, \epsilon\tau),\\
w &= w'(\epsilon x, x, y, z, \epsilon\tau, \tau) + \epsilon\bar{W}(\epsilon x, y, z, \epsilon\tau)
\end{aligned} \tag{22}$$

The solutions of the boundary layer equation (16) will be determined from the pressure at the base of the troposphere. In general, the boundary layer velocity is a function of all variables (but independent of height, z):

$$u^{\mathrm{B}} = u^{\mathrm{B}}(\epsilon x, x, y, \epsilon\tau, \tau) + \mathrm{O}(\epsilon), \qquad v^{\mathrm{B}} = v^{\mathrm{B}}(\epsilon x, x, y, \epsilon\tau, \tau) + \mathrm{O}(\epsilon) \tag{23}$$

We shall also need to define two different averages, the first over the zonal synoptic coordinate:

$$\bar{g}(X, y, z, t, \tau) = \lim_{L\to\infty} \frac{1}{2L} \int_{-L}^{L} g(X, x, y, z, t, \tau)\,\mathrm{d}x \tag{24}$$

and the second over the gravity wave time scale:

$$\langle g\rangle(X,x,y,z,t)=\lim_{T\to\infty}\frac{1}{2T}\int_{-T}^{T}g(X,x,y,z,t,\tau)\,\mathrm{d}\tau \tag{25}$$

and from these we can define the deviations from the spatial or temporal means:

$$g(x,\tau)=\bar{g}(\tau)+g'(x,\tau)=\langle g\rangle(x)+\tilde{g}(x,\tau)=\langle\bar{g}\rangle+\langle g'\rangle(x)+\bar{\tilde{g}}(\tau)+\tilde{g}'(x,\tau) \tag{26}$$

2.1. Synoptic scale and fast dynamics

Substituting Eqs. (22) into (14) and retaining order ϵ^0 yields the time dependent, synoptic scale, equatorial weak temperature gradient (SEWTG) equations:

$$\begin{aligned}
u'_\tau-yv'+p'_x&=\langle\bar{S}_u\rangle+\langle S'_u\rangle(x)+\bar{\tilde{S}}_u(\tau)+\tilde{S}'_u(x,\tau),\\
v'_\tau+yu'+p'_y&=\langle\bar{S}_v\rangle+\langle S'_v\rangle(x)+\bar{\tilde{S}}_v(\tau)+\tilde{S}'_v(x,\tau),\\
\theta'_\tau+N^2w'&=\langle\bar{S}_\theta\rangle+\langle S'_\theta\rangle(x)+\bar{\tilde{S}}_\theta(\tau)+\tilde{S}'_\theta(x,\tau),\\
p'_z&=\theta',\\
u'_x+v'_y+\frac{(\rho w')_z}{\rho}&=0
\end{aligned} \tag{27}$$

where the dependence on planetary scales, X, intraseasonal timescale, t, and vertical and meridional coordinate have been suppressed for conciseness of notation. The equations in (27) are essentially the forced linear anelastic equations. The solutions of the SEWTG equations can be divided into two general categories, fast and slow, and further subdivided according to the forcing from which they arise:

(1) Fast, free waves: gravity waves of all length scales, short Kelvin and mixed Rossby-gravity waves.
(2) Fast: waves of all types (Kelvin, gravity, Rossby and mixed Rossby-gravity) forced by fast time-dependent forcing:

$$\bar{\tilde{S}}(\tau)+\tilde{S}'(x,\tau).$$

(3) Slow: waves forced by (fast) time-independent forcing varying on the synoptic scale:

$$\langle S'\rangle(x)$$

This is the same forcing that has already been considered in the two previous MJO model papers (Majda and Biello, 2004; Biello and Majda, 2005).
(4) Slow: synoptic scale mean flows forced by (fast) time-independent forcing

$$\langle\bar{S}_v\rangle,\langle\bar{S}_u\rangle\quad\text{and}\quad\langle\bar{S}_\theta\rangle$$

which satisfy the geostrophic balance condition discussed below in Appendix A.
(5) Fast: synoptic scale mean flows forced by (fast) time-independent mean forcing which is not in geostrophic balance, i.e. the remainder of

$$\langle\bar{S}_u\rangle\quad\text{and}\quad\langle\bar{S}_\theta\rangle$$

Such waves necessarily cause secular growth of zonally symmetric "gravity" or "geostrophic adjustment" modes.

All of the terms are included here as a reminder of their importance especially in theories of moist dynamics or in further multiple scale theories which couple to meso-scales or smaller. However, only a small subset of them will be important in determining the synoptic scale flows of the MJO theory.

2.2. Synoptic scale balanced dynamics: SEWTG

The previous models of the MJO using the IPESD theory (Majda and Biello, 2004; Biello and Majda, 2005) did not consider the full generality of solutions to Eq. (27), and instead made three additional assumptions:

(1) The bulk averages of dynamics on the fast time scale, τ, are very weak and therefore not relevant.
(2) The planetary mean heating is order ϵ times the synoptic scale fluctuations. Therefore, the temperature forcing is

$$S_\theta = S'_\theta(X, x, y, z, t) + \epsilon \bar{S}_\theta(X, y, z, t) \tag{28}$$

(3) There are zonal momentum drag and thermal dissipation terms which are linear in the amplitudes of the zonal momentum and temperature, respectively. Furthermore, the typical momentum dissipation time is of order 5 days (Lin et al., 2005) and the thermal dissipation time is of order 15 days (Bretherton and Sobel, 2003). Therefore, the following additional forcing terms arise,

$$S_u = -\epsilon d_0(u' + \bar{U})$$

and

$$S_\theta = -\epsilon d_\theta(\theta' + \bar{\Theta})$$

where the values of the momentum and temperature dissipation make the nondimensionalized dissipations order one: $d_0 \approx 0.55$ and $d_\theta \approx 0.18$ (see Table 1).

As discussed in Biello and Majda (2005), the assumption in Eq. (28) about the large scale mean is consistent with the fact that planetary scale heating has strength 2–3 K per day while synoptic scale fluctuations are of order 10 K per day. In this setting the fast time average in Eq. (27) can be neglected, as can all dependence on the fast time scale, τ. The balanced synoptic scale anelastic equations are

$$\begin{aligned} -yv' + p'_x &= 0, \\ yu' + p'_y &= 0, \\ N^2 w' = S'_\theta, \quad \bar{S}'_\theta &= 0, \\ p'_z &= \theta', \\ u'_x + v'_y + \frac{(\rho w')_z}{\rho} &= 0 \end{aligned} \tag{29}$$

which are the SEWTG equations of Majda and Klein (2003), Majda and Biello (2004) and Biello and Majda (2005).

2.3. Planetary scale response: QLELWE

We now consider the zonal means of Eq. (14), among these are terms of second order and of zeroeth order in ϵ. The necessary and sufficient conditions that a forced wave equation have bounded solutions for all time is that the forcing be non-resonant with the linear operator and that the mean of the forcing in the direction of the wave characteristics vanish. Since all of the synoptic scale flows we consider are independent of the fast time scale, there only exists the possibility that higher order, nonlinear terms resonate with the fast time independent wave: this is the planetary scale mean flow. Therefore, the necessary and sufficient condition to solve the SEWTG equations is that the synoptic scale zonal mean of the terms in Eq. (14) vanish.

Using the assumptions of the previous subsection and taking the zonal synoptic scale mean of the scaled anelastic Eq. (14) we arrive at the anelastic quasi-linear equatorial long wave equation (QLELWE):

$$\begin{aligned}
\bar{U}_t - y\bar{V} + \bar{P}_X &= F^U - d_0\bar{U},\\
y\bar{U} + \bar{P}_y &= 0,\\
\bar{\Theta}_t + N^2\bar{W} &= F^\theta - d_\theta\bar{\Theta} + \bar{S}_\theta,\\
\bar{P}_z &= \bar{\Theta},\\
\bar{U}_X + \bar{V}_y + \frac{(\rho\bar{W})_z}{\rho} &= 0
\end{aligned} \tag{30}$$

The fluxes from the synoptic scales are given by

$$F^U = -(\overline{v'u'}_y) - (\overline{w'u'})_z, \qquad F^\theta = -(\overline{v'\theta'})_y - (\overline{w'\theta'})_z \tag{31}$$

Notice that all terms in Eq. (30) arise from second order in ϵ except the meridional geostrophic constraint which arises from the zero order terms in ϵ. This is a reflection of the fact that on the planetary zonal scale the gravity waves, which are not in meridional geostrophic balance, are fast and are thus filtered out by the asymptotic theory (see Majda, 2003, Chapter 9). What remains on the planetary zonal scale are only flows in meridional geostrophic balance: Kelvin and Rossby waves.

2.4. Dynamics in the boundary layer

Substituting the pressure boundary condition from Eq. (21) into the boundary layer equation (16) and again neglecting fast time derivatives, the boundary layer equations become:

$$\begin{aligned}
-yv^{\mathrm{B}} + du^{\mathrm{B}}\sqrt{1 + \left(\frac{|\vec{u}^{\mathrm{B}}|}{V_*}\right)^2} &= -p'_x + \mathrm{O}(\epsilon),\\
yu^{\mathrm{B}} + dv^{\mathrm{B}}\sqrt{1 + \left(\frac{|\vec{u}^{\mathrm{B}}|}{V_*}\right)^2} &= -p'_y - \bar{P}_y + \mathrm{O}(\epsilon)
\end{aligned} \tag{32}$$

where the pressure terms on the right-hand side correspond to the pressure in the free troposphere evaluated at $z = 0$.

The boundary layer is coupled to the free troposphere through the continuity of vertical velocity across $z = 0$ which provides a lower boundary condition on the vertical velocity in the free troposphere. The strength of this coupling is specified by the small relative boundary layer

thickness, Δ_B; therefore, it is a perfect candidate for rescaling. For a 0.5 km boundary layer and 16 km troposphere, the ϵ-rescaled boundary layer coupling parameter is defined as

$$\Delta \equiv \frac{\Delta_B}{\epsilon} \approx \frac{0.5/16}{1/10} \approx 0.3 \tag{33}$$

so that the combination:

$$\Delta\pi \approx 0.3\,\pi \sim O(1) \tag{34}$$

The boundary condition on the vertical velocity must be separated into its planetary mean and synoptic scale fluctuating component using the separation in Eq. (22) and the definition of the order one coupling parameter, Δ from Eq. (33):

$$(w' + \epsilon\bar{W})|_{z=0} = -\epsilon\pi\Delta[u_x^B + v_y^B + \epsilon u_X^B] \tag{35}$$

Taking the zonal synoptic average of both sides, using the fact that the zonal average of the fluctuating vertical velocity vanishes:

$$\tilde{w}' = 0 \tag{36}$$

and that flows have zero mean on the synoptic scales, yields:

$$\bar{u}_x^B = \lim_{L\to\infty} \frac{u^B(x=L) - u^B(x=-L)}{L} \longrightarrow 0 \tag{37}$$

Therefore, the boundary condition on the planetary scale mean vertical velocity at $z = 0$ is

$$\bar{W} = -\pi\Delta\bar{v}_y^B + O(\epsilon) \tag{38}$$

whereas the remainder yields the boundary condition for the synoptic scale fluctuations:

$$w' = O(\epsilon) = -\epsilon\pi\Delta(v_y^B - \bar{v}_y^B) + O(\epsilon^2) \tag{39}$$

Note from Eq. (39) that at leading order, the synoptic scale fluctuating component of the flow, from Eq. (29), is not affected by the boundary layer.

Finally, notice that the full geostrophic balance of the synoptic scale flows and meridional geostrophic balance of the planetary flows implies that the boundary layer pressure can be explicitly specified in terms of the zonal and meridional velocities at the base of the free troposphere. Therefore, to lowest order, the flow in the boundary layer is determined by

$$-yv^B + du^B\sqrt{1+\left(\frac{|\vec{u}^B|}{V_*}\right)^2} = -yv', \qquad yu^B + dv^B\sqrt{1+\left(\frac{|\vec{u}^B|}{V_*}\right)^2} = y(u' + \bar{U}) \tag{40}$$

where the right-hand sides are evaluated at $z = 0$.

A solution algorithm for Eq. (40) is provided in Appendix C.1 for the case of a general, nonlinear aerodynamic drag. In the case of a boundary layer drag coefficient which is independent of the total velocity, $|\vec{u}^B|$ (equivalently, $V_* \longrightarrow \infty$, which corresponds to a linear drag law), the lowest order term in Eq. (C.12) describes the boundary layer meridional velocity in terms of the zonal velocity at the base of the troposphere:

$$\bar{v}^B = \frac{yd}{y^2 + d^2}\bar{U}\bigg|_{z=0} \tag{41}$$

The interpretation of this expression is that eastward zonal velocities at the base of the troposphere near the equator drive boundary layer flows away from the equator and, according to Eq. (38), a

downward velocity in the troposphere must compensate. Conversely, westward winds at the base of the troposphere drive boundary layer flows toward the equator and a compensating upward Ekman pumping must occur in the free troposphere. Dimensionally, the U and v^{B} are both measured in the same units, 5 m/s whereas d is the boundary layer rate measured in units of the reciprocal of the equatorial deformation time, T_{E} and y is, of course, measured in terms of the equatorial deformation radius, L_{E}.

2.5. The IPESD theory for the Boussinesq equations

The MJO model outlined by Majda and Biello (2004) and Biello and Majda (2005) used the IPESD equations of Majda and Klein (2003) for the Boussinesq equations where both the density and buoyancy frequency are constant ($\rho = N = 1$) and the flow is specified in the following manner.

The total flow consists of planetary scale mean plus synoptic scale fluctuations as described in Eq. (22) which vary on synoptic scales x and y, in the vertical, z on long zonal planetary scale, $X = \epsilon x$ and on intraseasonal time scales, t. The small asymptotic parameter, ϵ, which measures the scale separation takes on the value $\epsilon \approx 0.1$. The coordinates are scaled so that $-10/3 \leq y \leq 10/3$, $0 \leq z \leq \pi$ and $-4/3 \leq X \leq 4/3$ describe the whole zonal extent of the equatorial troposphere from ± 5000 km meridionally and 16 km vertically. The unit of time is 3.3 days, which is useful in describing intraseasonal variations. Faster variations have been disregarded but can be included without significant differences. The velocity is measured in units of 5 m/s in the horizontal and 0.016 m/s in the vertical direction and the potential temperature is measured in units of 3.3 K.

The MJO model considers forcing only through latent heat release, upper troposphere drag dissipation, thermal dissipation and lower troposphere drag dissipation through coupling to a linear barotropic boundary layer at $z = 0$. The heating anomaly is specified a priori and is separated into its zonal synoptic scale fluctuating component and a weaker zonal planetary scale mean as in Eq. (28). The units for the heating anomaly are 10 K/day, which are typical of synoptic scale heating fluctuations in the tropics.

The synoptic scale flow is determined through the SEWTG balanced dynamics from Eq. (29) with rigid lid boundary conditions (39) at the top and bottom of the troposphere, forced by the synoptic scale heating fluctuations, S'_θ, from Eq. (28).

The planetary scale is governed by the quasi linear equatorial long wave Eq. (30) driven by upscale momentum and thermal fluxes, Eq. (31), and by planetary scale mean heating specified in Eq. (28). Again we assume a rigid lid boundary condition at the top of the troposphere, $\bar{W} = 0$ at $z = \pi$, (see Haertel and Kiladis, 2004, for validity) however the bottom boundary is coupled to the flow in the barotropic boundary layer below $z = 0$. The vertical velocity at the base of the free troposphere is a functional of the meridional momentum flux, Eq. (38), and this boundary layer momentum flux is determined by the zonal velocity at the base of the free troposphere through Eq. (41). The values of the nondimensionalized momentum drag, thermal dissipation and boundary layer thickness are given in Table 1.

3. Analytic expressions of the upscale flux arising from synoptic scale flows

One of the important features of the IPESD equations is that synoptic scale fluctuations in the flow and their resultant upscale momentum and temperature fluxes are analytically expressible in terms of the synoptic scale heating fluctuations. This is a very powerful tool for understanding the effect of different synoptic scale structures on planetary scale flows. In this section we shall

show the usefulness of this analytic tractability by setting up some plausible models for synoptic scale heating generalizing those in Majda and Biello (2004) and Biello and Majda (2005). We calculate the synoptic scale flow arising from this heating profile and the planetary scale flow which arises from the planetary scale mean heating and the upscale flux from the synoptic scales. By highlighting the steps in this computation, we show that the model of Majda and Biello (2004) and Biello and Majda (2005) forms the archetypal congestus/supercluster MJO model, and the effect of changing the structure of the heating can be analytically expressed through these formulae.

Consider a simple model for the synoptic scale fluctuating component of the latent heat release consisting of first and second baroclinic mode heating (which are dominant modes in the observations, Mapes and Houze, 1995):

$$S'_\theta = F(X,t)(G^1_x(X,x,y,t)\sin(z) + G^2_x(X,x,y,t)\sin(2z)) \tag{42}$$

which with G^1, G^2 being periodic functions of x, ensures that the zonal integral of S'_θ is zero. A planetary scale mean heating can be incorporated into this framework simply by adding a weaker mean heating which also consists of first and second baroclinic components; since the weaker planetary scale mean heating only affects planetary scale flows in a linear fashion (see Eq. (30)), we shall not consider it further in this section. The profiles of fluctuating heating in (42) are general enough to incorporate the synoptic scale fluctuations from deep convective, stratiform and congestus wave trains of convection as are indicated in observations (Lin and Johnson, 1996).

Of a large scale envelope function, $F(X,t)$, which zonally localizes the latent heat release over an envelope of convection (for example, the Western Pacific warm pool), and the sum of a first and second baroclinic heating component with spatially and temporally varying amplitudes, G^1_x, G^2_x.

Using this heating profile, the synoptic scale balanced flow can easily be solved in the following fashion. Since the equations in (29) are linear, each vertical baroclinic mode of the flow can be solved separately and summed up at the end to yield the total flow. From Eq. (29) with $N = \rho = 1$, the vertical component of the balanced flow is exactly equal to the heating rate on the synoptic scale. Taking the x derivative of the meridional geostrophic balance condition minus the y derivative of the zonal geostrophic balance condition and expressing the horizontal divergence of the flow in terms of the vertical velocity (equivalently the heating rate) yields the expression for the meridional component of the flow, v. Both the meridional and vertical components of the flow can be substituted into the incompressibility condition, which can then be integrated to yield the zonal velocity, u', subject to the condition that its zonal mean be zero. The pressure can be solved by integrating either of the geostrophic balance constraints, again requiring that its zonal mean be zero, and hydrostatic balance allows to determine the potential temperature in terms of the pressure. Therefore, the heating rate profile in Eq. (42) yields the synoptic scale flow:

$$\begin{aligned}
w' &= G^1_x \sin(z) + G^2_x \sin(2z),\\
v' &= y[G^1_x \cos(z) + 2G^2_x \cos(2z)],\\
u' &= -[(2G^1 + yG^1_y)\cos(z) + 2(2G^2 + yG^2_y)\cos(2z)],\\
p' &= y^2[G^1 \cos(z) + 2\,G^2 \cos(2z)],\\
\theta' &= -y^2[G^1 \sin(z) + 4\,G^2 \sin(2z)]
\end{aligned} \tag{43}$$

The resulting upscale momentum flux contains structure in all of the vertical wavenumbers which can be expressed as sums or differences of the first two baroclinic waves; i.e. the upscale response drives the barotropic and first four baroclinic modes.

The definition of the momentum and thermal flux convergence is given in Eq. (31) and the definition planetary scale mean is given in Eq. (24). Upon substituting the expressions for the synoptic scale flow from Eq. (43) into the flux expression (31) it is clear that the resultant expression for the flux is a sum of bilinear functions of the horizontal structure of the heating, G^1, G^2. We make use of three bilinear operators: the first is essentially the zonally averaged Jacobian and is antisymmetric in its arguments:

$$A(F,G) = \frac{\overline{F_x G_y - F_y G_x}}{2} \tag{44}$$

the second is symmetric:

$$S(F,G) = \frac{\overline{F_x G_y + F_y G_x}}{2} \tag{45}$$

and the third is also antisymmetric, but involves only derivatives in x:

$$\Upsilon(F,G) = \frac{\overline{F_x G - G_x F}}{2} = \overline{F_x G} = -\overline{F G_x} \tag{46}$$

Upon integration by parts, all of the components of the flux convergences can be expressed in terms of these operators acting on G^1 and G^2. In particular, we shall simplify the notation by defining:

$$\begin{aligned} &S^{11} = S(G^1, G^1), \qquad S^{22} = S(G^2, G^2), \qquad S^{12} = S(G^1, G^2), \\ &A^{12} = A(G^1, G^2), \qquad \Upsilon^{12} = \Upsilon(G^1, G^2) \end{aligned} \tag{47}$$

3.1. The eddy flux convergence arising from general first and second baroclinic synoptic scale heating

Using the definitions of the bilinear operators in Eq. (47) the momentum flux convergence is

$$\begin{aligned} F^U = &\left[\frac{y^2}{2}(S^{11} + 4S^{22})\right]_y + \left[2y^2 S_y^{12} + \frac{7}{2} y S^{12} - 3\Upsilon^{12} - \frac{3}{2} y A^{12}\right] \cos(z) \\ &+ \left[\frac{1}{2} y^2 S_y^{11} + 2y S^{11}\right] \cos(2z) \left[2y^2 S_y^{12} + \frac{17}{2} y S^{12} + 3\Upsilon^{12} + \frac{3}{2} y A^{12}\right] \cos(3z) \\ &+ 4\left[\frac{1}{2} y^2 S_y^{22} + 2y S^{22}\right] \cos(4z) \end{aligned} \tag{48}$$

Many of these terms can be explicitly traced to particular components of the flux, in particular:

- Both barotropic forcing terms arise solely from the horizontal flux of zonal momentum $(\overline{uv})_y$.
- The term in Υ in the first baroclinic forcing arises solely from the vertical transport of zonal momentum $(\overline{uw})_z$.
- All of the remaining terms do not come from either of the two individual components of the flux.

The upscale flux of temperatures yields a flux convergence which contains only first and third baroclinic components:

$$F^{\theta} = \left[\frac{15}{2}y^2\Upsilon^{12} + 3y^3\Upsilon^{12}_y\right]\sin(z) + \left[\frac{15}{2}y^2\Upsilon^{12} + y^3\Upsilon^{12}_y\right]\sin(3z) \tag{49}$$

and neither of these components can uniquely be traced to either the meridional or vertical components of the temperature flux.

Though these expressions are useful to shed some light on the effects of the forcing terms, full insight will be gained after the further simplification below. For now, we emphasize certain general properties:

- We will show below that the terms in Υ^{12} and A^{12} are ubiquitous in models of the MJO (Biello and Majda, 2005), whereas the terms in S arise in specific examples and can be seen as perturbations around a basic model. Therefore, the basic structure of the momentum forcing is

$$F^{U} \propto \cos(z) - \cos(3z) \tag{50}$$

  whose maxima occur at about 5 and 11 km heights.
- The temperature flux convergence contains the ubiquitous terms in Υ^{12} which also drive the first and third baroclinic modes, but these are multiplied by functions of latitude, y. Therefore, the temperature flux convergence is always weak near the equator.
- The barotropic, second and fourth baroclinic modes are driven only by upscale momentum flux convergence and their components contain only terms in S also multiplied by factors of y. Therefore, these components are always weaker above the equator than the ubiquitous, Υ terms.
- The functions G^j are mean zero and are formally extended over an infinite zonal synoptic scale (recall the limit in the synoptic scale average in Eq. (24)). Equivalently, the synoptic scale convective envelope can be simply a finite zonal synoptic region over which the functions G^j are periodic and mean zero. Irrespective, the G^j can always be expressed as a Fourier sum or integral over wavenumbers in the synoptic scale zonal direction, for example:

$$G^j = \sum_{k=1} H_{jk}(y)\sin(k\,x + \phi_k).$$

  Upon taking the zonal synoptic scale average, from Eq. (24), only terms of the same zonal wavenumber couple to one another and contribute to the various bilinear functions which constitute the components of the flux convergence.

Therefore, in order to understand the effects of the structure of synoptic scale heating on the upscale flux convergences, we need only consider structures which contain a single wavenumber in the zonal synoptic direction. The effect on the planetary scales of more general zonal structures is simply a linear superposition of the single wave structure. In particular, the integration implies that many classes of synoptic scale heating give the same flux convergence, so that the details of the zonal synoptic scale structure are not important in calculating the planetary scale effects.

3.2. Explicit computation of the flux convergence

With the above considerations, we can consider the most general heating profiles which consist of one zonal synoptic wavenumber:

$$\begin{aligned} G^1 &= H_1(y)\sin(x+\phi_1(y)) \quad \text{and} \\ G^2 &= H_2(y)\sin(x+\phi_2(y)) \Longrightarrow S'_\theta \\ &= F(X)[H_1(y)\cos(x+\phi_1(y))\sin(z) + H_2(y)\cos(x+\phi_2(y))\sin(2z)] \end{aligned} \tag{51}$$

Notice that H_j and ϕ_j are both functions of the meridional coordinate and, in general, are also functions of time and the planetary scale zonal coordinate. The functional dependence on time and zonal planetary scale are parametric from the perspective of calculating the flux convergence and are not explicitly shown until the discussion of the solution of the planetary scale flows.

Therefore, the bilinear forms become:

$$\begin{aligned} \Upsilon^{12} &= \tfrac{1}{2}H_1H_2\ \sin(\phi_2-\phi_1), \\ A^{12} &= \tfrac{1}{4}\left[H_1H_2\ \sin(\phi_2-\phi_1)\right]_y \equiv \tfrac{1}{2}\Upsilon^{12}_y, \\ S^{11} &= \tfrac{1}{2}(H_1)^2\phi_{1y}, \\ S^{22} &= \tfrac{1}{2}(H_2)^2\phi_{2y}, \\ S^{12} &= \tfrac{1}{4}[(H_1H_{2y}-H_2H_{1y})\sin(\phi_2-\phi_1) + H_1H_2(\phi_{1y}+\phi_{2y})\cos(\phi_2-\phi_1)] \end{aligned} \tag{52}$$

Notice that the term $H_1H_{2y} - H_2H_{1y}$, which appears in the expression for S^{12} can be rewritten as

$$H_1H_{2y} - H_2H_{1y} = H_1H_2\left(\frac{\mathrm{d}\ln(H_2)}{\mathrm{d}y} - \frac{\mathrm{d}\ln(H_1)}{\mathrm{d}y}\right) = H_1H_2\frac{\mathrm{d}}{\mathrm{d}y}\ln(H_2/H_1) \tag{53}$$

In this form, it appears as the original meridional structures multiplied by the difference of the reciprocal of their meridional length scales (i.e. $l_1^{-1} \sim (\mathrm{d}\ln(H_1)/\mathrm{d}y)$, etc.). Therefore, it vanishes unless the meridional extent of the first and second baroclinic heating are different.

Notice also that the phase gradient, ϕ_y, measures the meridional/zonal tilt of the zonally fluctuating heating structure. Therefore, for positive phase gradients, the heating contours locally tilt from the northwest to the southeast whereas for negative phase gradients, they tilt from the southwest to the northeast.

We can now list some very general properties of the bilinear structures and therefore of the flux convergences:

- If there is no phase lag, nor any difference in the meridional extent of the first and second baroclinic heating, then the flux convergences are everywhere zero.
- The most common example is of first and second baroclinic heating modes having meridionally independent phase, $\phi_{1y} = \phi_{2y} = 0$ with a phase lag, $\phi_1 \neq \phi_2$, and the same meridional structure, $H_1 = H_2 = H$. In this case all of the symmetric bilinear forms vanish and the momentum flux convergence contains only first and third baroclinic modes. The temperature flux convergence also contains both first and third baroclinic modes. This is the "ubiquitous" example referred to above: it describes both westward tilted superclusters and lower troposphere

congestus heating and yields the canonical MJO example from previous papers (Majda and Biello, 2004; Biello and Majda, 2005).

- A simple perturbation to the canonical case considers synoptic scale heating where the meridional extent of the second baroclinic mode is greater than the first baroclinic heating mode with lagged phases which are independent of latitude. This case describes, for example, superclusters with broader stratiform decks. Clearly, the bilinear form S^{12} is no longer zero and the upscale flux still projects only onto the first and third baroclinic modes, though breaking the symmetry described in Eq. (50).
- Heating profiles with horizontally tilted structures have $\phi_{iy} \neq 0$ and contribute to S^{ii}. Therefore, local tilts in the horizontal direction drive barotropic, second and fourth baroclinic momentum flux convergences. These terms arise from a meridional upscale transport of zonal momentum. Such effects are emphasized in Moncrieff's (2004)phenomenological models.

The MJO models of Majda and Biello (2004) and Biello and Majda (2005) considers precisely the simplest of these examples: first and second baroclinic synoptic heating fluctuations of equal meridional extent with vertical tilt (phase lag) and no horizontal tilt. In particular:

$$S'_\theta = F(X)H(y;\lambda)[\cos(x)\sin(z) - \alpha(X)\cos(x+\phi)\sin(2z)] \tag{54}$$

where $\alpha > 0$ and $\phi > 0$ describes deep convective superclusters while $\alpha < 0$ and $\phi > 0$ describes lower troposphere congestus heating. In these models, $H(y,\lambda) = \mathrm{e}^{-(y+y_0)^2/\lambda(X)^2}$ is used to describe the meridionally localized equatorial, $y_0 = 0$, or off equatorial, $y_0 \neq 0$, heating profile. In the examples considered below, we revisit the planetary scale flows resulting from this synoptic scale heating profile and consider more general cases with synoptic scale heating tilted meridionally so that the meridional momentum flux is non-zero.

4. The effect of meridional momentum flux

Using the MJO models discussed in Biello and Majda (2005) (hereafter referred to as the "canonical MJO models") we consider four examples which are modulations of these models which include meridional momentum flux and one example whose synoptic scale fluctuations only result in upscale meridional momentum flux. The canonical MJO models employ a first and second baroclinic heating profile both for the fluctuating and planetary mean components similar to that given in Eq. (54). The fluctuating and mean heating in the canonical MJO models are

$$\begin{aligned} S'_\theta(X,x,y,z,t) &= F(X-st)H(y;\lambda)\,[\cos(x)\,\sin(z) - \alpha(X-st)\cos(x+\phi_0)\,\sin(2z)]\,, \\ \bar{S}_\theta(X,y,z,t) &= F(X-st)H(y;\lambda)\,[\sin(z) - \bar{\alpha}(X-st)\sin(2z)] \end{aligned} \tag{55}$$

where the convective envelope is simply a clipped cosine:

$$F(X) = \begin{cases} \cos\left(\frac{\pi X}{2L_*}\right) & |X| < L_* \\ 0 & |X| \geq L_* \end{cases} \tag{56}$$

and $L_* = 0.417$ implies that the convective activity has a zonal extent of 10,000 km. The meridional structure of the convection is a Gaussian:

$$H(y;\lambda) = \mathrm{e}^{-(y+y_0)^2/\lambda^2} \tag{57}$$

with a typical meridional extent of 1500 km ($\lambda = 1$) and the maximum of heating centered either at the equator or 450 km south; $y_0 = 0, 0.3$, respectively. The convective envelope travels at an

eastward speed equal to 5 m/s ($s = 0.1$). The heating maxima are located in the top (bottom) half of the troposphere for $\alpha, \bar{\alpha} > 0$ and the in the bottom half of the troposphere for $\alpha, \bar{\alpha} < 0$. The parameter ϕ_0 determines the phase lag of the second baroclinic mode compared to the first and does not depend on y in this model. When the meridional gradient of the phase is zero, there is no barotropic, second or fourth baroclinic mode forcing. In this case, it was shown in Majda and Biello (2004) and Biello and Majda (2005) that the flux convergences depend on the parameters α, F and ϕ_0 solely through the combination:

$$\kappa = \tfrac{3}{4} F(X - st)^2 \alpha(X - st)\, \sin(\phi_0) \tag{58}$$

and both flux convergences are proportional to κ:

$$\begin{aligned} F^U &= \kappa(\cos(z) - \cos(3z))(2H^2 + yHH_y), \\ F^\theta &= -\kappa y^2 \left\{ \sin(z)[5H^2 + 4yHH_y] + \sin(3z)[5H^2 + 4/3 yHH_y] \right\} \end{aligned} \tag{59}$$

The flux convergences for the case of positive κ (supercluster) along with their meridional and vertical components are shown in Figs. 1 and 2. In the canonical MJO models, the convection varies between westward tilted supercluster to the west of the convective envelope and lower troposphere congestus convection to the east of the convective envelope and simple linear functions were used:

$$\alpha(X - st) = -\frac{8(X - st)}{3L_*}, \qquad \bar{\alpha}(X - st) = -\frac{3(X - st)}{2L_*} \tag{60}$$

Figs. 3 and 4 show horizontal slices of the planetary scale flow arising from the congestus/supercluster MJO model with heating centered at the equator and 450 km south using the parameters described above; these examples are considered in Biello and Majda (2005). The zonal flow above the equator, which is also the location of the maximum heating, is shown in Fig. 5. This diagram is essentially the same above the center of the heating in the off-equatorial heating model. For an extensive discussion of the results, we refer the reader to Biello and Majda (2005).

4.1. Equatorially symmetric meridional momentum flux

The most straightforward way to see the effects of meridional momentum flux is to add an equatorially symmetric meridional tilt to the synoptic scale heating of the canonical MJO model with heating centered at the equator (Figs. 3 and 5). The vertical tilts in the synoptic scale heating of the canonical MJO model yield a momentum flux convergence which drives only the first and third vertical baroclinic modes. The addition of a meridionally tilted synoptic scale heating adds barotropic, second and fourth baroclinic momentum forcing to the planetary scale mean flows. Since the tilts are equatorially symmetric, the resultant upscale flux convergences will also be equatorially symmetric.

The tilt of the first and second baroclinic modes are the same except for a phase lag and depend quadratically on distance from the equator:

$$\phi_1 = \gamma \frac{y^2}{2}, \qquad \phi_2 = \gamma \frac{y^2}{2} + \phi_0 \tag{61}$$

For $\gamma > 0$ the heating contours are tilted poleward/westward whereas for $\gamma < 0$ the heating contours are tilted poleward/eastward. As before, the vertical tilt is described by the constant phase lag, ϕ_0.

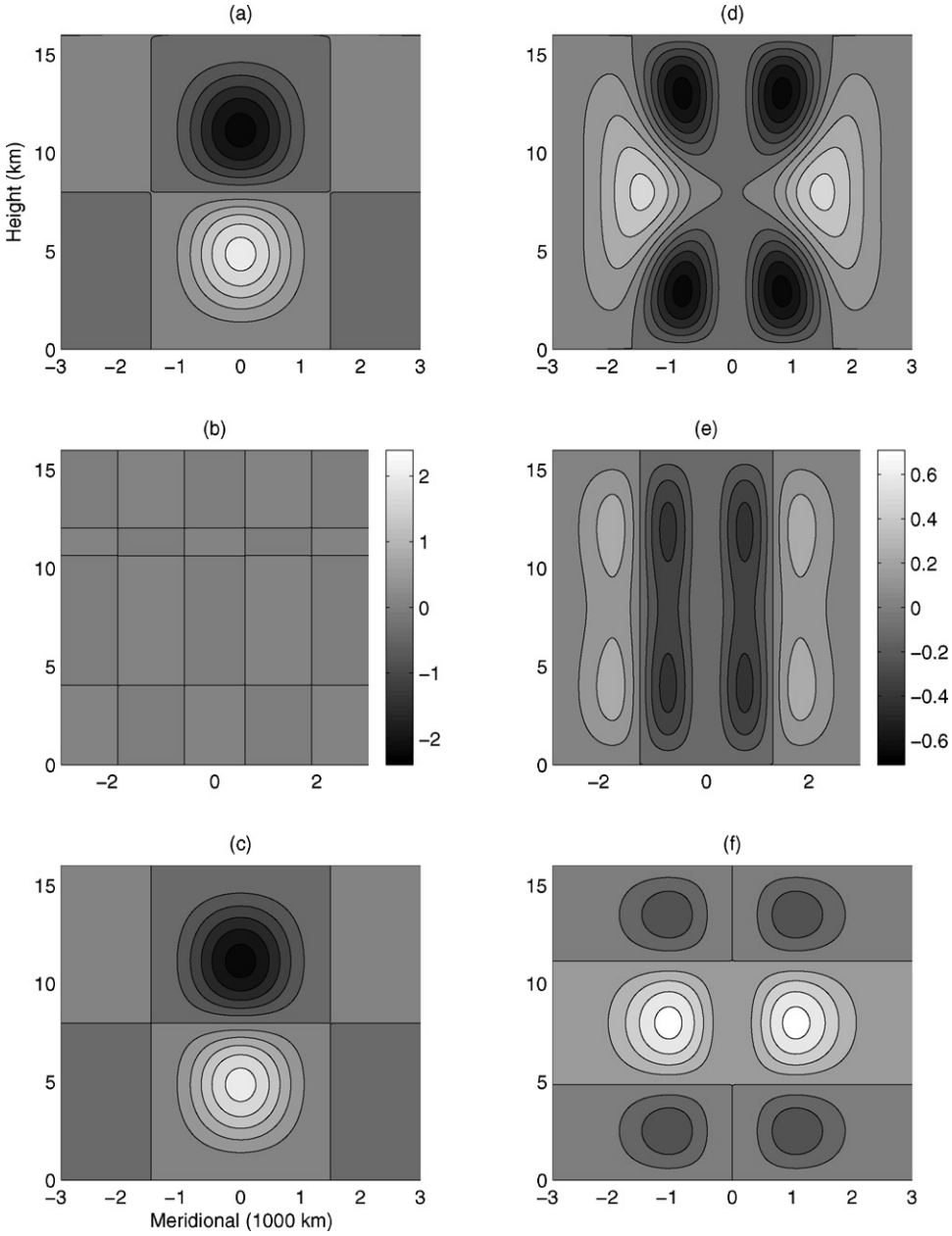

Fig. 1. The eddy flux convergences as a function of latitude and height in the troposphere for equatorially symmetric heating in the supercluster portion of the convective envelope: (a) total momentum flux convergence; (b) meridional component of momentum flux convergence; (c) Vertical component of momentum flux convergence; (d–f) are the same as (a)–(c) except for the temperature flux convergence. The scale on the left is for figures (a)–(c) whereas that on the right is for figures (d)–(f); both are nondimensionalized scales.

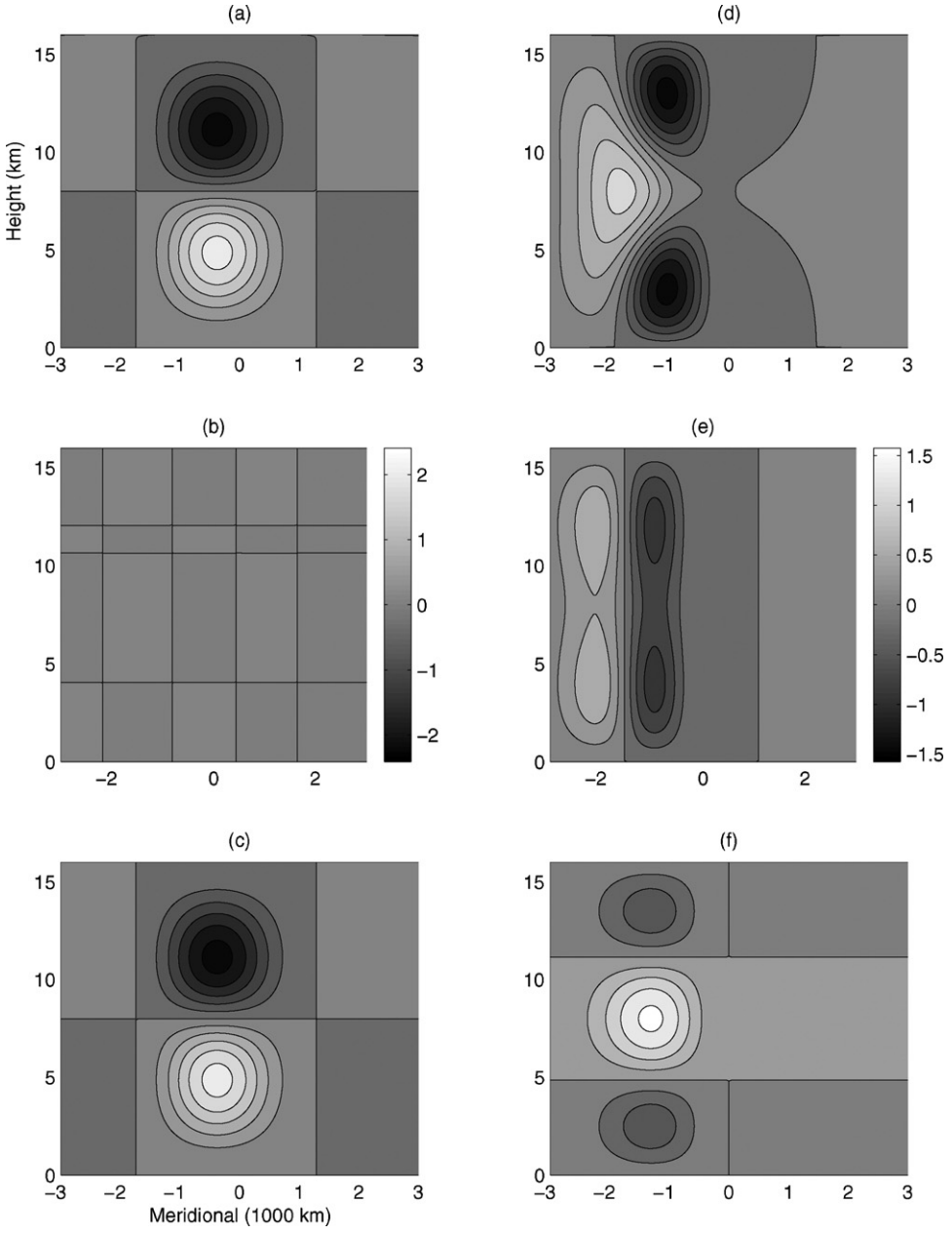

Fig. 2. The eddy flux convergences as a function of latitude and height in the troposphere in the supercluster convection region for heating centered at 450 km south. The frames are the same as in Fig. 1.

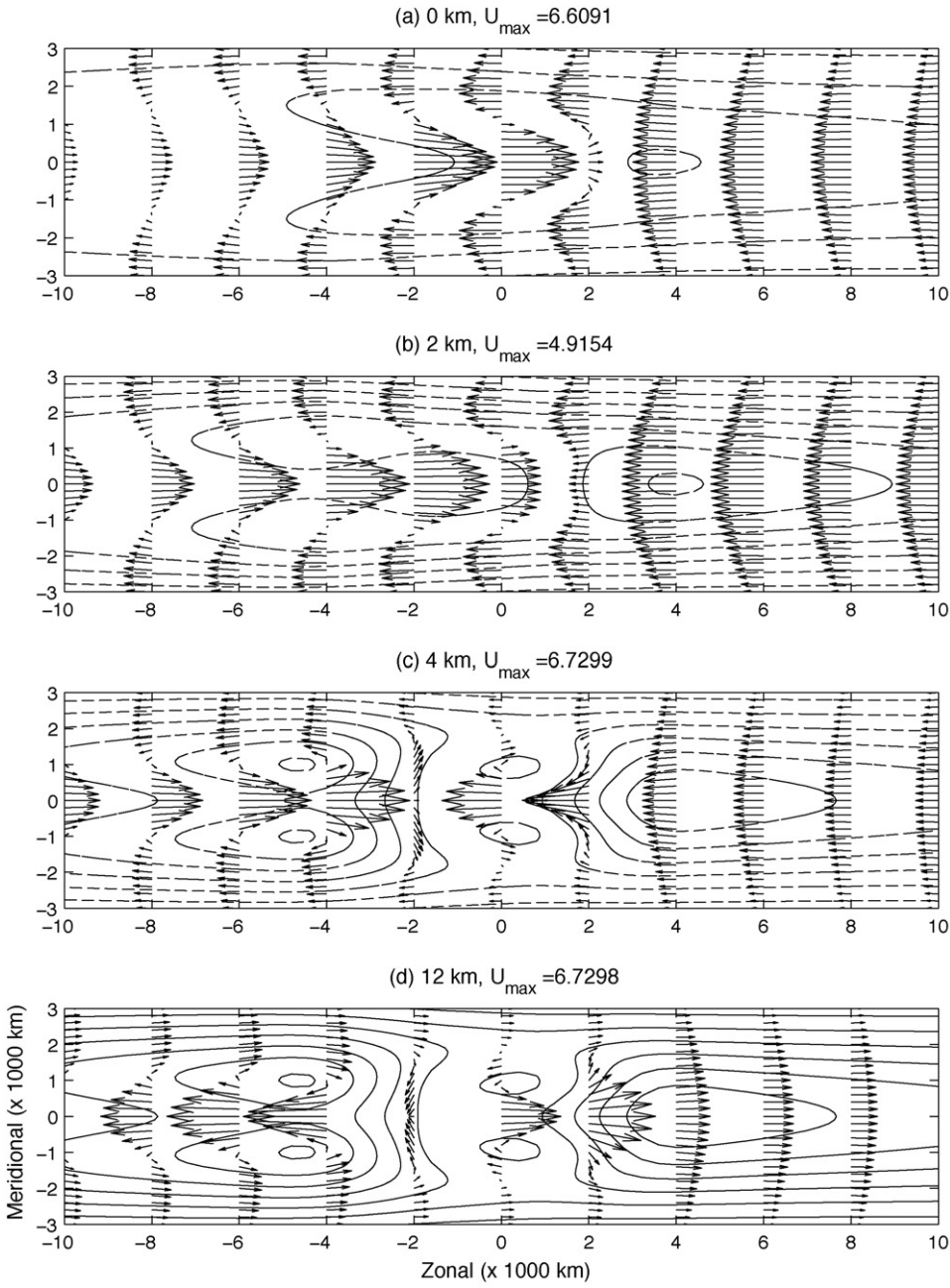

Fig. 3. Zonal velocity and pressure contours after saturation without boundary layer drag in the equatorially symmetric congestus/supercluster model of the MJO.

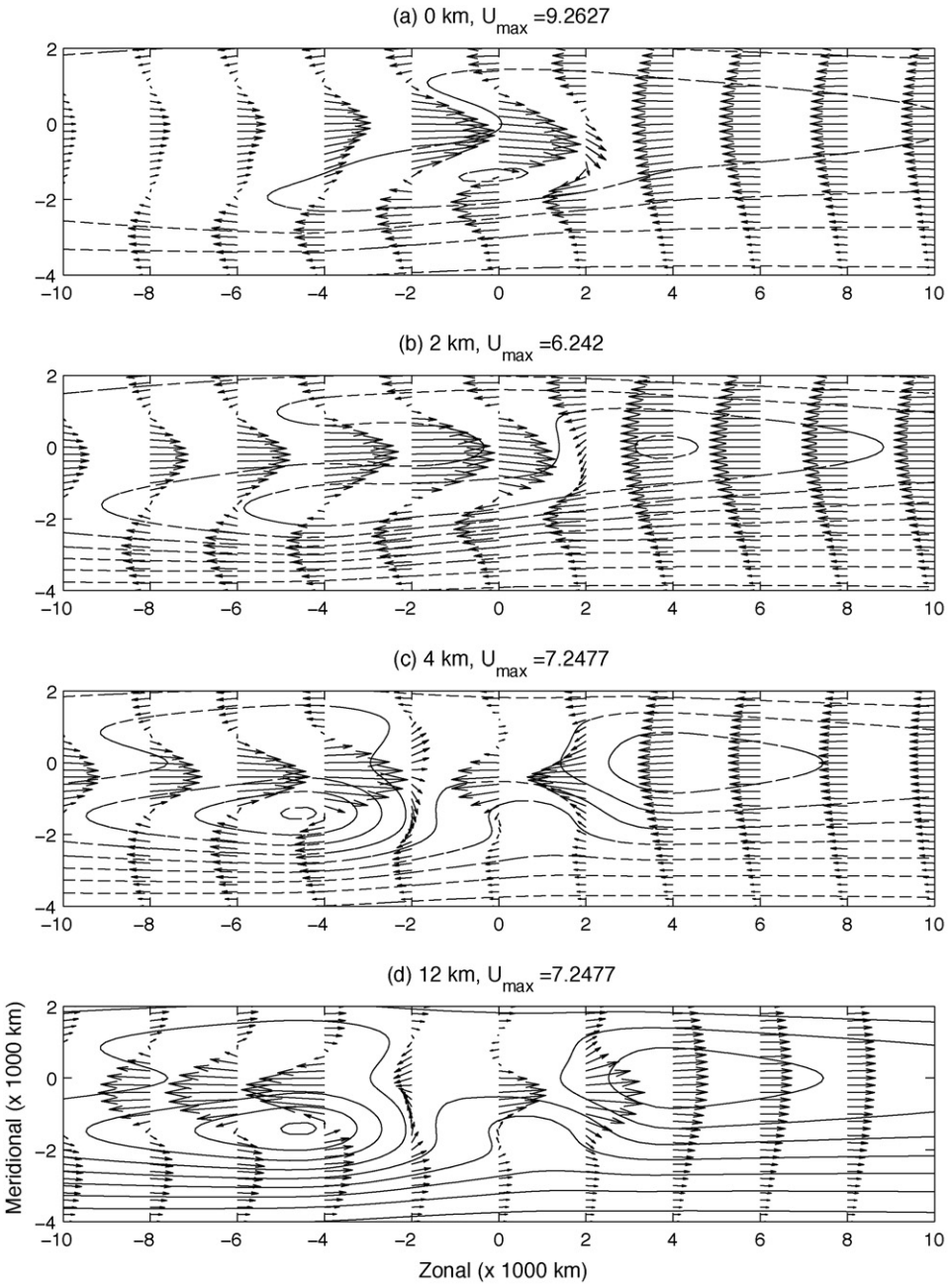

Fig. 4. Compare with Fig. 3, the horizontal velocity field at various heights for the canonical 450 km S MJO model.

A natural picture of the synoptic scale heating fluctuations has the superclusters in the western portion and the lower troposphere congestus heating in the eastern portion of the convective envelope meridionally tilted in opposite directions. In particular, congestus cloud decks are observed to move from east to west (Lin and Johnson, 1996; Wheeler and Kiladis, 1999) and it is natural that they undergo a backward tilt, i.e. poleward/eastward. The deep convective superclusters travel from west to east and are naturally tilted poleward/westward. In the SEWTG model, a convective envelope with westward tilts in the west and eastward tilts in the east is achieved by linearly interpolating $\gamma(X)$ within the convective envelope:

$$\gamma(X) = -\frac{X}{L_*} \tag{62}$$

in much the same fashion as the congestus/supercluster structure was modulated by a linear interpolant for α in (60) above. For a meridional tilt which is quadratic in latitude, the synoptic scale heating contours look like arrows in the horizontal plane pointing toward the center of the convective activity.

There is no simple closed form expression for the upscale fluxes in this example, however, there is now a sharp top/bottom asymmetry in the zonal momentum forcing. The upscale flux in

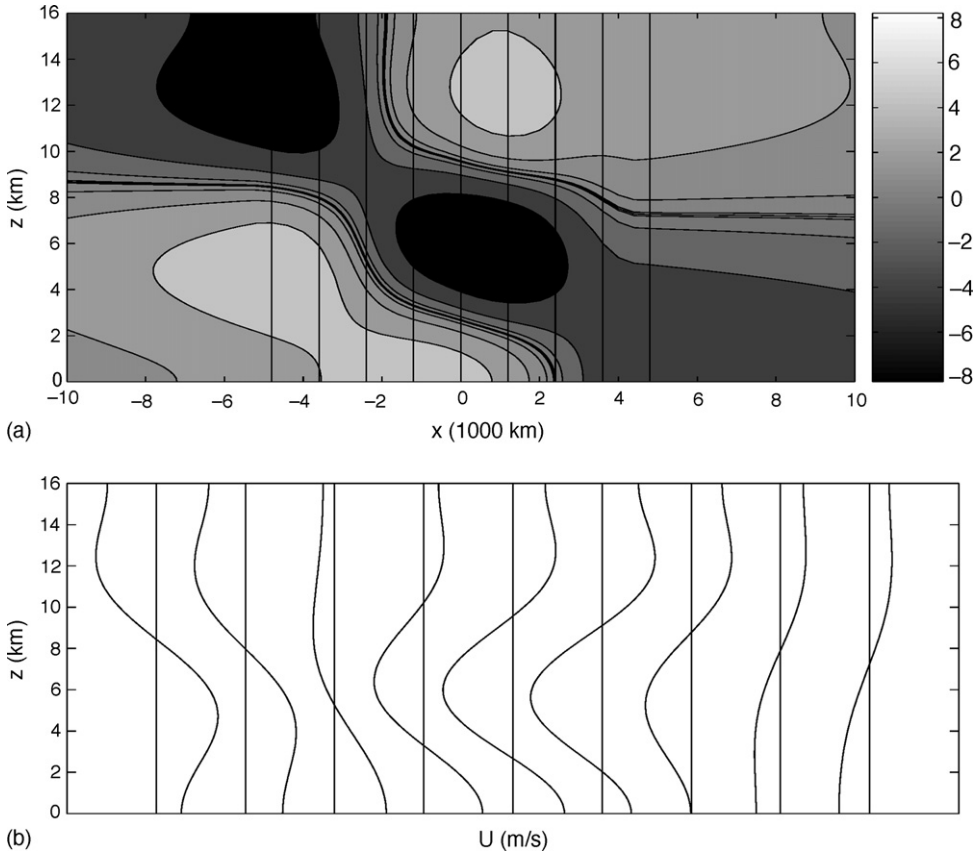

Fig. 5. Zonal velocity above the heating region after saturation without boundary layer drag in the equatorially symmetric congestus/supercluster model of the MJO. The flow is very similar for heating centered at 450 km south.

the center of the supercluster portion of the convective envelope is shown in Fig. 6 whereas that in the congestus portion is shown in Fig. 7. The momentum forcing in the supercluster region is qualitatively similar to the canonical model except for strong westerlies being driven at the top of the troposphere. On the other hand, the momentum forcing in the congestus convection region is

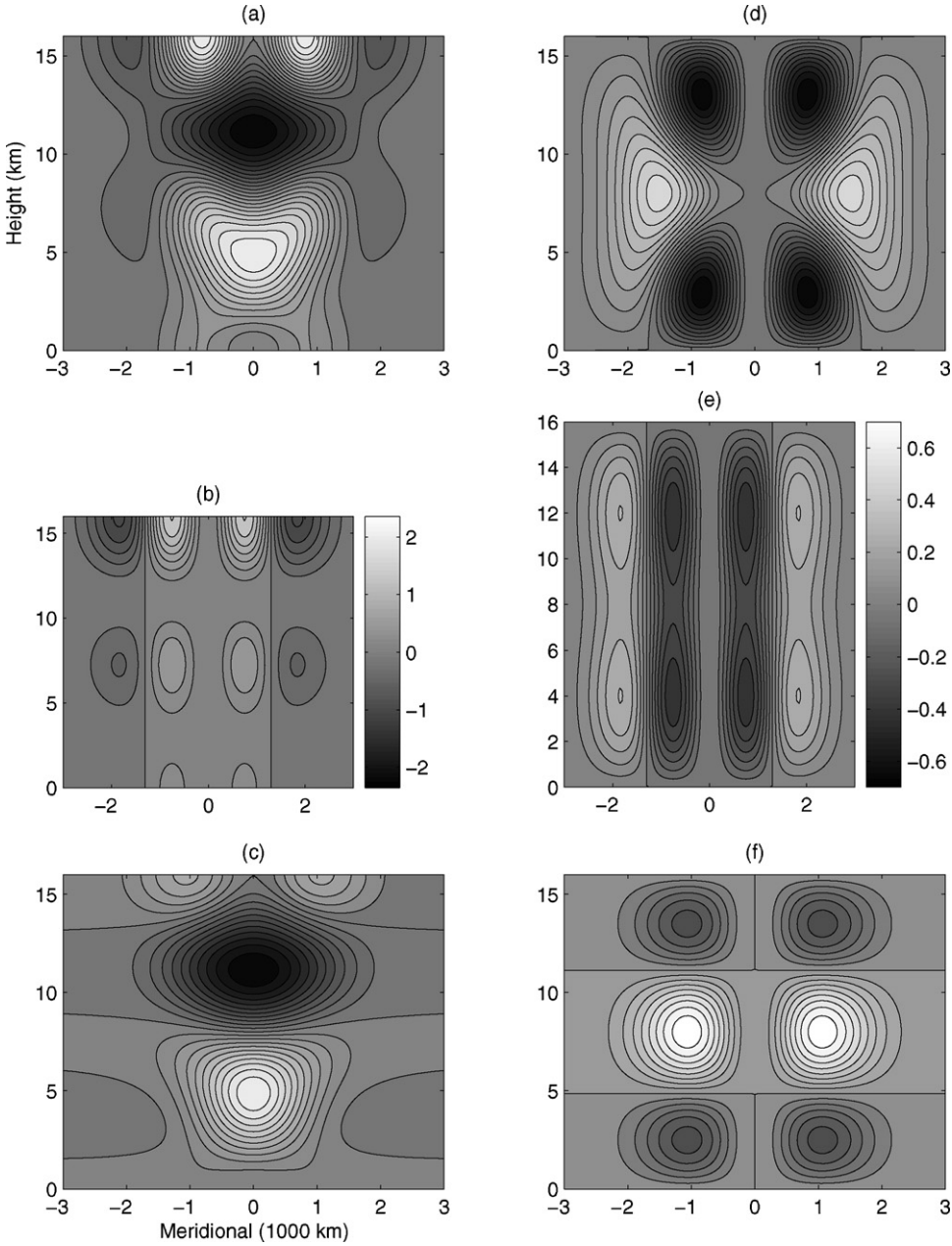

Fig. 6. The eddy flux convergences as a function of latitude and height in the troposphere for equatorially symmetric heating with quadratic tilt in the supercluster portion of the convective envelope.

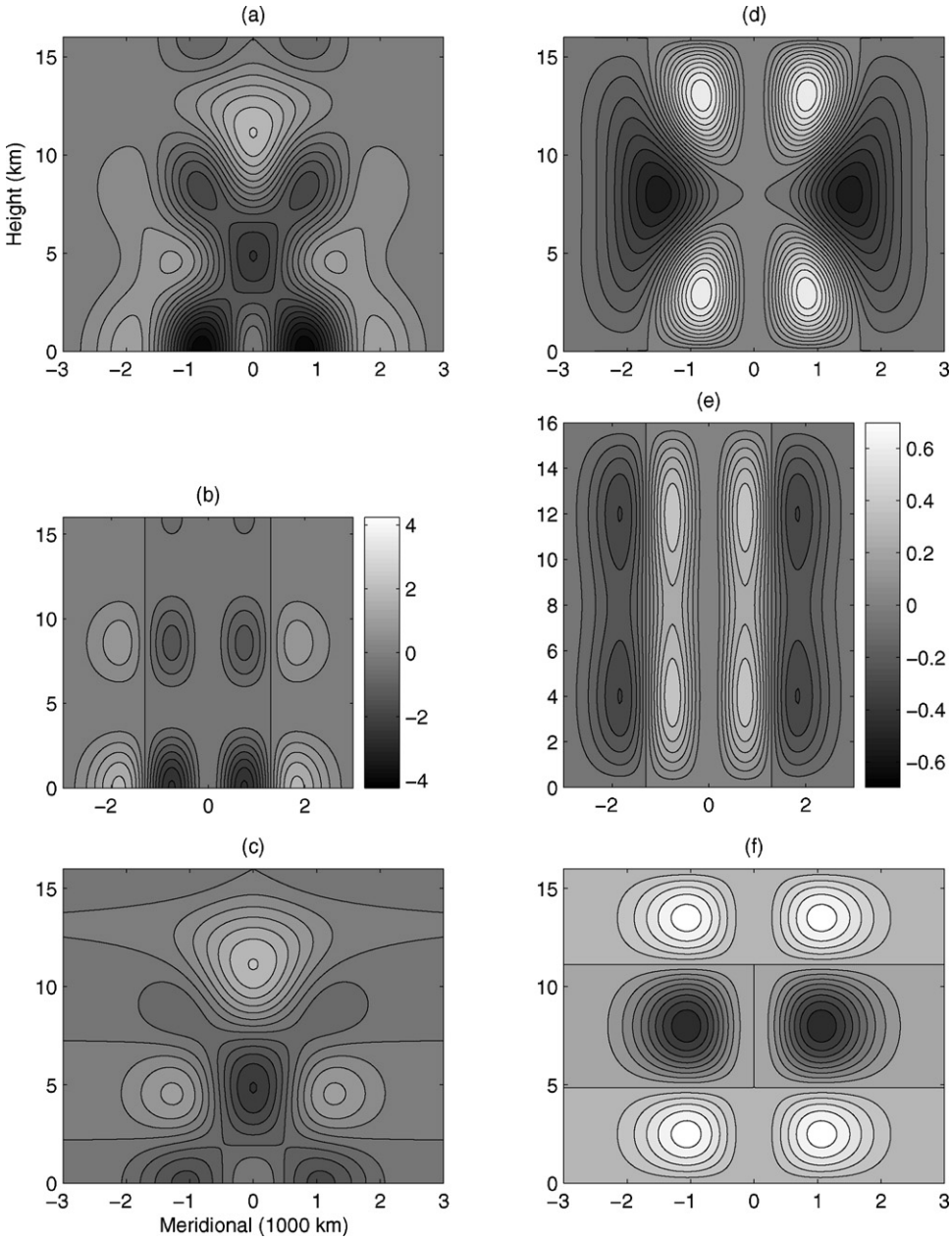

Fig. 7. The eddy flux convergences as a function of latitude and height in the troposphere for equatorially symmetric heating with quadratic tilt in the congestus portion of the convective envelope.

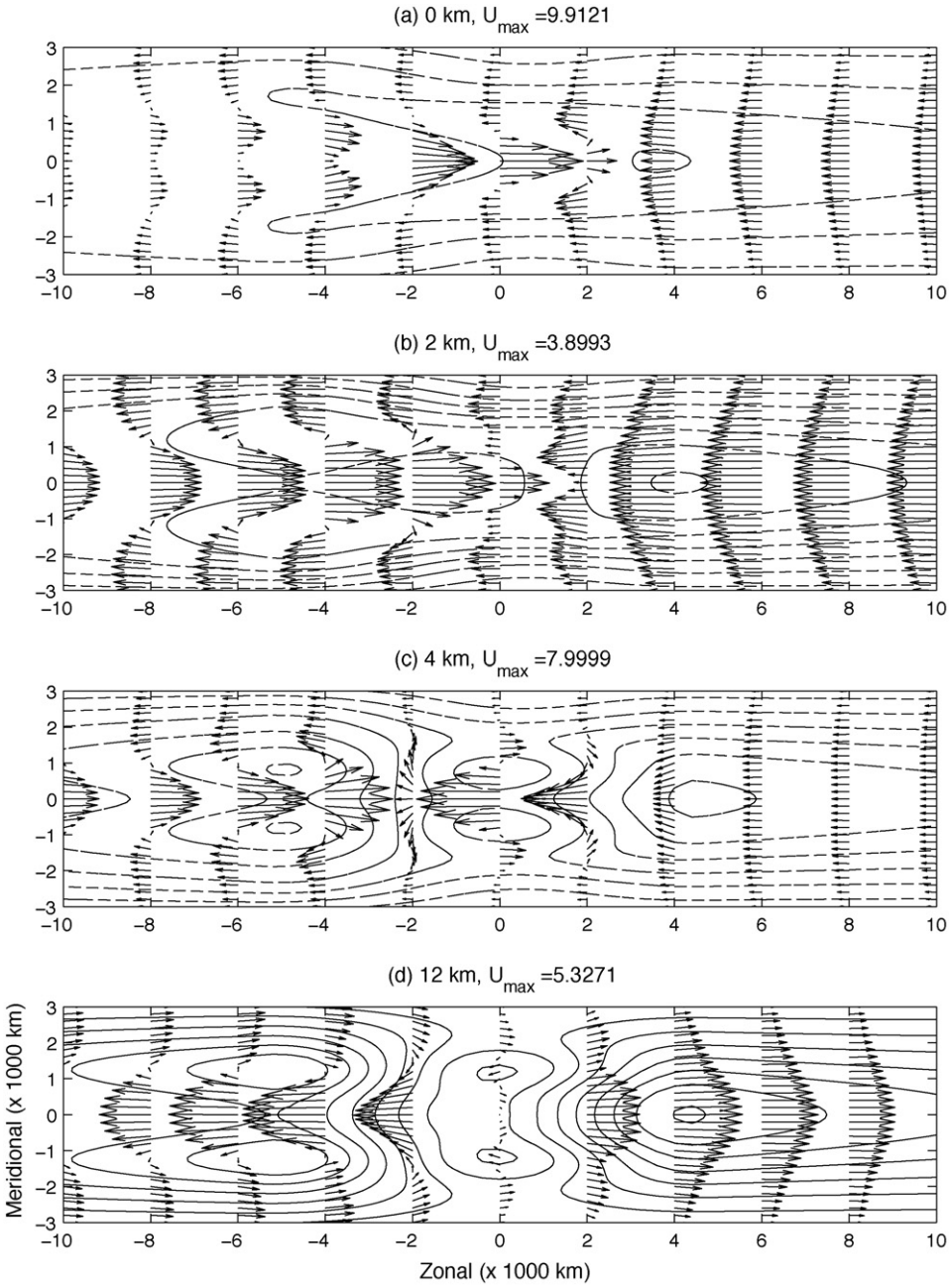

Fig. 8. Compare with Fig. 3, the horizontal velocity field at various heights for the meridionally tilted, equatorial symmetric MJO model.

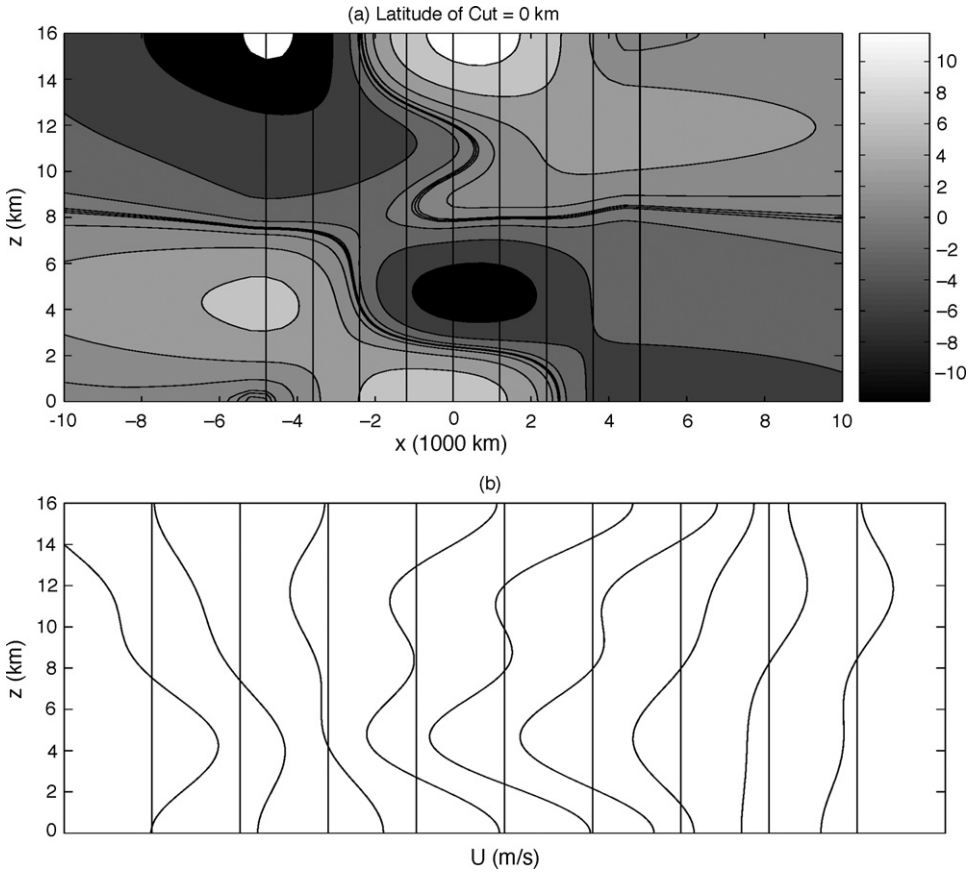

Fig. 9. Zonal velocity over equator for the meridionally tilted, equatorial symmetric MJO model.

significantly different than in the canonical example. In particular, there is strong easterly forcing down to the base of the troposphere and away from the equator; this is the primary consequence of the meridional flux of zonal momentum.

The resultant planetary scale flows, shown in Fig. 8, have zonal winds which are more equatorially confined at the base of the troposphere, with maximum zonal flows which are 50% stronger than the canonical example shown in Fig. 3. At higher levels, the flow remains much the same, the trailing Rossby gyres being slightly broader meridionally in the present example, and the maximum zonal flow weakens at 2 and 12 km and strengthens at 4 km heights. Fig. 9 shows that the westerlies above the equator are very sharply tilted westward with height. This is in stark contrast to the gradual upward/westward tilt of the canonical equatorial MJO in Fig. 3. We conclude that symmetric meridional tilts can sharply confine the wind burst near the equator, amplify its intensity and significantly change its vertical structure.

4.2. Meridional momentum flux due to constant meridional tilts

As discussed in Section 3.2 a meridional/zonal tilt in either of the synoptic scale heating modes generates a meridional component of the momentum flux convergence and thereby drives

barotropic and the even vertical baroclinic modes on planetary scales. In this section we consider the effect of phases which are linear functions of the meridional coordinate, y, so that the resultant momentum flux convergence acquires an antisymmetric component about the equator. In particular the phase is given by

$$\phi_i = \gamma y + \phi_{0,i} \tag{63}$$

where γ_i measure the slope of the meridional/zonal tilt of the heating fluctuations. For $\gamma_i < 0$ the tilt is Southwest to Northeast (SW/NE) whereas for $\gamma_i > 0$ the tilt is Northwest to Southeast (NW/SE) and a constant phase lag exists between first and second baroclinic modes, $\phi_{0,i}$. For the examples in this section, the tilts of the first and second baroclinic modes are the same:

$$\gamma_i = -0.25 \tag{64}$$

Therefore, there is a relatively strong $x : y = 4 : 1$ meridional tilt.

Though the same meridional tilt for congestus convection and superclusters may not be a likely scenario in the real atmosphere, the use of such a simple tilt allows us to identify the novel aspects of the momentum flux convergence which arise from meridional tilt. In particular, the momentum flux convergence is no longer of opposite signs in the congestus portion of the heating as compared to the supercluster portion. Rather, the momentum flux convergence has vertical top/bottom of troposphere symmetry between the supercluster and congestus heating regions.

4.2.1. Equatorial centered heating with SW/NE tilt

The flux convergences in the supercluster portion of the heating region associated with the heating profiles centered at the equator with vertical and SW/NE meridional tilt are shown in Fig. 10. Due to the symmetries of the flux convergences in this model, in the congestus portion of the heating region the momentum flux convergence is exactly flip symmetric with respect to the middle of the troposphere (as discussed above) whereas the temperature flux convergence changes sign everywhere (positive/negative symmetric, as in the canonical MJO models). The result is that there is absolutely no difference in the temperature flux convergence profiles in the entire heating region as compared to the canonical MJO model since it can only change if there is a difference in the meridional tilts of the first and second baroclinic synoptic scale fluctuating heating. However, due to the meridional component of the momentum flux convergence, the total momentum flux convergence is moderately changed near the base of the troposphere in the supercluster model, but is dramatically changed there in the congestus model. In both the congestus and supercluster portion of the convection, there is a region of westerly forcing at the base of the troposphere at about 500 km south of the equator. Clearly, if the meridional tilts had been in the opposite direction, NW/SE, the center of the momentum forcing would be north of the equator.

The planetary scale flow for the tilted equatorial MJO model is shown in Fig. 11. The zonal winds at the base of the troposphere are much stronger than in the canonical model and their maximum occurs at 500 km south of the equator. There is an asymmetry in the pressure contours in the trailing Rossby waves which reverses its latitude at higher altitudes; this corresponds to a northward bend in the winds and pressure in the middle troposphere. A contour plot of the zonal momentum above the equator (the center of heating) is shown in Fig. 12 and the same contours are shown above 500 km south (the location of the maximum of the wind burst at the base of the troposphere) in Fig. 13. An upward/westward tilt in the zonal flow is clear in Fig. 12, which is also a characteristic of the observations and of the canonical MJO model. However, the structure of the tilt is quite different above the maximum of the wind burst (Fig. 13). In fact, the westerly wind burst enters sharply as a "bullet" near the base of the troposphere, with a sharp westward vertical

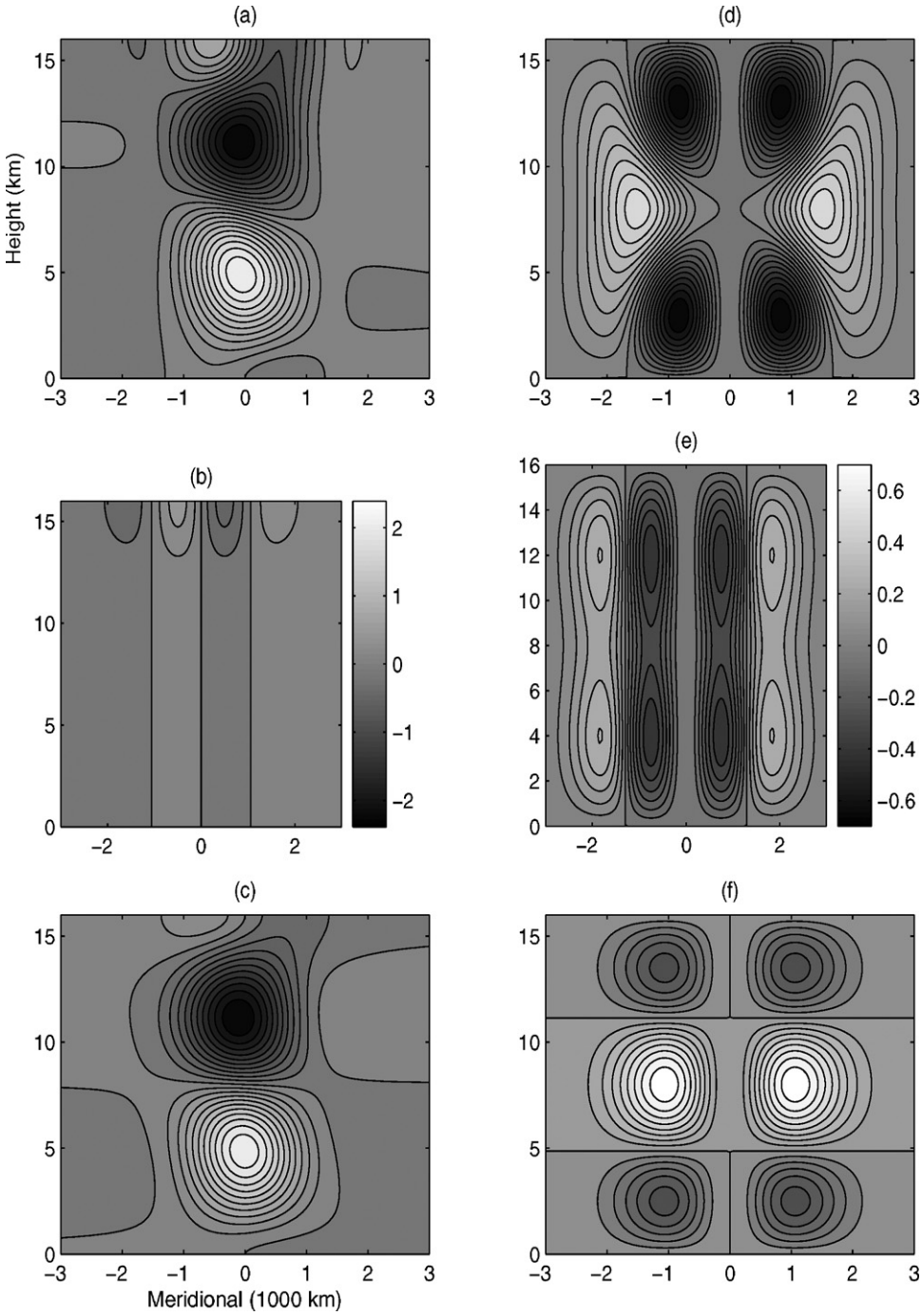

Fig. 10. Upscale momentum and thermal flux convergences along with their vertical and meridional components for the vertically/meridionally tilted synoptic scale equatorial supercluster model. In the congestus portion of the heating region, each component of the momentum flux convergence is simply flipped about the middle height of the troposphere whereas the temperature flux convergence is everywhere the negative of its value in the supercluster region.

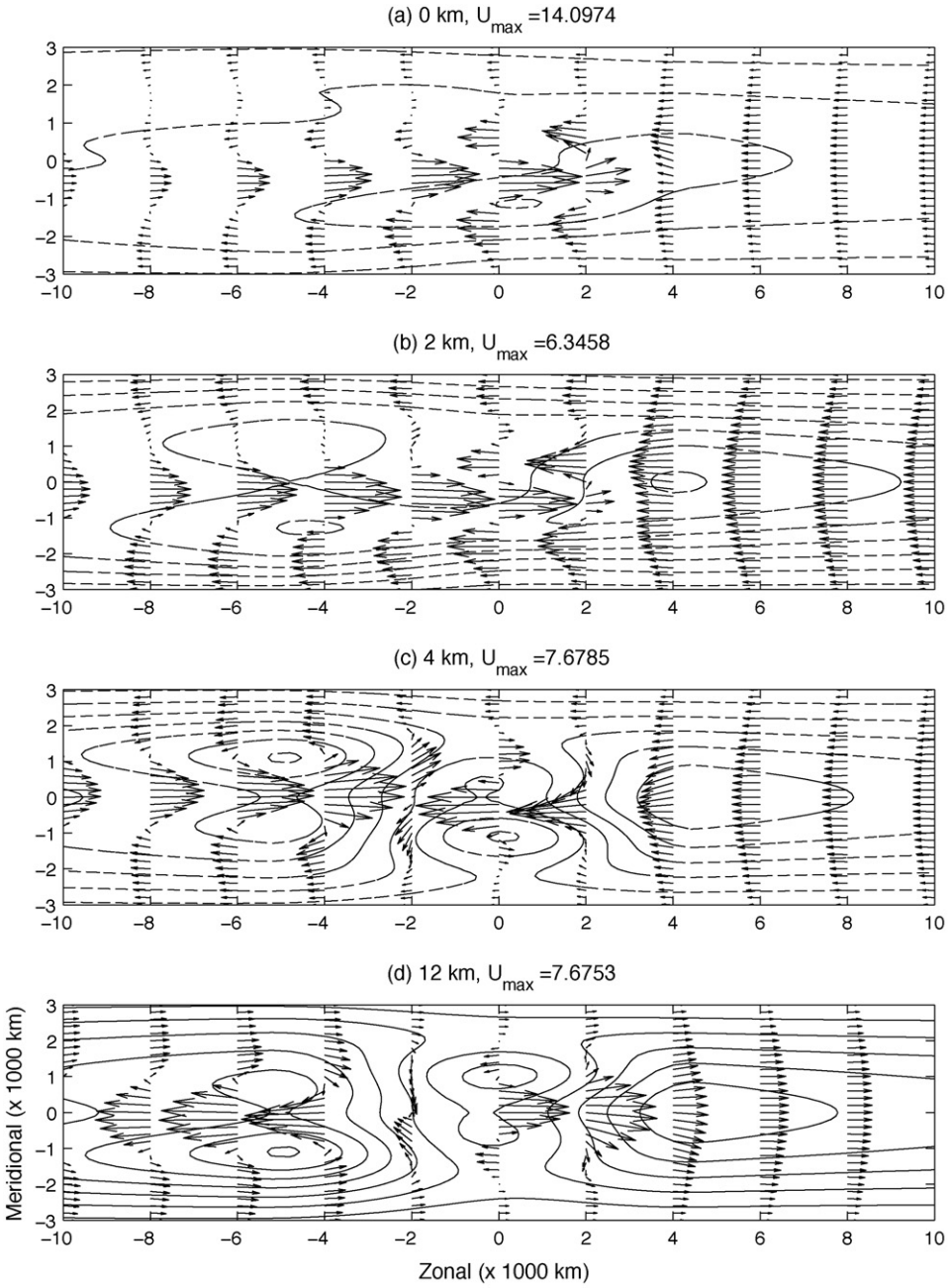

Fig. 11. Compare with Fig. 3, the horizontal velocity field at various heights for the SW/NE tilted, equatorial symmetric MJO model.

lag above. These results are not inconsistent with observations, since the latter either observe above one station near the equator (Johnson and Lin, 1997), report composite data (Maloney and Hartmann, 1998) or data which is meridionally averaged near the equator.

4.2.2. Heating centered at 450 km south with SW/NE tilt

The flux convergences in the supercluster portion of the heating region associated with the heating profiles centered at 450 km south with vertical and SW/NE meridional tilt are shown in Fig. 14. As in the equatorially centered example, the symmetries of the synoptic scale heating profile imply that the momentum flux convergence is exactly flip symmetric with respect to the middle of the troposphere, whereas the temperature flux convergence changes sign everywhere in the congestus portion as compared to the supercluster portion of the heating region. Again, the meridional momentum flux is the dominant new feature in these examples, shifting the westerly maximum of the momentum flux convergence southward over the supercluster region and driving westerlies in the congestus region at the base of the troposphere.

The zonal winds are again much greater at the base of the troposphere, reaching 20 m/s and their maximum occurs at about 700 km south of the equator. In the resultant planetary

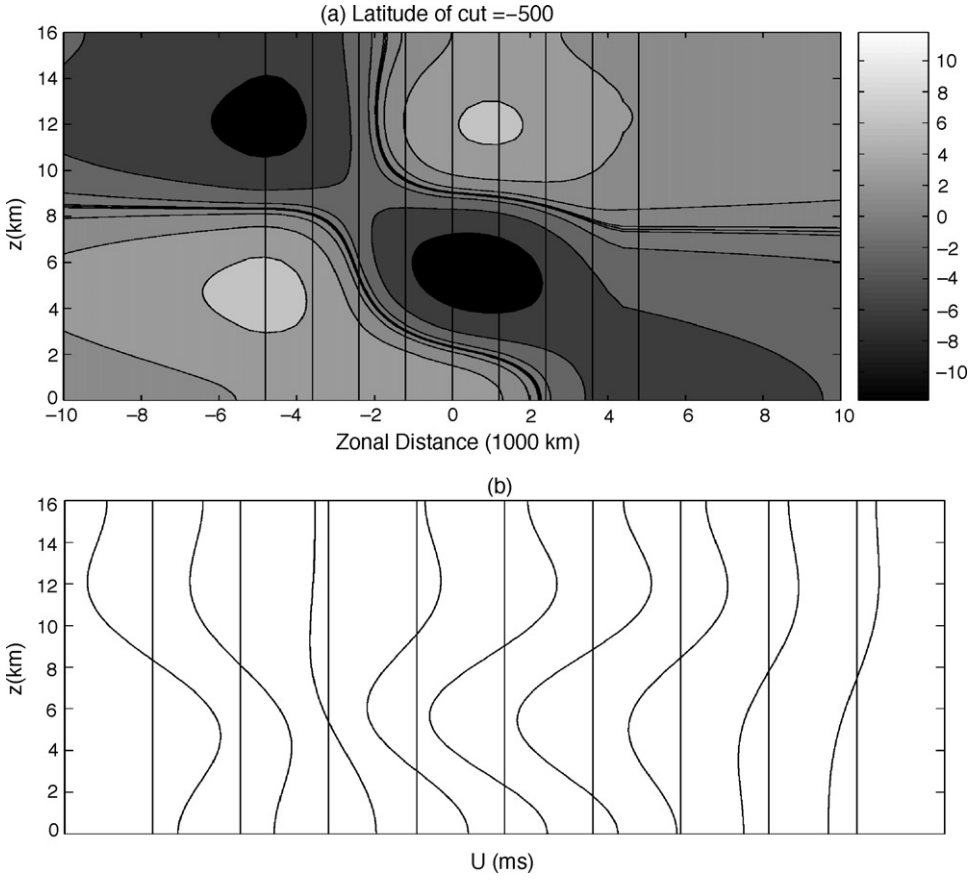

Fig. 12. Zonal velocity over equator for the SW/NE tilted, equatorial symmetric MJO model.

scale flow the westerlies encroach very far forward into the congestus convection region as is evidenced in Figs. 15 and 16. Though most of the features of the canonical MJO example remain, the upward/westward tilt is not pronounced, neither above the center of convection (16), nor above the wind burst maximum (17). Again, in the trailing Rossby gyres, there is a northward bend in both the pressure and zonal velocity in the middle troposphere (Fig. 17).

4.2.3. Heating centered at 450 km south with NW/SE tilt

The flux convergences in the supercluster portion of the heating region associated with the heating profiles centered at 450 km south with vertical and NW/SE meridional tilt are shown in figure are shown in Fig. 18. Again, the congestus region has a momentum flux convergence which is flip symmetric about the midplane and a temperature flux convergence which is negative compared with the flux convergences in the supercluster portion of the heating region. Since the meridional tilt is opposite that of the previous cases, it is clear that now the maximum of the westerly momentum flux convergence at the base of the troposphere shifts northward both in the supercluster and the congestus portion of the convective envelope.

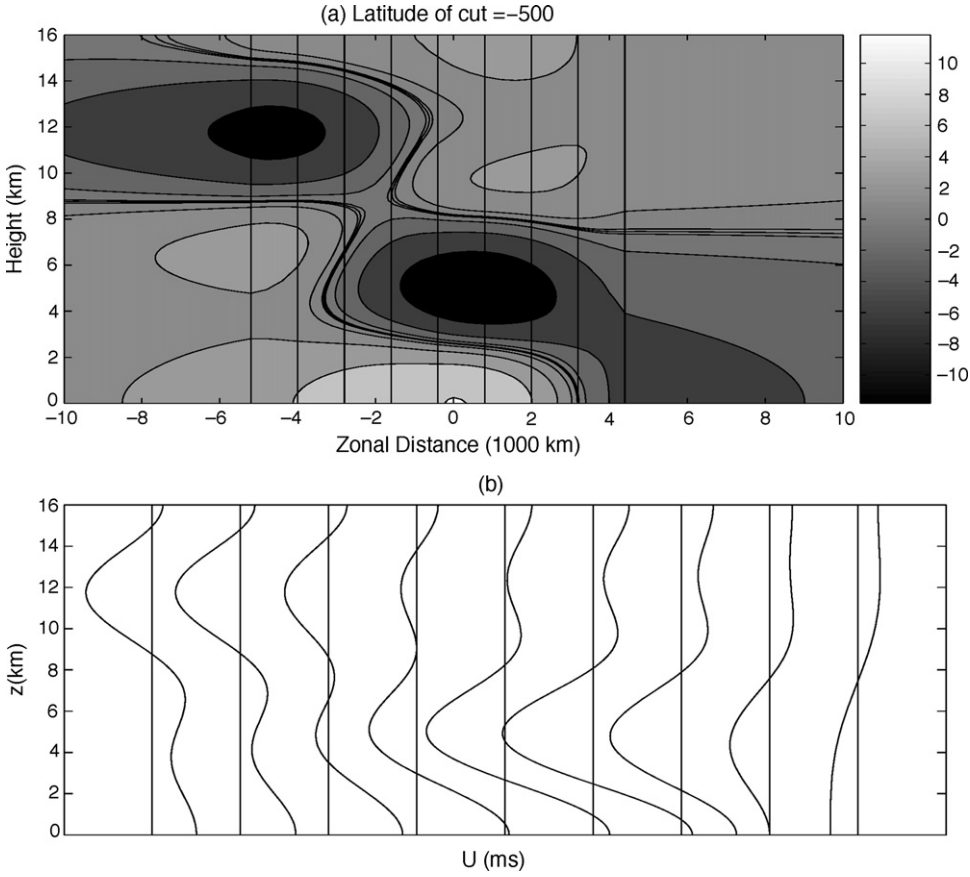

Fig. 13. Zonal velocity over 500 km south (the location of the wind burst maximum) for the SW/NE tilted, equatorial symmetric MJO model.

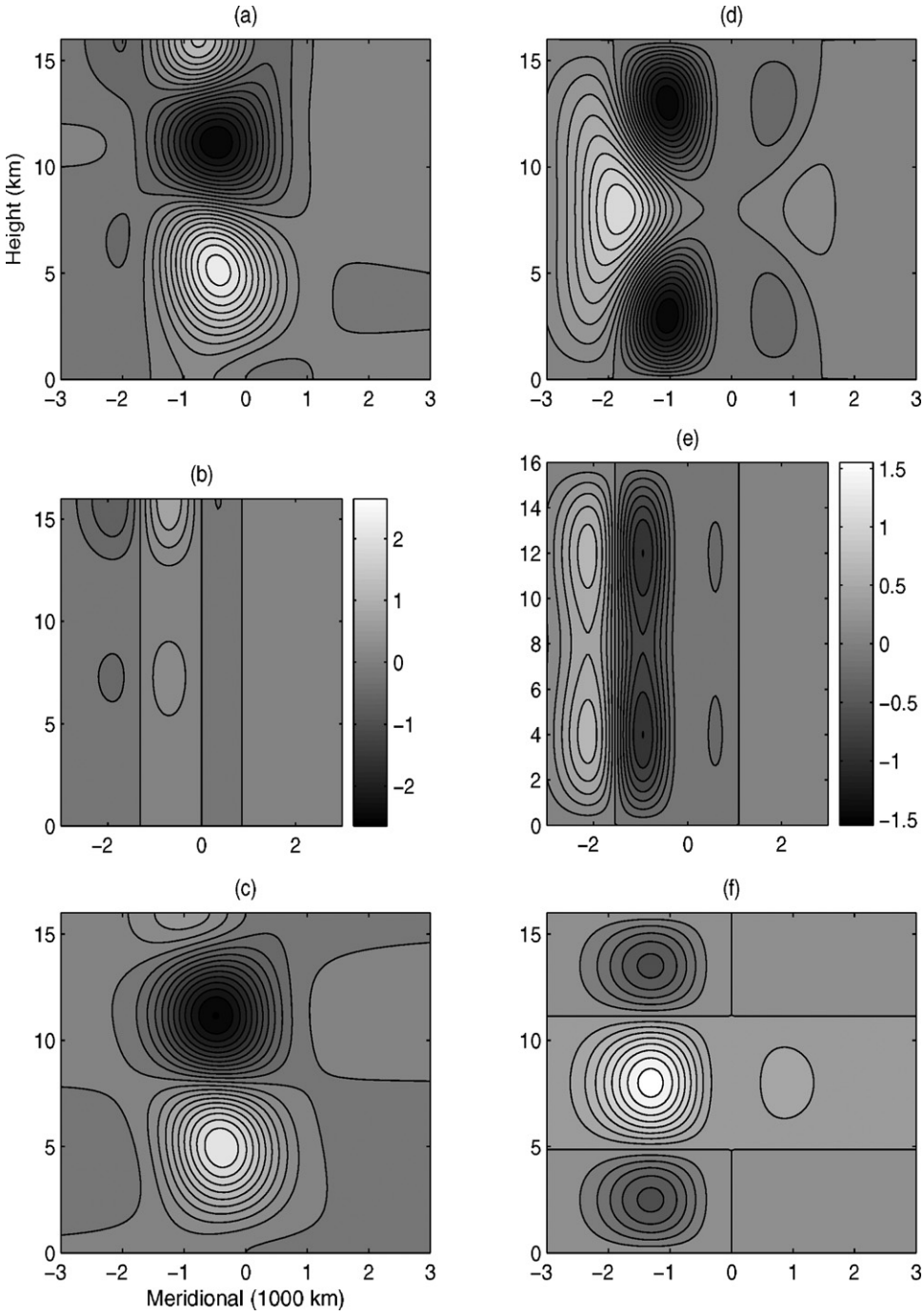

Fig. 14. Upscale momentum and thermal flux convergences along with their vertical and meridional components for the vertically/meridionally tilted, synoptic scale, 450 km S, SW/NE supercluster model. In the congestus portion of the heating region, each component of the momentum flux convergence is simply flipped about the middle height of the troposphere whereas the temperature flux convergence is everywhere the negative of its value in the supercluster region.

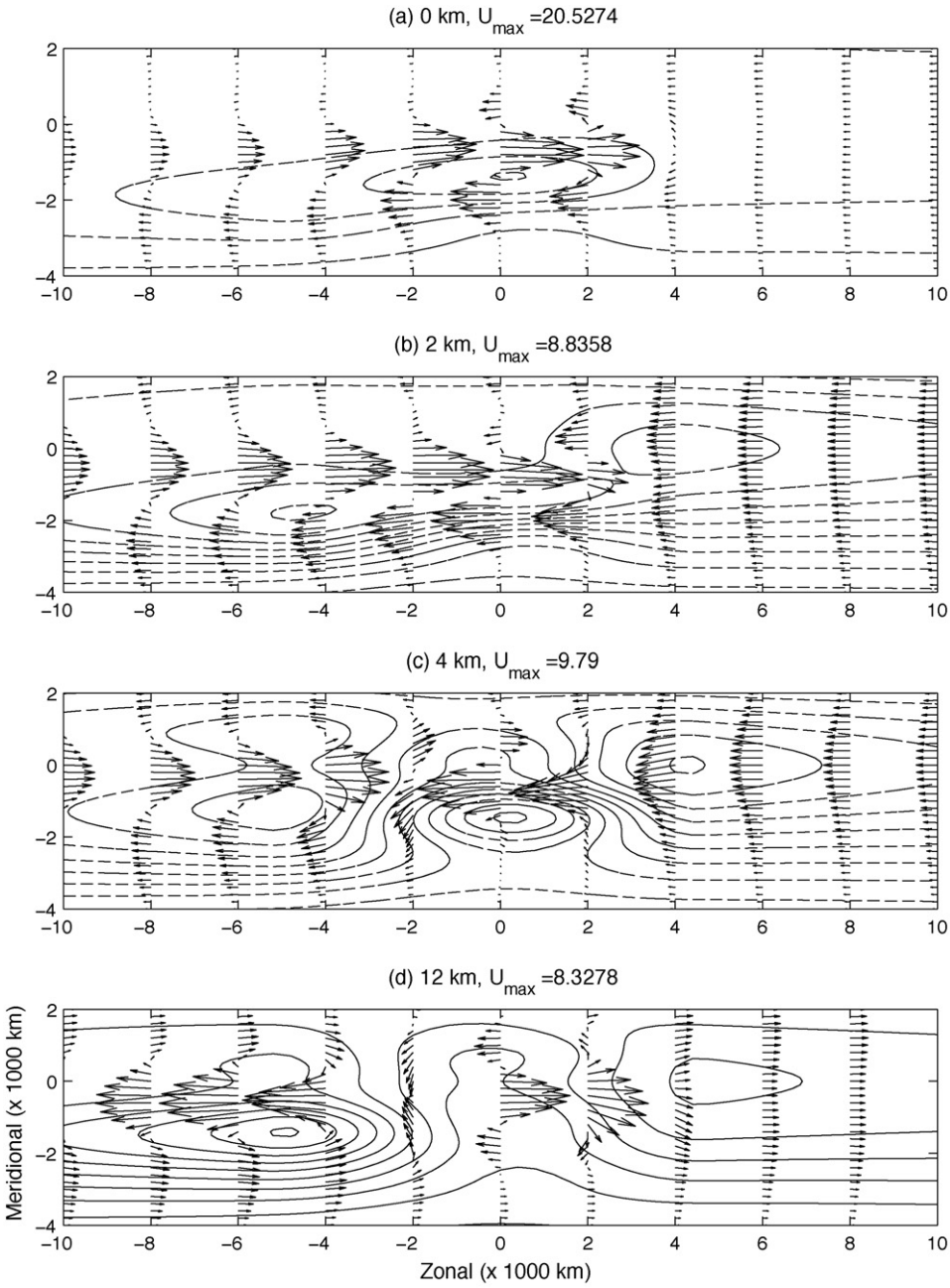

Fig. 15. Compare with Fig. 4, the horizontal velocity field at various heights for the 450 km S, SW/NE tilted MJO model.

The maximum of the wind burst now occurs at 200 km north of the equator and is weaker than in the previous examples (Fig. 19). In this example, the trailing Rossby gyre bends southward in the middle troposphere. The westerlies above the wind burst maximum (200 km in Fig. 20) still do not have a pronounced tilt, but rather have the same "bullet" structure as before. South of the maximum wind burst, at the maximum of the heating, there is a very distinct tilt in the profile of the westerlies which is more characteristic of the canonical MJO example and the MJO data (Fig. 21).

We can therefore conclude some general principles from these four examples. First, SW/NE tilts tend to move the maximum of the wind burst southward whereas NW/SE tilts tend to move the maximum northward. Secondly, there is a southward tilt in the middle troposphere in the trailing Rossby gyres in the SW/NE tilted examples and a northward tilt in the NW/SE case. Thirdly, the $(x : y) = (4 : 1)$ tilt used in these examples result in much stronger winds at the base of the troposphere. Fourthly, heating with meridional synoptic scale tilts tends to generate planetary scale westerlies with dramatically different upward/westward tilts than were seen in the canonical MJO examples. The zonal winds seem to encroach sharply in the lower few kilometers of the troposphere and then more gradually at about 4–6 km. However, the gradual tilt characteristic of

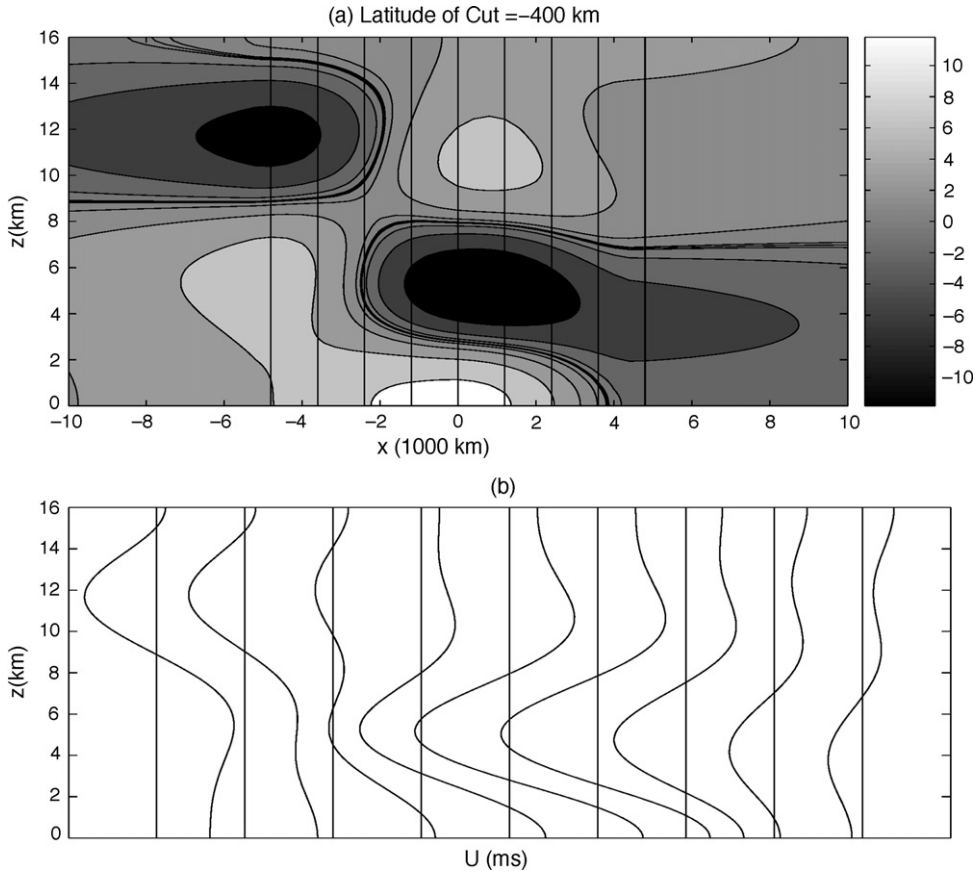

Fig. 16. Zonal velocity over 400 km south for the 450 km S, SW/NE tilted MJO model.

the canonical MJO model does persist south of the maximum of the wind burst. In conjunction with observations, these results can be used to constrain the amount of meridional tilt associated with the convection which gives rise to a reasonable MJO.

4.3. Synoptic scale heating fluctuations without vertical tilts: the effect of meridional tilts alone

The previous models all considered the effect of meridional tilts as an addition to vertical tilts: the question can be asked, what of meridional tilts, alone? Moncrieff (2004) has invoked meridional tilts as the dominant mechanism to explain the MJO planetary structure and this hypothesis can be tested in a straightforward fashion using the IPESD theory.

A plausible model retains the mean heating profile, $\bar{S}_\theta$ as in Eqs. (55) and (60) which accounts for lower troposphere congestus heating in the east of a moving convective envelope and upper troposphere heating from deep convection in the west of the envelope. The synoptic scale fluctuations considered thus far invoke some vertical tilt in the congestus convection region which causes, among other things, a net upward transport of westward zonal momentum (the negative of

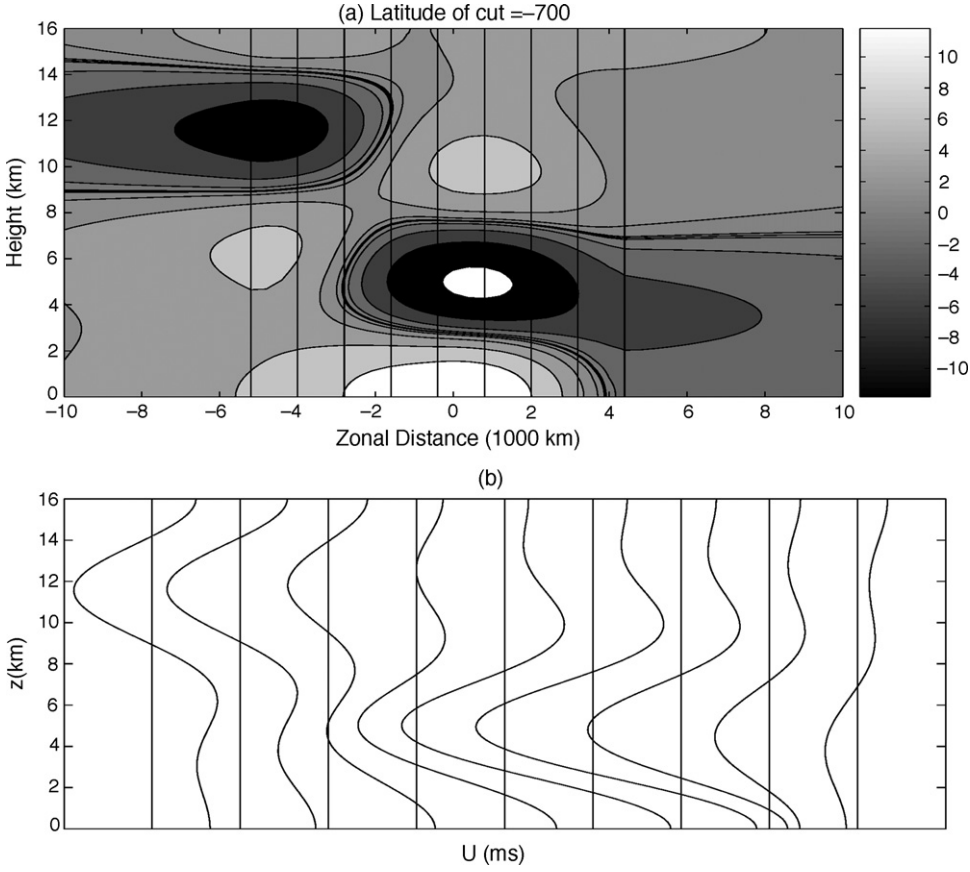

Fig. 17. Zonal velocity over 700 km south (the location of the wind burst maximum) for the 450 km S, SW/NE tilted MJO model.

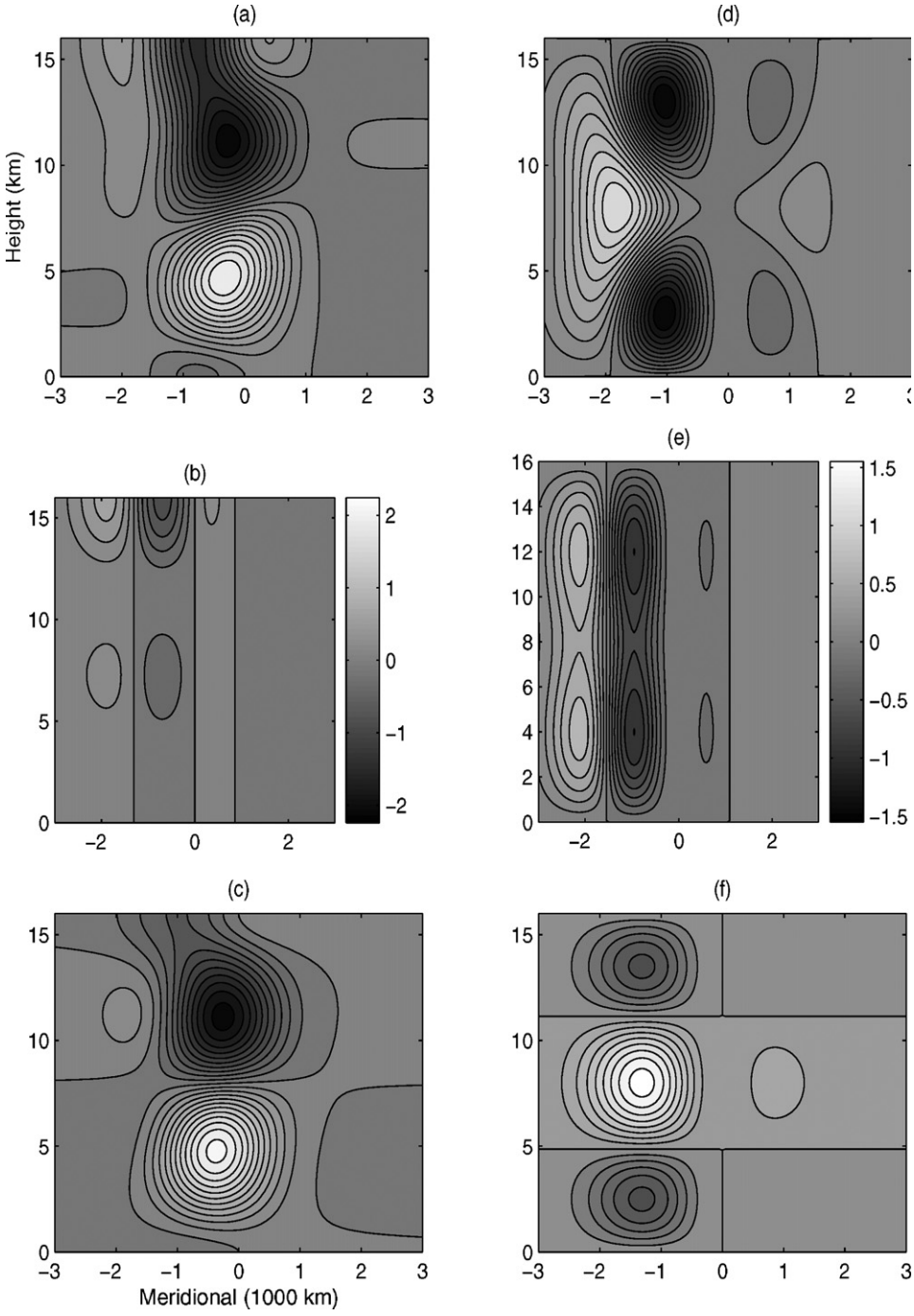

Fig. 18. Upscale momentum and thermal flux convergences along with their vertical and meridional components for the vertically/meridionally tilted, synoptic scale, 450 km S, NW/SE supercluster model. In the congestus portion of the heating region, each component of the momentum flux convergence is simply flipped about the middle height of the troposphere whereas the temperature flux convergence is everywhere the negative of its value in the supercluster region.

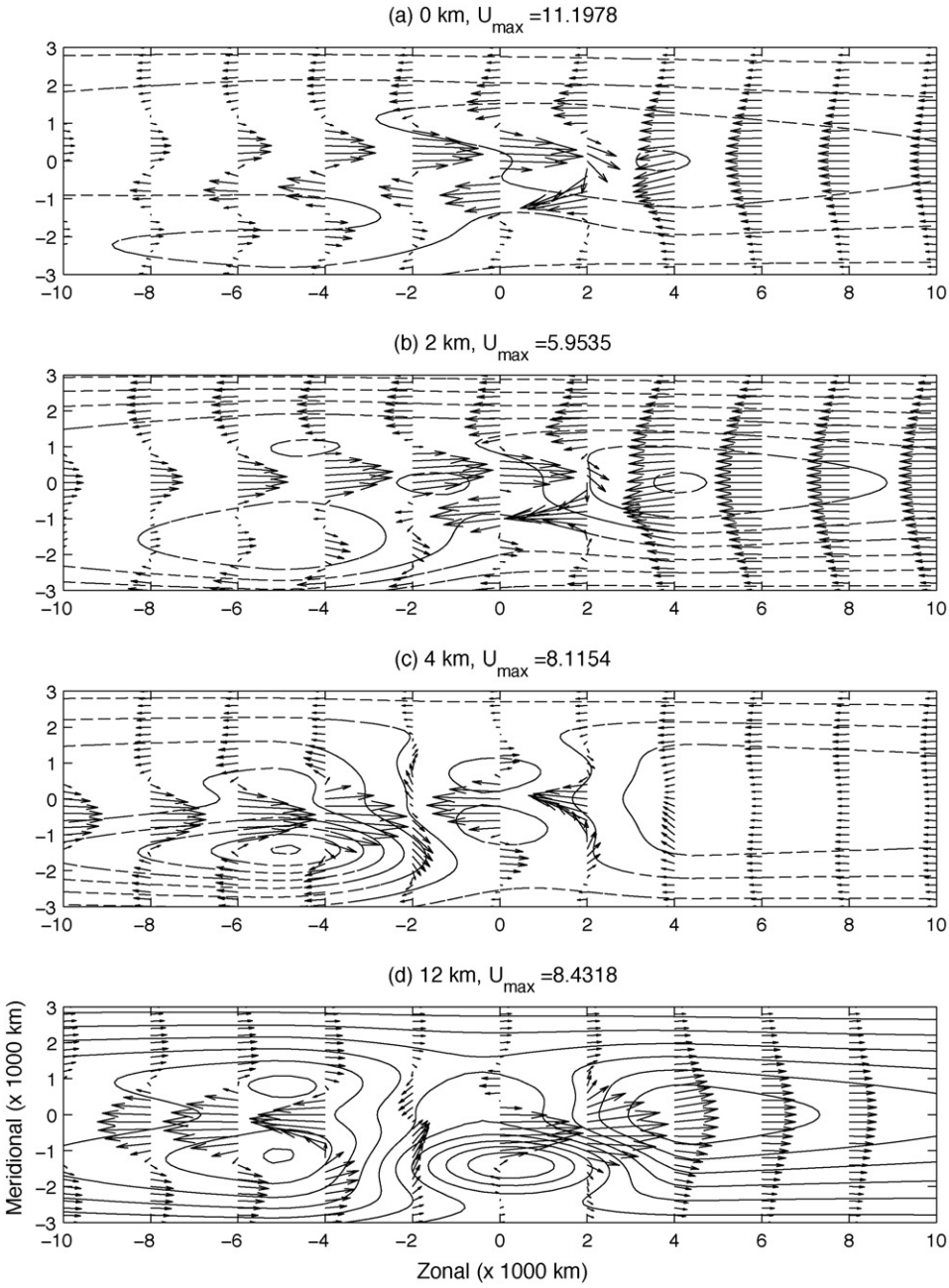

Fig. 19. Compare with Fig. 3, the horizontal velocity field at various heights for the 450 km S, NW/SE tilted MJO model.

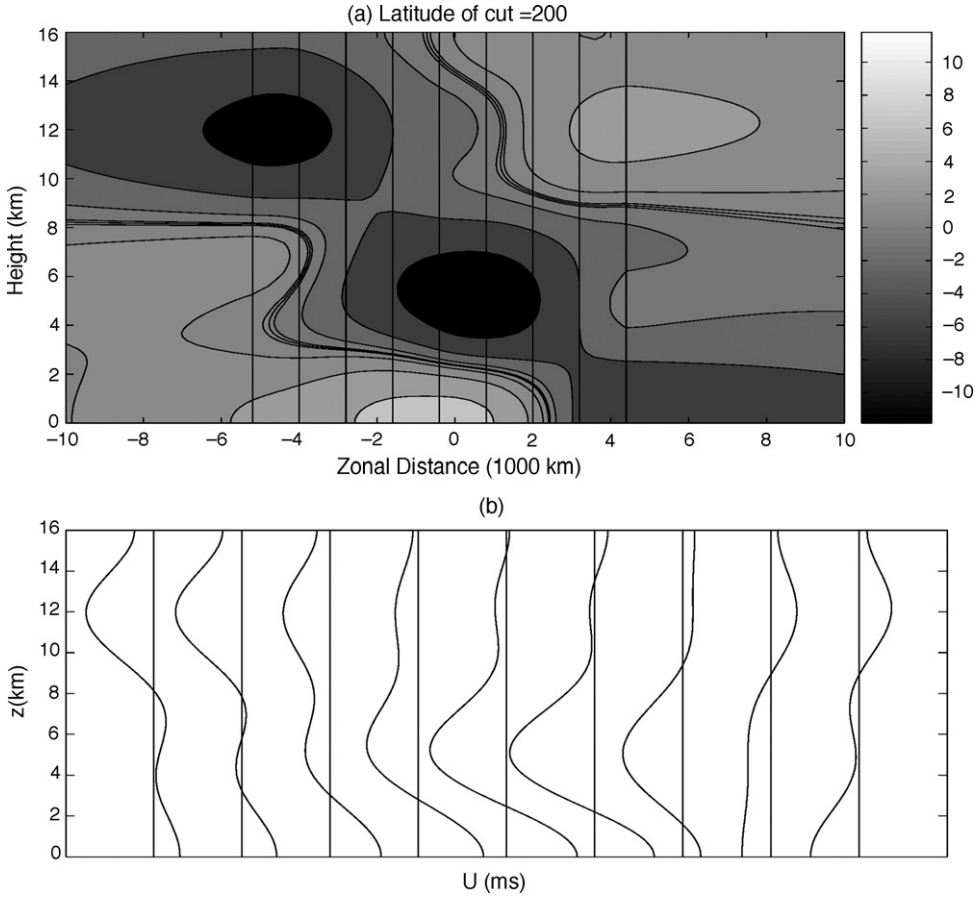

Fig. 20. Zonal velocity above 200 km north (the location of maximum wind burst) in the 450 km S, NW/SE tilted MJO model.

the forcing in Fig. 1). If instead the congestus heating is untilted (vertically, and also meridionally) then, as the formulae in Eqs. (48), (49) and (52) indicate, there can be no upscale fluxes in this region.

On the other hand, Moncrieff (2004) has suggested that the meridional tilt of superclusters produces predominantly meridional fluxes of momentum. A supercluster model consisting of the first and second baroclinic modes and containing meridional tilts produces upscale zonal momentum fluxes which project on the barotropic mode and the first four vertical baroclinic modes and temperature fluxes which project on the first and third baroclinic modes as in Eqs. (48) and (49). As was evidenced by the example in Section 4.1, the forcing profile in such examples can be very complicated, thereby making it difficult to isolate essential aspects of the forcing. Instead, we consider a purely first baroclinic synoptic scale heating fluctuation with symmetric, and westward zonal tilts.

Therefore, the parameters of the model are $H_2(y) = 0$ and $\phi_1(y) = 0.25y^2$, constant as a function of longitude, corresponding to westward/poleward tilted synoptic scale first baroclinic heating. The resultant upscale flux is purely due to momentum flux, no upscale temperature

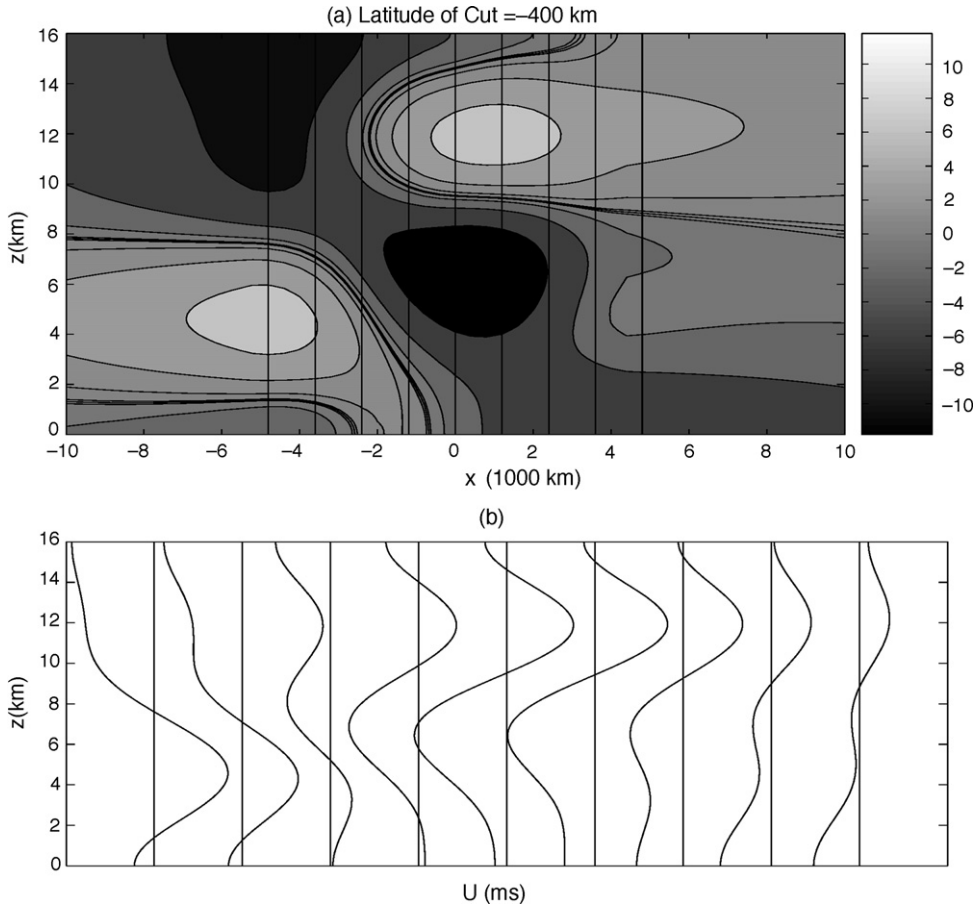

Fig. 21. Zonal velocity above 400 km south in the 450 km south, NW/SE tilted MJO model.

flux, and the self-coupling of the first baroclinic mode drives a barotropic and second baroclinic response on the planetary scales. The forcing as a function of height and longitude is shown in Fig. 22.

The resultant planetary scale flow is shown in Fig. 23 and the vertical profile of the zonal flow in Fig. 24. The flow near the equator has a significant region of westerlies in the lower half troposphere whose leading edge moves westward with height (Fig. 23). However, the maximum westerlies occur at the base of the troposphere, Fig. 24, but nonetheless have the characteristic vertical tilt evident in observations (Lin and Johnson, 1996). The westerly wind burst in the lower troposphere looks more like a split jet west of its leading edge. This splitting can be reduced for less meridional tilt, or for constant tilt as a function of latitude. There are no leading pairs of anticyclones which straddle the heating region, nor are the cyclones there particularly strong. This is a consequence of the lack of tilt in the congestus convection region which is the primary cause of the leading anticyclones (Biello and Majda, 2005). Finally, the outflow in the upper half troposphere (Fig. 23(d)) is much weaker than in Fig. 3 and essentially consists of an easterly wind to the east of the heating region and broad, weaker westerlies, due solely to the mean heating, in the west.

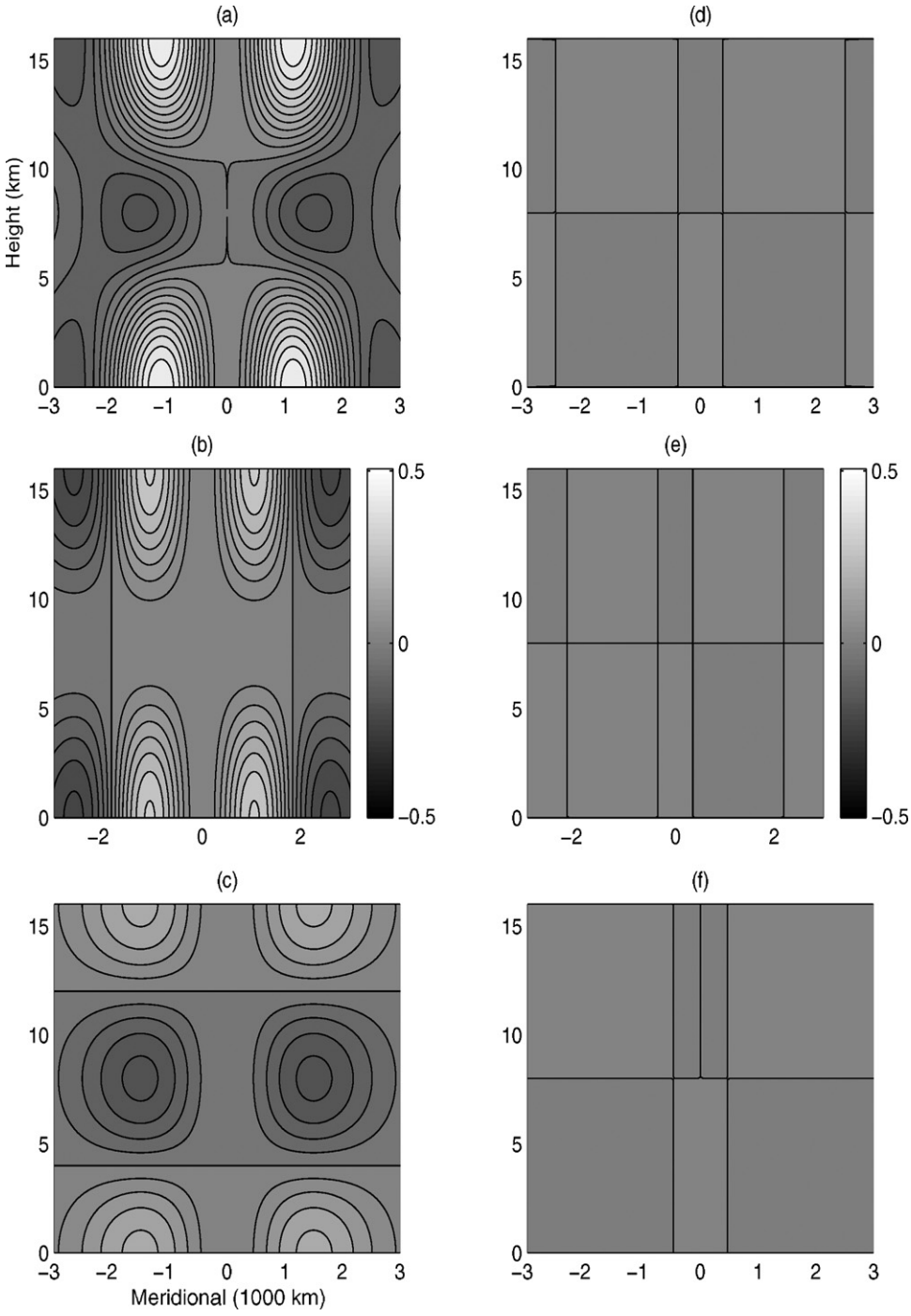

Fig. 22. Upscale momentum and thermal flux convergences along with their vertical and meridional components for the westward meridionally tilted, first baroclinic, synoptic scale heating model. The synoptic scale fluctuations are confined to the western half of the envelope.

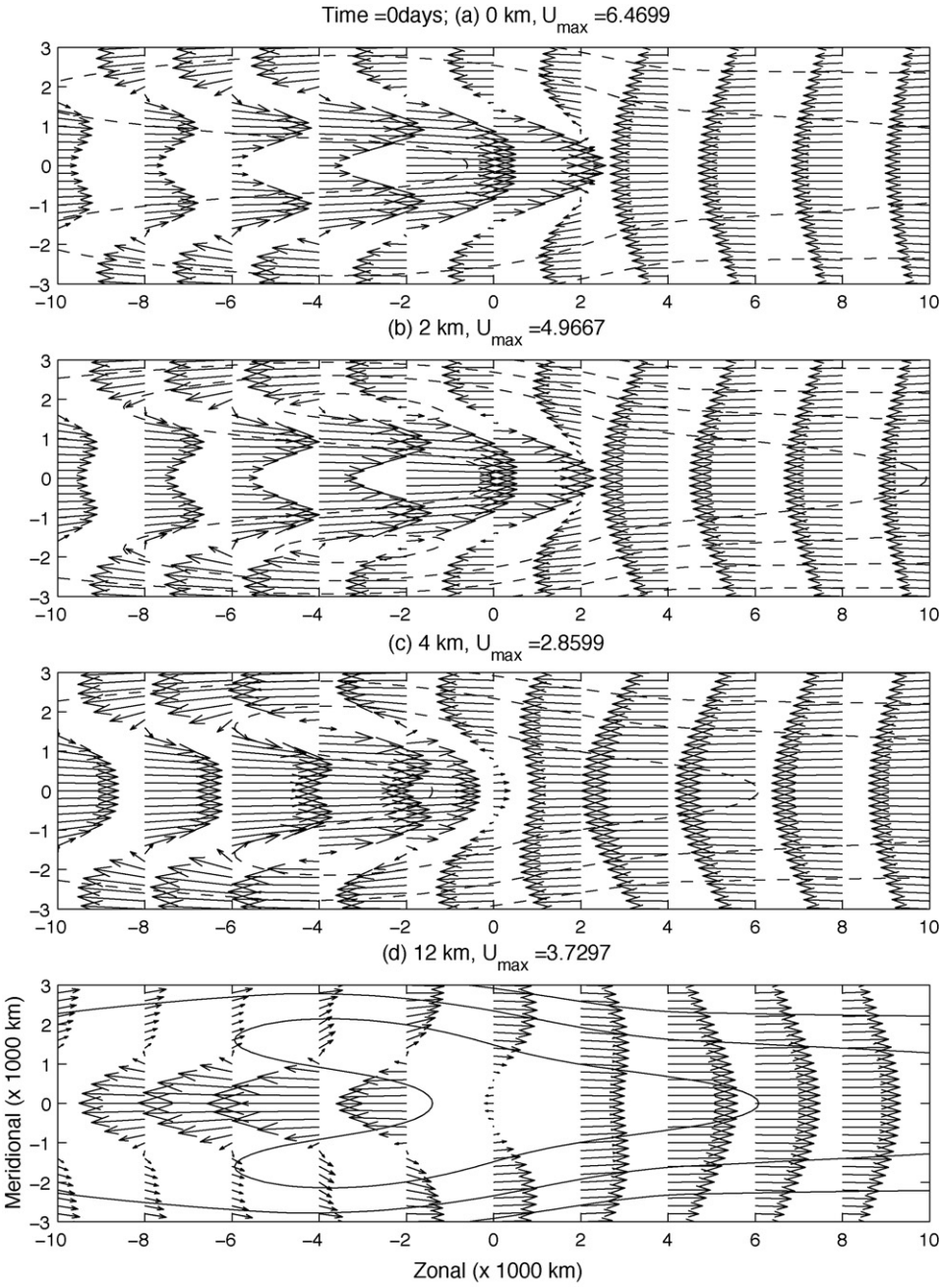

Fig. 23. Compare with Fig. 3, the horizontal velocity field at various heights for the first baroclinic meridional tilt model with mean heating.

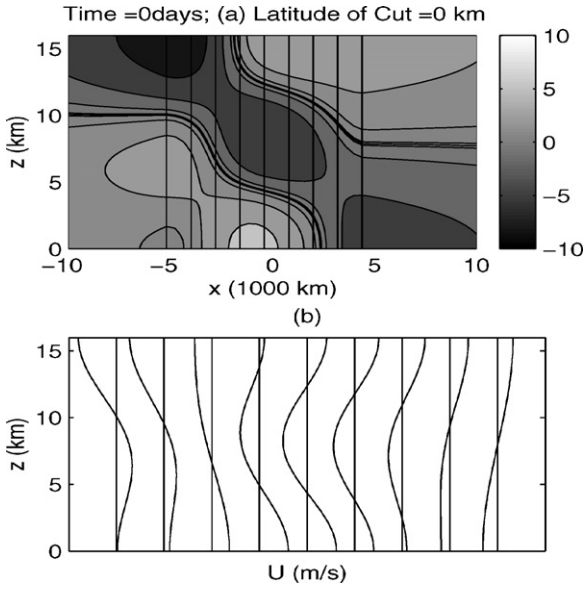

Fig. 24. Zonal velocity above the equator in the first baroclinic meridional tilt model.

Therefore, the meridionally tilted MJO model has some features of the observational record but lacks those essential features that are produced by vertical tilt and upscale transport from congestus convection. Whether a modified model which emphasizes meridional tilts can reproduce the features of the planetary scale observational record remains to be explored.

5. The effect of boundary layer dissipation

Ekman friction is driven by meridional velocity convergence in the boundary layer. Using Eqs. (30) and (41) in the linear boundary layer theory in the absence of forcing, it is straightforward to show that the energy on planetary scales is dissipated according to

$$\frac{\mathrm{d}}{\mathrm{d}t}\int \frac{\bar{U}^2+\bar{\Theta}^2}{2}\,\mathrm{d}x\,\mathrm{d}y\,\mathrm{d}z = -\int [d_0\bar{U}^2+d_\theta\bar{\Theta}^2]\,\mathrm{d}x\,\mathrm{d}y\,\mathrm{d}z - \pi\Delta\,\mathrm{d}\int\left(\frac{y^2}{y^2+d^2}\right)\bar{U}^2\Big|_{z=0}\mathrm{d}x\,\mathrm{d}y \tag{65}$$

The form of the second integral in Eq. (65) has several important consequences for the dissipation of energy. Firstly, it is clear that Ekman dissipation only acts in the presence of flows with non-zero zonal velocity at the base of the troposphere. Thus, the interpretation of Ekman dissipation as a boundary drag term: any flow with vanishing zonal velocity at the base of the free troposphere will not experience Ekman drag. Secondly, the energy dissipation rate per unit area in the horizontal direction is weighted by the y dependent kernel:

$$K(y/d) = \frac{(y/d)^2}{(y/d)^2+1} \tag{66}$$

It is clear that zonal winds near the equator ($|y| < y_d \equiv d$) are not significantly dissipated by Ekman friction; in particular, equatorial zonal winds are not dissipated at all. As discussed in Appendix C.1, for a 1 day boundary layer dissipation time:

$$d = \frac{8.33\,\text{h}}{1\,\text{day}} \approx 0.35 \Longrightarrow y_d \approx 520\,\text{km} \tag{67}$$

which implies that the energy of the flow within about 520 km of the equator are not significantly affected by Ekman friction. Nonetheless, Ekman friction is degenerate (see Biello and Majda, 2004) which can lead to a significant redistribution of energy among various vertical modes, in particular spinning up the barotropic component of the flow.

5.1. Boundary layer dissipation and the MJO models

The following examples consider the effects of linear boundary layer dissipation on the examples that were considered in Biello and Majda (2005). In particular we use the MJO congestus/supercluster heating model which has bottom heavy mean heating to the east and top heavy mean heating to the west which is either equatorially symmetric, or symmetric about 450 km south. The fluctuating component is associated with lower troposphere congestus cloud clusters on the eastern side of the heating region and upper troposphere, westward tilted superclusters on the western side of the heating region. The upscale momentum and temperature fluxes in the supercluster region are shown in Figs. 1 and 2. All of the examples were run using a 0.5 km thick boundary layer and the results are shown after 100 days of integration. The momentum dissipation time is 5 days in the free troposphere and 1 day in the barotropic boundary layer whereas the thermal dissipation time is 15 days.

Figs. 25 and 26 show the planetary scale velocity and pressure contours at four different heights in the troposphere and should be compared with the canonical MJO examples at the two latitudes which can be found in Figs. 3 and 4.

The principal effect of boundary layer friction, as evidenced by comparing Figs. 3 with 25 and Figs. 4 with 26 is to dissipate the flow at the base of the troposphere outside of the heating region. The higher in the troposphere, the weaker the effect of the boundary layer friction. Boundary layer dissipation confines the westerly wind burst to the equatorial region in both the example of equatorially centered heating and of heating at 450 km south (Figs. 25 and 26). In particular the Rossby gyres at the base of the troposphere along with the off-equatorial easterlies leading the heating region are all significantly weakened. The westerly wind burst itself and the easterlies within the congestus convective region along the equator remain strong despite boundary layer friction. These facts are precisely in accord with the interpretation of the energy dissipation given in Eq. (65).

In the example of off-equatorial heating the wind burst is sharply focused at the equator by Ekman friction (Fig. 26). At higher levels in the troposphere the flow is again only weakly affected, however at 2 km heights, it is clear that the easterlies at latitudes of 2000 km south are also much weaker due to boundary layer friction. Fig. 27 shows the effect of boundary layer dissipation on the example of Fig. 8 from Section 4; this example uses synoptic scale heating fluctuations which tilt eastward/poleward in the congestus portion of the convective envelope and westward/poleward in the supercluster portion. Despite the fact that the meridional tilt confined the westerly wind burst near the equator as compared to the canonical MJO model, the boundary layer dissipation further confines it equatorially. Furthermore, in this example, the effect of the boundary layer is felt at higher levels in the lower troposphere; especially at 2 km where the pressure contours to the

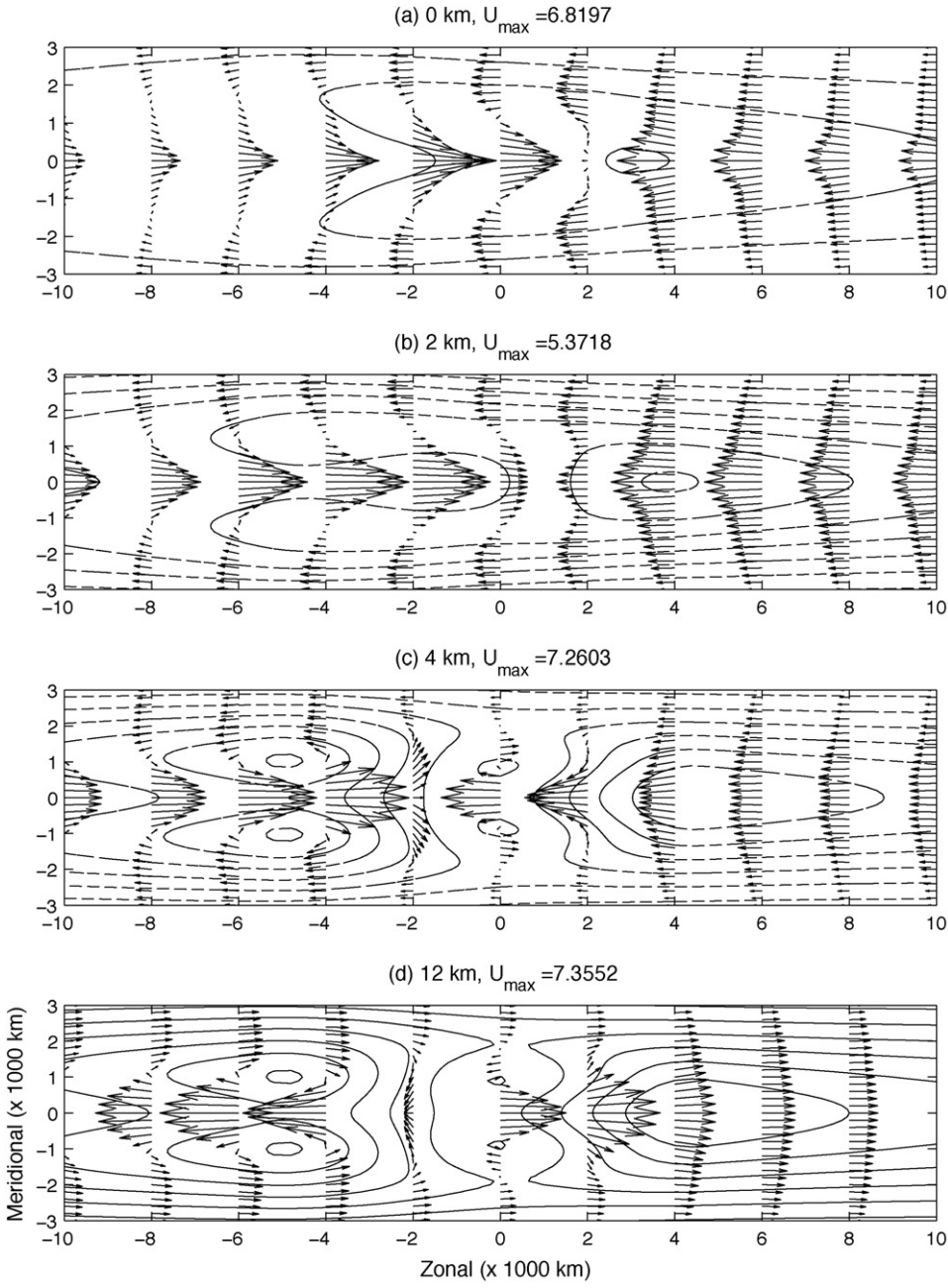

Fig. 25. Compare with Fig. 3, the horizontal velocity field at various heights for the equatorial symmetric MJO heating model including boundary layer dissipation.

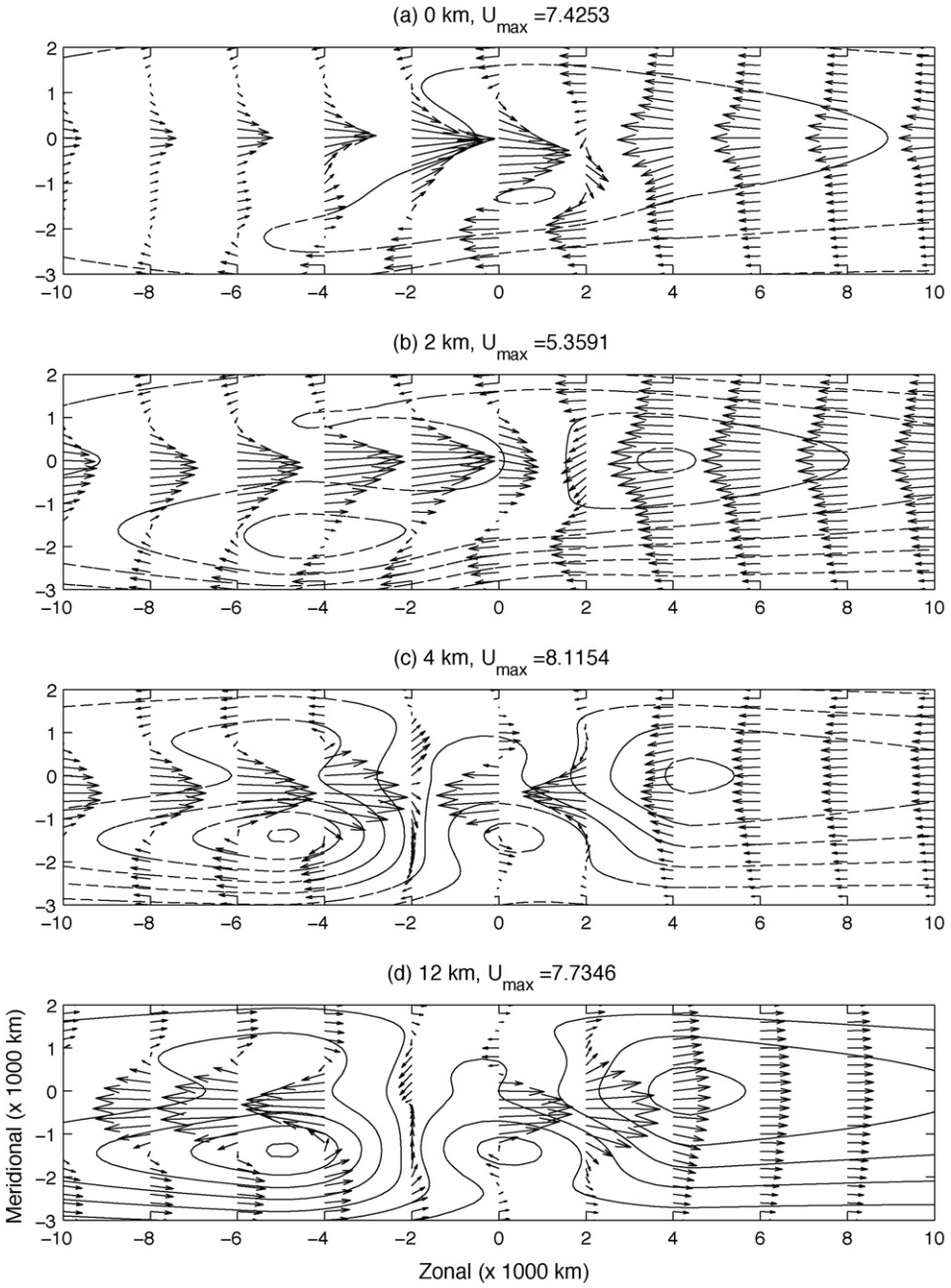

Fig. 26. Compare with Fig. 4, the horizontal velocity field at various heights for MJO heating centered at 450 km south including boundary layer dissipation.

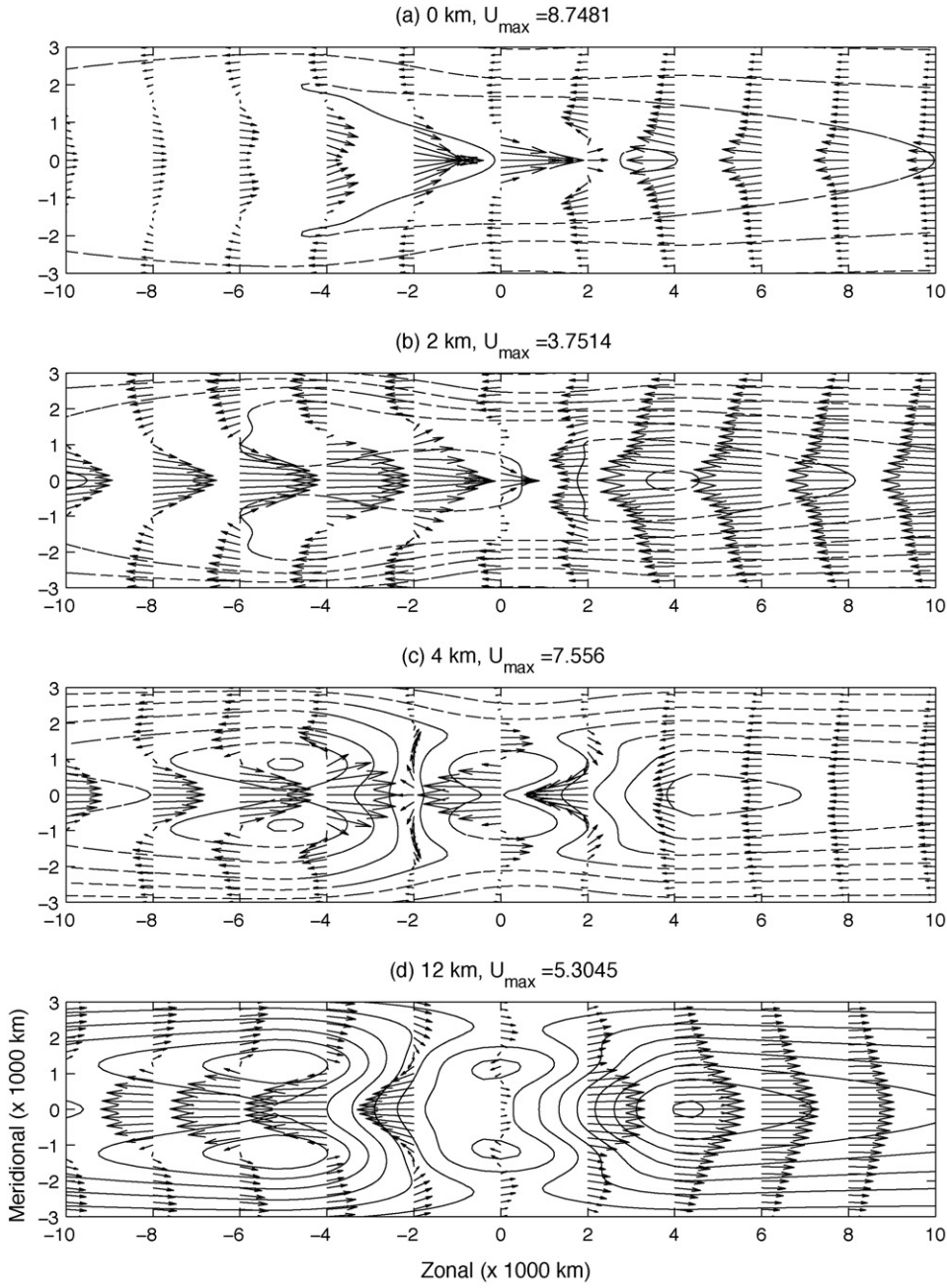

Fig. 27. Compare with Fig. 8, the horizontal velocity field at various heights for the equatorial symmetric and meridionally titled heating model including boundary layer dissipation.

west of the convective activity are significantly distorted. This deeper penetration is do to ability of the boundary layer dissipation to affect the barotropic modes and the even vertical baroclinic modes: a small perturbation to the former communicates itself through the whole vertical extent of the troposphere.

5.2. The effect of varying the boundary layer dissipation rate

The energy dissipation due to Ekman friction in the lower boundary layer is given in Eq. (65). In particular, the quantity:

$$-\pi\Delta d \int K(y/d)\bar{U}^2\Big|_{z=0} \,\mathrm{d}x\,\mathrm{d}y \tag{68}$$

describes the dissipation of energy. We wish to study the effect of varying d on the structure of the westerly wind burst and note that there are two effects. First, as already discussed, a larger dissipation rate, d, sets a larger meridional zone within which Ekman dissipation is not effective. Secondly, however, the larger dissipation rate increases the absolute amount of dissipation through the prefactor $\pi\Delta d$.

Fig. 28(a) and (b) shows the flow at the base of the troposphere for the canonical equatorial MJO model using boundary layer dissipation times of a half day and 1 day, respectively; these figures are to be contrasted with Fig. 25(a) which uses a 1 day dissipation time. For boundary layer dissipation times of 0.5, 1, and 2 days, the nondimensionalized dissipation rates are $d = 0.70, 0.35$ and 0.175 which correspond to length scales of approximately 1000, 500 and 250 km, respectively. So, although the dissipation rate in the free troposphere ($\propto \Delta d$) decreases with increasing boundary

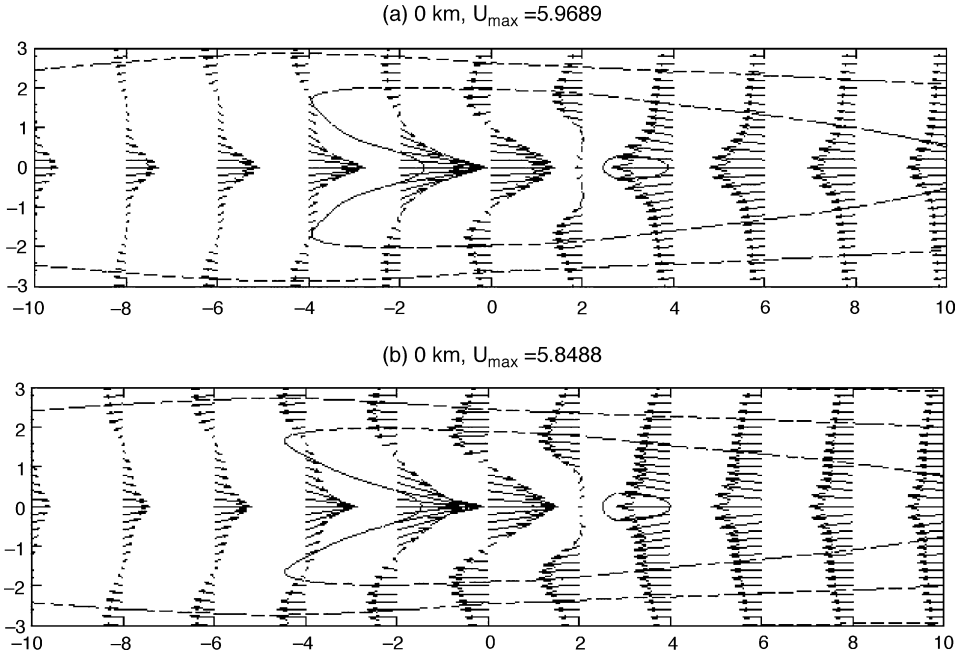

Fig. 28. Compare with Fig. 25; the horizontal velocity field at the base of the troposphere for the equatorial symmetric MJO heating model using (a) a 0.5 day and (b) a 2 day boundary layer dissipation rate.

layer dissipation time ($\propto d^{-1}$), the meridional region over which the boundary layer dissipation does not play a role also decreases ($\propto d$).

Comparing the results in Fig. 28 (a) and (b) with Figs. 25 and 3 reveals that the westerly jet at the equator is meridionally sharpened by the boundary layer dissipation, but that the dissipation rate d does not have a significant effect on the structure of the jet. This is clearly a consequence of the fact that the jet is equatorially confined within the meridional dissipation length scale. The main difference is seen at higher latitudes where the increased boundary layer dissipation rate is much more effective at dissipating the return flow at the base of the troposphere. The flow at higher levels is not shown because it is little effected by the boundary layer dissipation.

6. Discussion

We have systematically derived the IPESD model including lower boundary layer Ekman drag from the hydrostatic, anelastic, equatorial β-plane primitive equations; this is a different starting point than was used in the original IPESD derivation presented in Majda and Klein (2003). The IPESD model is a multiscale theory which describes the interaction of synoptic scales and planetary scales in a systematic, asymptotic fashion. Synoptic scale flows are driven by synoptic scale heating fluctuations through balanced dynamics described in Eq. (29). The dynamical planetary scale Eq. (30) drive flows which are forced by planetary scale mean heating and upscale fluxes from the synoptic scale circulations given by Eq. (31).

The effects of an equatorial Ekman boundary layer beneath the free troposphere are systematically incorporated by including a barotropic layer at the base of the free troposphere in which drag dissipation occurs. This layer is coupled to the free troposphere through the continuity of pressure and vertical velocity across their common interface. The flow in the boundary layer drives a vertical flow at the base of the free troposphere (Eq. (38)) and is, itself, driven by the zonal velocity at the base of the free troposphere (Eq. (41)).

A very useful feature of the IPESD theory is that the synoptic scale flows can be solved analytically in terms of the synoptic scale fluctuating heating, Eq. (43). Therefore, the temperature and momentum flux convergences also have an analytic representation in terms of the synoptic scale heating fluctuations as given in Eqs. (48) and (49). Due to the synoptic scale averaging of the theory, many aspects of the flux convergence are insensitive to the details of the synoptic scale circulations. However, as is shown in Eq. (52), non-trivial flux convergences are a consequence of either vertical or meridional tilts in the synoptic scale heating fluctuations.

The MJO model considered in Biello and Majda (2005) focused on a moving convective envelope of congestus clouds and deep westward tilted superclusters. These models exploited the upward/westward tilt of the superclusters and lower troposphere heating of the congestus clouds to attain an MJO planetary scale structure in excellent qualitative agreement with the observations. The models considered in this present work add the effects of meridionally tilted heating which drives a barotropic, second and fourth vertical baroclinic mode response on planetary scales due to a non-zero meridional component of the zonal momentum flux. In the simplest, equatorially symmetric example, the heating fluctuations due to tilted superclusters and lower troposphere congestus clouds proceed toward one another in such manner that they converge at the center of a moving convective envelope. The anomalies plausibly tilt meridionally away from the direction

of travel making them tilt westward/poleward in the supercluster region and eastward/poleward in the congestus convective region. We have shown that the planetary scale flows resulting from such heating are similar to the canonical MJO models discussed in Biello and Majda (2005) with the novel feature that the westerly wind burst at the base of the troposphere increases in amplitude by 50% and becomes more equatorially confined by the meridional component of the zonal momentum flux convergence.

We have also considered meridional tilts in the synoptic scale heating which are antisymmetric with respect to the equator. A southwest/northeast tilt in the heating shifts the maximum westerly wind burst southward whereas a northwest/southeast tilt shifts the maximum wind burst northward. When off-equatorial heating profiles are meridionally tilted, the two effects can either enhance the wind burst away from the equator or force it closer to the equator; this may lead to interesting mechanisms for shutting down an MJO event which tends too far poleward and away from regions of high SST.

Lower boundary layer dissipation due to Ekman friction provides another mechanism for equatorially confining the westerly wind burst at the base of the troposphere. The momentum dissipation rate in the boundary layer defines a meridional band near the equator within which zonal flows in the free troposphere are only weakly affected by the dissipation. In all of the examples we considered, Ekman friction equatorially confined the westerly wind burst at the base of the troposphere and its effect decreased with height as would be expected from the analytic formula for the energy dissipation.

Acknowledgments

The authors thank Mitch Moncrieff for inspiring the meridionally tilted heating model of Section 4.3. The research of Andrew Majda is partially supported by a grant from the Office of Naval Research, ONR # N00014-96-1-0043 and two National Science Foundation grants, NSF # DMS-0456713 and NSF-FRG # DMS-0139918. Joseph Biello was supported as a postdoctoral research associate with A. Majda through National Science Foundation grant, NSF-FRG # DMS-0139918.

Appendix A. Strong planetary scale mean heating: advection effects in planetary scale flows

The IPESD models allow for the possibility of mean heating on the planetary scales which is as strong as 10 K/day and zonal and meridional forcing of order 15 m/s/day. While these heating effects on the planetary scale are much stronger than observed planetary scale heating, nevertheless, it is interesting to see how they couple affect the IPESD models (Majda and Klein, 2003). In this case the planetary scale mean forcing contributes at the lowest order, and the flow does not meaningfully separate into zonal means and synoptic scale fluctuations. Rather it separates into components which respond to the mean forcing and those in meridional geostrophic balance. We can focus on the planetary mean component only since it is straightforward to add synoptic scale fluctuations to these equations and follow the construction of Sections 2.2 and 2.3. Therefore, the forcing is given by

$$S_u = \bar{S}_u(X, y, z, t), \qquad S_v = \bar{S}_v(X, y, z, t), \quad \text{and} \quad S_\theta = \bar{S}_\theta(X, y, z, t) \tag{A.1}$$

and the resultant flows are still expressible as a synoptic scale fluctuating component and planetary mean as in Eq. (22).

The lowest order dynamics determine the unbalanced circulations:

$$-y\bar{v} = \bar{S}_u, \qquad y\bar{u} + \bar{p}_y = \bar{S}_v, \qquad \bar{w} = \bar{S}_\theta, \qquad \bar{p}_z = \bar{\theta}, \qquad \bar{v}_y + \bar{w}_z = 0 \tag{A.2}$$

while any fluctuating component is solved as in the previous discussion of SEWTG; the mean and fluctuating component combine linearly to give the total. Unless the means of the forces are in geostrophic balance, these equations cannot be solved; the assumption of fast time independence is not valid and secular growth can occur on the fast time scale as noted in Section 2.1. Geostrophic balance arises upon applying the incompressibility constraint and yields:

$$\bar{S}_{\theta_z} - \left(\frac{\bar{S}_u}{y}\right)_y = 0 \tag{A.3}$$

Clearly the vertical/meridional flow is

$$\bar{v} = -\frac{\bar{S}_u}{y}, \qquad \bar{w} = \bar{S}_\theta \tag{A.4}$$

and could also be expressed in terms of a stream function. There is an indeterminacy in selecting the solution for $\bar{u}$, $\bar{p}$ and $\bar{\theta}$ since there are only two equations for the three unknowns. We can remove this indeterminacy by requiring that the incompressibility condition which arises at next order not acquire any terms from the planetary zonal derivative of a zonal flow. We therefore require:

$$\bar{u} \equiv 0 \tag{A.5}$$

which necessitates the solutions:

$$\bar{p} = \int_0^y \bar{S}_v \, \mathrm{d}y \quad \text{and} \quad \bar{\theta} = \int_0^y \bar{S}_{vz} \, \mathrm{d}y \tag{A.6}$$

having the additional property that $\bar{p}(y=0) = \bar{\theta}(y=0) = 0$.

The solutions at second order now contain no direct forcing, as there is no possible way to split this forcing from the stronger forcing which drives the lower order SEWTG. It is a misnomer to call these the planetary scale equations since planetary scale flows must contain the means from the first order solutions also. However, the second order equations still have the same structure of the planetary long wave equations since they describe the forcing over longer time scales of geostrophically balanced equatorial long waves by an inhomogeneous component.

Collecting the second order terms plus the zeroeth order meridional geostrophic balance constraint, we arrive at

$$\begin{aligned}
\bar{D}_t\bar{U} - y\bar{V} + \bar{P}_X &= -d_0\bar{U} + F^U - \bar{p}_X, \\
y\bar{U} + \bar{P}_y &= 0, \\
\bar{D}_t\bar{\Theta} + \bar{W} &= -d_\theta\bar{\Theta} + F^\theta - \bar{D}_t\bar{\theta} - d_\theta\bar{\theta}, \\
\bar{P}_z &= \bar{\Theta}, \\
\bar{U}_X + \bar{V}_y + \bar{W}_z &= 0
\end{aligned} \tag{A.7}$$

where the advective derivative is defined with respect to the meridional/vertical circulation:

$$\bar{D}_t = \partial_t + \bar{v}\partial_y + \bar{w}\partial_z \tag{A.8}$$

Notice that the pressure, $\bar{p}$, and potential temperature, $\bar{\theta}$, from the first order equations explicitly contribute to the forcing in both the temperature and zonal momentum in Eq. (A.7). Additionally, the flux convergence terms are included to account for the synoptic scale flow fluctuations which arise in the case that there is a strong synoptic scale heating fluctuation. Both flux convergence terms are defined as in Eq. (31).

A final note is necessary to understand the coupling of the free troposphere to the boundary layer at the base of the troposphere. The total pressure is given by the third equation in (22) and its x and y derivatives are used to express the right-hand side of Eq. (40) in terms of the horizontal velocity at the base of the troposphere. In this case of strong mean forcing, there is no synoptic scale derivative of the pressure so the right-hand side of the first equation in (40) is equal to zero. Furthermore, the pressure is not in meridional geostrophic balance with the zonal momentum, but rather we can express it using:

$$-p_y = -\bar{P}_y - \bar{p}_y = y\bar{U} - \bar{S}_v \tag{A.9}$$

It is this expression for the meridional derivative of the pressure which constitutes the right-hand side of the second equation in (40) and drives the flow in the boundary layer.

Appendix B. Density weighted coordinates and the relationship of the anelastic and Boussinesq IPESD models

The anelastic IPESD theory can be simplified somewhat by transforming to a set of density weighted coordinates. At this point all variables have been nondimensionalized and, in particular the background density, $\rho(z)$ and pressure, $P_0(z)$, have been scaled to one at the base of the free troposphere (Majda and Klein, 2003). Consider the transformation to a scaled vertical coordinate:

$$\mathrm{d}\tilde{z} = \rho(z)\,\mathrm{d}z \tag{B.1}$$

which, upon substituting the definition of the background pressure from the lowest order hydrostatic balance (Majda and Klein, 2003):

$$\frac{\mathrm{d}P_0(z)}{\mathrm{d}z} = -\rho(z) \tag{B.2}$$

integrates to become:

$$\tilde{z} = 1 - P_0 \tag{B.3}$$

Therefore, the density weighted coordinate, $\tilde{z}$ is a pressure coordinate. The polytropic relation implies:

$$P_0 = \rho^\gamma \tag{B.4}$$

and, for a diatomic ideal gas, the ratio of specific heats is $\gamma = 4/3$. Therefore, the pressure stratification is given by

$$P_0(z) = \left[1 - \frac{z}{4}\right]^4 \tag{B.5}$$

meaning that the pressure vanishes at heights of $z = 4$. This is to be compared with the Boussinesq examples where we have been putting a rigid lid at $z = \pi$. Therefore, we have the following

relationship between the domain of the actual vertical height, the pressure and the density scaled vertical height:

$$z \in [0, 4], \quad P_0 \in [1, 0], \quad \tilde{z} \in [0, 1] \tag{B.6}$$

Now we can transform the SEWTG equations to density weighted coordinates by redefining the vertical velocity, heating rate and temperature while leaving the other variables unchanged:

$$\tilde{w} = \rho w', \qquad \tilde{u} = u', \qquad \tilde{v} = v', \qquad \tilde{S}_\theta = \frac{\rho S'_\theta}{N^2}, \qquad \tilde{\theta} = \frac{\theta'}{\rho}, \qquad \tilde{p} = p' \tag{B.7}$$

so that the synoptic scale equations become exactly those of the Boussinesq SEWTG:

$$\begin{aligned} -y\tilde{v} + \tilde{p}_x &= 0, \\ y\tilde{u} + \tilde{p}_y &= 0, \\ \tilde{w} = \tilde{S}_\theta, \qquad \bar{\tilde{S}}_\theta &= 0, \\ \tilde{p}_{\tilde{z}} &= \tilde{\theta}, \\ \tilde{u}_x + \tilde{v}_y + \tilde{w}_{\tilde{z}} &= 0 \end{aligned} \tag{B.8}$$

The upscale fluxes become:

$$F^U = -(\overline{\tilde{v}\tilde{u}})_y - (\overline{\tilde{w}\tilde{u}})_{\tilde{z}}, \qquad F^\theta = -(\overline{\rho\tilde{v}\tilde{\theta}})_y - (\overline{\rho\tilde{w}\tilde{\theta}})_{\tilde{z}} \tag{B.9}$$

so that the momentum flux convergence is the same as that in the Boussinesq equations whereas the thermal flux convergence gains a factor of ρ. The transformation is less useful in simplifying the planetary scale equations. Making the same substitutions for the mean flows as for the fluctuating flows in Eq. (B.7) yields:

$$\begin{aligned} \tilde{U}_t - y\tilde{V} + \tilde{P}_X &= F^U - d_0\tilde{U}, \\ y\tilde{U} + \tilde{P}_y &= 0, \\ \tilde{\Theta}_t + \frac{N^2}{\rho^2}\tilde{W} &= \frac{F^\theta}{\rho} - d_\theta\tilde{\Theta} + \frac{\bar{S}_\theta}{\rho}, \\ \tilde{P}_{\tilde{z}} &= \tilde{\Theta}, \\ \tilde{U}_X + \tilde{V}_y + \tilde{W}_{\tilde{z}} &= 0 \end{aligned} \tag{B.10}$$

Clearly the difference between this equation and that of the Boussinesq QLELWE lies in the equation for the potential temperature, $\tilde{\Theta}$. In this nondimensionalization, the density varies from $\rho(\tilde{z} = 0) = 1$ to $\rho(\tilde{z} = 1) = 0$ and is given by

$$\rho(\tilde{z}) = (1 - \tilde{z})^{3/4} \tag{B.11}$$

which can cause serious singularities in the equation for potential temperature. The density in the thermal flux term essentially cancels that in the denominator. The direct heating term is also divided by the density, but this term is benign as long as direct heating vanishes rapidly enough with height. The main effect is the factor which multiplies $\bar{W}$ in the heat equation. Clearly this can have a strong effect at the top of the troposphere and the solutions can look qualitatively quite different from those of the Boussinesq equations.

Appendix C. On solving the equatorial long wave equations in the IPESD model with boundary layer dissipation

In this section we detail the algorithm for computing planetary scale flows. This gives us the opportunity to discuss both linear and nonlinear dissipation in Appendix C.1 and barotropic/baroclinic mode splitting in Appendix C.2. An algorithm for solving the barotropic modes is presented in Appendix C.3, and for solving the baroclinic modes in Appendix C.4. The baroclinic algorithm requires the correct meridional basis functions to solve for the Rossby and Kelvin waves and so the parabolic cylinder function basis for baroclinic modes is outlined in Appendix C.4.1. The section concludes with a comment about the relationship of equatorial potential vorticity to the amplitudes of the modes we integrate (Appendix C.5).

C.1. Analytic solution of the boundary layer equations

In the limit of $V_* \longrightarrow \infty$, the boundary layer equations are linear and the flow in the boundary layer is simply a linear functional of the flow at the base of the free troposphere. In the general case of nonlinear boundary layer drag, we will have to resort to numerical solutions of the boundary layer equations. Nonetheless after a few analytic manipulations we will find that there exists an analytic solution to the meridional and zonal velocities in the boundary layer.

Define the magnitude of the total velocity at the base of the troposphere as

$$|U| = \sqrt{(u' + \bar{U})^2 + (v')^2} \tag{C.1}$$

Squaring both sides of the equations in (40) and adding them together yields a quadratic equation for the magnitude of the boundary layer velocity:

$$(y^2 + d^2)|\vec{u}^{\mathrm{B}}|^2 + d^2 \frac{|\vec{u}^{\mathrm{B}}|^4}{V_*^2} = y^2[(u' + \bar{U})^2 + (v')^2] \tag{C.2}$$

Choosing the positive root of the quadratic equation and re-expressing it so that in the limit $V_* \longrightarrow \infty$ the linear solution is explicitly evident, we find:

$$|\vec{u}^{\mathrm{B}}| = \frac{|y||U|}{\sqrt{d^2 + y^2}} \sqrt{\frac{2}{1 + \sqrt{1 + (4d^2y^2|U|^2)/((d^2 + y^2)^2 V_*^2)}}} \tag{C.3}$$

This expression can be used to explicitly evaluate the value of the nonlinear dissipation by substituting into the expression:

$$\tilde{d} = d\sqrt{1 + \left(\frac{|\vec{u}^{\mathrm{B}}|}{V_*}\right)^2} \tag{C.4}$$

By eliminating the zonal boundary layer velocity, u^{B}, from the right hand side of Eq. (40) we can calculate the meridional boundary layer velocity, whose meridional derivative sets the vertical velocity of the Ekman pump at the base of the free troposphere in Eq. (38). Therefore, the meridional boundary layer velocity is given by

$$v^{\mathrm{B}} = \frac{y\tilde{d}(u' + \bar{U}) + y^2 v'}{\tilde{d}^2 + y^2} \tag{C.5}$$

while the zonal velocity is

$$u^{\mathrm{B}} = \frac{y^2(u' + \bar{U}) - y\tilde{d}v'}{\tilde{d}^2 + y^2}. \tag{C.6}$$

A solution strategy goes as follows. Calculate the total velocity in the boundary layer from the total velocity at the base of the troposphere using Eq. (C.3) and substitute into Eq. (C.4) to get the value of the nonlinear dissipation, $\tilde{d}$. Now substitute the nonlinear dissipation, $\tilde{d}$, into Eq. (C.5) and, again using the horizontal velocity at the base of the troposphere, u', $\bar{U}$, and v' calculate the meridional boundary layer velocity, v^{B}. The vertical velocity in the troposphere evaluated at $z = 0$ is proportional to the meridional derivative of the zonal synoptic average of this velocity, $\bar{v}^{\mathrm{B}}_y$; this is the required quantity in order to close the equations and the synoptic scale average must, in general, by computed numerically. Note that, in general, the synoptic and planetary scale solutions are nonlinearly coupled in computing this mean.

The dissipation rate in the boundary layer has been scaled to the equatorial deformation time scale, $T_{\mathrm{E}} = 8.33\,\mathrm{h}$. Therefore, for a 1 day boundary layer drag dissipation time we find:

$$d = \frac{8.33\,\mathrm{h}}{1\,\mathrm{day}} \approx 0.35 \tag{C.7}$$

Since the boundary layer dissipation rate enters the expressions for the dissipation in combination with y it is clear that it sets a length scale, y_{d}, over which the boundary layer dissipation is most effective; therefore we find:

$$d = 0.35 \Longrightarrow y_{\mathrm{d}} \approx 520\,\mathrm{km} \tag{C.8}$$

At 520 km north/south of the equator, the boundary layer is most effective at dissipating zonal velocity.

C.1.1. Simplified behavior when $|U|/V_* \ll 1$

Some physical insight can be gained by expanding the nonlinear boundary layer dissipation in a power series in small values of $|U|/V_*$, which is the ratio of the total velocity at the base of the troposphere compared to the turbulent velocity. Therefore, we find:

$$\tilde{d} \approx d\left[1 + \frac{|\vec{u}^{\mathrm{B}}|^2}{2V_*^2}\right] \quad \text{and} \quad |\vec{u}^{\mathrm{B}}|^2 \approx \frac{y^2|U|^2}{d^2 + y^2} \tag{C.9}$$

so that, upon serious manipulation we arrive at

$$v^{\mathrm{B}} = \frac{yd(u' + \bar{U}) + y^2v'}{d^2 + y^2} - \frac{y^3d}{(d^2 + y^2)^3}\frac{(u' + \bar{U})^2 + (v')^2}{2V_*^2}\left[(d^2 - y^2)(u' + \bar{U}) + 2ydv'\right] \tag{C.10}$$

and therefore the synoptic scale mean meridional velocity in the boundary layer is

$$\bar{v}^{\mathrm{B}} = \frac{yd\bar{U}}{d^2 + y^2} - \frac{y^3d}{2V_*^2(d^2 + y^2)^3}[\overline{(u' + \bar{U})^2 + (v')^2}][\overline{(d^2 - y^2)(u' + \bar{U}) + 2ydv'}] \tag{C.11}$$

which simplifies to

$$\bar{v}^{\mathrm{B}} = \frac{yd}{y^2 + d^2}[\bar{U} - \Lambda(y)(\mu_0 + \mu_1\bar{U} + \mu_3\bar{U}^3)] \tag{C.12}$$

where

$$\Lambda(y) = \frac{y^2}{2V_*^2(d^2+y^2)^2},$$
$$\mu_0 = [(d^2-y^2)\kappa_1 + 2dy\kappa_2],$$
$$\mu_1 = [(d^2-y^2)E + 4dy\Omega 2],$$
$$\mu_3 = (d^2-y^2) \tag{C.13}$$

and

$$E = 3(\bar{u}')^2 + (\bar{v}')^2, \qquad \kappa_1 = \overline{u'((u')^2+(v')^2)},$$
$$\Omega = \overline{u'v'}, \qquad \kappa_2 = \overline{v'((u')^2+(v')^2)} \tag{C.14}$$

The expression for E is asymmetric in u', v', due to the factor of "3". This is not mysterious and simply arises from the meridional average of $(u'+\bar{U})^3$ whereas the term in $(v')^2$ arises from the meridional average of $(u'+\bar{U})(v')^2$.

C.2. Barotropic/baroclinic mode splitting for planetary scales

Using the Boussinesq IPESD with a rigid boundary at the top of the troposphere and the Ekman flux at the bottom of the troposphere, the vertical velocity can be expressed as a linearly decreasing function of height plus a function which satisfies homogeneous boundary conditions at $z = 0, \pi$. Using $\bar{W} = 0$ at $z = \pi$ and $\bar{W} = -\pi\Delta\bar{v}_y^{\mathrm{B}}$ at $z = 0$ from Eq. (38) we find:

$$\bar{W} = -(\pi - z)\Delta\bar{v}_y^{\mathrm{B}} + f(z) \tag{C.15}$$

where $f(z)$ satisfies homogeneous boundary conditions. $f(z)$ can be split up into a sine series and we choose the standard baroclinic mode splitting:

$$\bar{W} = -(\pi - z)\Delta\bar{v}_y^{\mathrm{B}} + \sum_j W^j\sqrt{2}\sin(jz) \tag{C.16}$$

so that

$$\bar{W}_z = \Delta\bar{v}_y^{\mathrm{B}} + \sqrt{2}\sum_j jW^j\cos(jz) \tag{C.17}$$

The velocities in the plane and the pressure are expanded in cosines in the vertical direction:

$$\begin{bmatrix}\bar{U}\\ \bar{V}\\ \bar{P}\end{bmatrix} = \begin{bmatrix}U^0\\ V^0\\ P^0\end{bmatrix} + \sqrt{2}\sum_{j=1}\begin{bmatrix}U^j\\ V^j\\ P^j\end{bmatrix}\cos(jz) \tag{C.18}$$

Defining the inner product:

$$\langle f, g\rangle = \frac{1}{\pi}\int_0^\pi fg\,\mathrm{d}z \tag{C.19}$$

the expansions (C.16) and (C.18) are substituted into the equations in (30) and, upon eliminating Θ, projected onto $\cos(jz)$. This splits the system into a barotropic mode:

$$U_t^0 - yV^0 + P_x^0 = F^{U,0}, \qquad yU^0 + P_y^0 = 0, \qquad U_x^0 + V_y^0 = -\Delta\bar{v}_y^{\mathrm{B}} \tag{C.20}$$

and a family of baroclinic modes for $j \geq 1$:

$$\begin{aligned} U_t^j - yV^j + P_x^j &= F^{U,j}, \\ j^2 P_t^j + U_x^j + V_y^j + \sqrt{2}\Delta \bar{v}_y^{\mathrm{B}} &= -jF^{\theta,j} - jS^j, \\ yU^j + P_y^j &= 0 \end{aligned} \tag{C.21}$$

For the sake of conciseness, the expressions for the forcing include the damping terms and are given by

$$\begin{aligned} F^{U,0} &= \frac{1}{\pi}\int_0^\pi [F^U - d_0\bar{U}]\mathrm{d}z, \\ F^{U,j} &= \frac{\sqrt{2}}{\pi}\int_0^\pi \cos(jz)[F^U - d_0\bar{U}]\,\mathrm{d}z, \\ F^{\theta,j} &= \frac{\sqrt{2}}{\pi}\int_0^\pi \sin(jz)[F^\theta - d_\theta\bar{\Theta}]\,\mathrm{d}z \\ \text{and} \quad S^j &= \frac{\sqrt{2}}{\pi}\int_0^\pi \sin(jz)\bar{S}_\theta\,\mathrm{d}z \end{aligned} \tag{C.22}$$

As was mentioned above, the free solutions of the quasi-linear equatorial long wave equations are simply Kelvin and Rossby waves. The eigenfunctions of these waves form a complete basis over which any flow can be projected and therefore the total flow can be computed. In particular, for the Rossby component of the waves, the potential vorticity is integrated and, using the meridional geostrophic balance, the velocity and pressure of the planetary scale flows are calculated.

The computational scheme we employ begins with the long wave equations which have already been split into barotropic and baroclinic components, (C.20) and (C.21). The upscale fluxes and direct heating are assumed to have been calculated already from the synoptic scales. Furthermore, the meridional velocity in the boundary layer is simply a linear functional of the total zonal velocity at the base of the troposphere and, as such, is known at each time.

C.3. An algorithm for the evolution of the barotropic modes

For the barotropic mode it is convenient to define a finite meridional extent to the β-plane channel, $-L_{\mathrm{C}} < y < L_{\mathrm{C}}$ where $L_{\mathrm{C}} = 5000$ km in order to capture as many barotropic modes as possible. This allows us to easily integrate the meridional Fourier transform of the barotropic velocity, $\tilde{U}$ which is given by

$$U^0(x, y, t) = \frac{1}{\sqrt{2\pi}}\sum_k \tilde{U}^0(x, t)\,\mathrm{e}^{il_k y} \tag{C.23}$$

where

$$l_k = \frac{\pi k}{L_{\mathrm{C}}} \tag{C.24}$$

Taking two y derivatives of Eq. (C.20) we can eliminate V^0

$$U^0_{yyt} + U^0_x + \Delta[y\bar{v}^{\mathrm{B}}]_{yy} = F^{U,0}_{yy} \tag{C.25}$$

and then evaluate the Fourier transform:

$$\tilde{U}_t^0 - \frac{\tilde{U}_x^0}{l_k^2} = \tilde{F}^{U,0} - \Delta\,[\tilde{y\bar{v}^{\mathrm{B}}}] \tag{C.26}$$

where the last term is simply the Fourier transform of the product. This equation is a simply advection for each mode and can, in fact, be solved explicitly. Practically, we implement a numerical advection/integration scheme.

Upon integrating the Fourier components of the zonal component of the barotropic flow we can calculate the meridional velocity by first calculating the zonal velocity in physical space using Eq. (C.23). Then the divergence condition in Eq. (C.20) can be meridionally integrated to give the meridional velocity:

$$V^0(X, y) = V^0(X, -L_{\mathrm{C}}) - \Delta\bar{v}^{\mathrm{B}} - \int_{-L_{\mathrm{C}}}^{y} U_X^0(X, y')\,\mathrm{d}y' \tag{C.27}$$

This integral has a free function, $V^0(X, -L_{\mathrm{C}})$ which must be determined by some channel boundary conditions. Since antisymmetric barotropic modes will have vanishing meridional velocity at the channel boundary, L_{C}, and we would like to include these modes, therefore we should not impose "no penetration" boundary conditions on the channel. Instead, a "zero meridional momentum" for the whole channel is a useful boundary condition; that is to say, the total meridional momentum of the channel must vanish at every latitude:

$$\int_{-L_{\mathrm{C}}}^{L_{\mathrm{C}}} V^0(X, y)\,\mathrm{d}y = 0 \tag{C.28}$$

This completes the computation of the barotropic modes.

C.4. An algorithm for the evolution of the baroclinic modes

It is convenient to define the Riemann invariants:

$$Q^j = \frac{1}{\sqrt{2}}\left(P^j + \frac{U^j}{j}\right), \qquad R^j = \frac{1}{\sqrt{2}}\left(P^j - \frac{U^j}{j}\right), \qquad S^j = \frac{V}{j^2\sqrt{2}} \tag{C.29}$$

and the operators:

$$L_{\pm}^j = \frac{\mathrm{d}}{\mathrm{d}y} \pm jy \tag{C.30}$$

which will be used to solve for the baroclinic modes from Eq. (C.21). Taking linear combinations of the baroclinic equation (C.21) the Riemann invariants evolve according to

$$\begin{aligned} Q_t^j + \frac{Q_x^j}{j} + L_-^j S^j &= F^{Q,j} - \frac{\Delta\bar{v}_y^{\mathrm{B}}}{j^2}, \\ R_t^j - \frac{R_x^j}{j} + L_+^j S^j &= F^{R,j} - \frac{\Delta\bar{v}_y^{\mathrm{B}}}{j^2}, \\ L_+^j Q^j + L_-^j R^j &= 0 \end{aligned} \tag{C.31}$$

where

$$F^{Q,j} = \frac{1}{j\sqrt{2}}(F^{U,j} - F^{\theta,j} - S^j), \qquad F^{R,j} = \frac{-1}{j\sqrt{2}}(F^{U,j} + F^{\theta,j} + S^j) \tag{C.32}$$

The equations for the baroclinic modes are then projected onto a basis of parabolic cylinder functions which clearly separates the Kelvin, Rossby and mixed Rossby-gravity components of the flow.

C.4.1. Basis

The parabolic cylinder function of degree m is

$$D_m(\eta) = 2^{-m/2} H_m\left(\frac{\eta}{\sqrt{2}}\right) \mathrm{e}^{-\eta^2/4} \tag{C.33}$$

where the H_m are the Hermite polynomials:

$$\begin{aligned} &H_0(\xi) = 1, \quad H_1(\xi) = 2\xi, \qquad H_2(\xi) = 4\xi^2 - 2, \\ &H_3(\xi) = 8\xi^3 - 12\xi, \quad H_4(\xi) = 16\xi^4 - 48\xi^2 + 12 \end{aligned} \tag{C.34}$$

etc. For each j an orthonormal basis is given by

$$\phi_m^j(y) = \left(\frac{\sqrt{j}}{m!\sqrt{\pi}}\right)^{1/2} D_m(y\sqrt{2j}) = \left(\frac{\sqrt{j}}{2^m m!\sqrt{\pi}}\right)^{1/2} H_m(y\sqrt{j})\mathrm{e}^{-(jy^2)/2} \tag{C.35}$$

The operators $L_\pm$ from Eq. (C.30) act on the basis as follows:

$$L_-^j \phi_m^j = -\sqrt{2j(m+1)}\phi_{m+1}^j, \qquad L_+^j \phi_m^j = \sqrt{2jm}\phi_{m-1}^j \tag{C.36}$$

Eq. (C.31) are solved using the expansion:

$$\begin{bmatrix} Q^j \\ R^j \\ S^j \end{bmatrix} = \begin{bmatrix} K^j \phi_0^j \\ 0 \\ S_0^j \phi_0^j \end{bmatrix} + \sum_{m=1}^{\infty} \begin{bmatrix} Q_m^j \phi_{m+1}^j \\ R_m^j \phi_{m-1}^j \\ S_m^j \phi_m^j \end{bmatrix} \tag{C.37}$$

where the amplitude of the forced Kelvin waves are given by K^j, the various Rossby waves are given by the sum over m. S_0^j is a meridional velocity due to the component of the forcing projected onto a mixed Rossby-gravity wave and is necessitated by the constraints.

C.4.2. Kelvin waves

The forced Kelvin wave is a solution to Eq. (C.31) with $R = S = 0$; the meridional velocity of the Kelvin wave is identically zero. The amplitude of the Kelvin wave is given by K in Eq. (C.37) and it is clear that the constraint in (C.31) is trivially solved for this mode.

Therefore, the forced damped Kelvin wave is governed by

$$K_t^j + j^{-1} K_X^j = F_0^{Q,j} - \frac{\Delta_B}{j^2}[v_y^B]_0 \tag{C.38}$$

where subscripts on the forcing and dissipation terms denote inner product with ϕ_m^j.

C.4.3. Forcing of a mixed Rossby-gravity component

In the theory of equatorial long waves, the mixed Rossby-gravity (MRG) waves are filtered out by the assumption of slow temporal evolution of the long waves. Nonetheless, general equatorial forcing may project onto the same components as the MRG, yet there is no zonal velocity or pressure associated with this mode. Instead, the constraints imply that any forcing along the mixed Rossby-gravity component simply generates a compensating meridional flow given by

$$-\sqrt{2j}S_0^j = F_1^{Q,j} - \frac{\Delta_B}{j^2}[v_y^B]_1 \tag{C.39}$$

C.4.4. Equatorial baroclinic Rossby waves

The constraint in Eq. (C.31) suggests that a convenient new variable is

$$\Omega^j \equiv L_+^j Q^j - L_-^j R^j \tag{C.40}$$

Operating L_+^j on the first equation minus L_-^j on the second equation in (C.31) yields

$$\Omega_t^j + (L_+^j L_-^j - L_-^j L_+^j)S^j = L_+^j F^{Q,j} - L_-^j F^{R,j} - (L_+^j - L_-^j)\frac{\Delta \bar{v}_y^B}{j^2} \tag{C.41}$$

whereas adding these two equations gives:

$$j^{-1}\Omega_X^j + (L_+^j L_-^j + L_-^j L_+^j)S^j = L_+^j F^{Q,j} + L_-^j F^{R,j} - (L_+^j + L_-^j)\frac{\Delta \bar{v}_y^B}{j^2} \tag{C.42}$$

We shall return to Eq. (C.41) in the next section when discussing potential vorticity. For now, note that ϕ_m^j is an eigenfunction of either operator $L_+^j L_-^j$ or $L_-^j L_+^j$. Since Ω^j can be expanded in term of ϕ_m^j and, using its definition in Eq. (C.40) and the expansion of Q and R, we find

$$\Omega_m^j = \sqrt{2j}(\sqrt{m+1}Q_m^j + \sqrt{m}R_m^j) \tag{C.43}$$

Furthermore, projecting the constraint in Eq. (C.31) onto the functions ϕ_m^j yields

$$\sqrt{m+1}Q_m^j = \sqrt{m}R_m^j \tag{C.44}$$

so that the two Eqs. (C.43) and (C.44) determine Q_m^j and R_m^j in terms of Ω_m^j for each Rossby wave.

In order to close this system of equations the expressions for Ω^j must be projected onto the various ϕ_m^j and the quantity, S_m^j must be eliminated from the resulting equations. For conciseness, define

$$\Delta_m^j \equiv \frac{\Delta}{j^2}[\bar{v}_y^B]_m \tag{C.45}$$

so that the governing equation for Ω_m^j is

$$\Omega_{m,t}^j - \frac{\Omega_{m,x}^j}{(2m+1)j} = \frac{2\sqrt{2jm(m+1)}}{2m+1}\left\{\sqrt{m}F_{m+1}^{Q,j} + \sqrt{m+1}F_{m-1}^{R,j} - \sqrt{m}\Delta_{m+1}^j - \sqrt{m+1}\Delta_{m-1}^j\right\} \tag{C.46}$$

whose unforced solutions are clearly traveling at the Rossby wave speeds.

Finally we must reconstruct the primary variables of the problem, P, U and V,

$$U^j = \frac{j}{\sqrt{2}} \left\{ K^j \phi_0^j + \sum_{m=1} \frac{\Omega_m^j}{2\sqrt{2}j} \left[\frac{\phi_{m+1}^j}{\sqrt{m+1}} - \frac{\phi_{m-1}^j}{\sqrt{m}} \right] \right\} \tag{C.47}$$

and pressure

$$P^j = \frac{1}{\sqrt{2}} \left\{ K^j \phi_0^j + \sum_{m=1} \frac{\Omega_m^j}{2\sqrt{2}j} \left[\frac{\phi_{m+1}^j}{\sqrt{m+1}} + \frac{\phi_{m-1}^j}{\sqrt{m}} \right] \right\} \tag{C.48}$$

The meridional velocity is expanded in terms of ϕ_m^j:

$$V^j = \sum_{m=0} V_m^j \phi_m^j \tag{C.49}$$

where

$$V_m^j = \frac{\Omega_{m,X}^j}{\sqrt{2}(2m+1)} + \frac{\sqrt{j}}{2m+1} \left\{ \sqrt{m} \left[\tilde{F}_{m-1}^{R,j} - \tilde{\Delta}_{m-1}^j \right] - \sqrt{m+1} \left[\tilde{F}_{m+1}^{Q,j} - \tilde{\Delta}_{m+1}^j \right] \right\} \tag{C.50}$$

where the subscripts everywhere denote projection onto ϕ_m^j. The forcing and dissipation are now given by

$$\tilde{F}^{Q,j} = \frac{1}{\sqrt{2}}(F^{U,j} - F^{\theta,j}), \qquad \tilde{F}^{R,j} = \frac{-1}{\sqrt{2}}(F^{U,j} + F^{\theta,j}), \qquad \tilde{\Delta}^j = \frac{\Delta_{\mathrm{B}}}{j}[v_y^{\mathrm{B}}] \tag{C.51}$$

The meridional velocity associated with forcing along a mixed Rossby-gravity component ($m = 0$) is included in Eq. (C.50) by recognizing that $\Omega_0^j \equiv 0$ and any quantities with negative subscripts are identically zero.

In this manner, the baroclinic modes can now be integrated for any forcing.

C.5. Potential vorticity in the long wave equations

We shall now show how the quantity Ω^j is related to the actual potential vorticity in the Boussinesq version of the long wave equations. Define the potential vorticity:

$$\Omega^* = y - \bar{U}_y + y\Theta_z \equiv y + \Omega' \tag{C.52}$$

Using the long wave equations with $\rho = N = 1$ in (30), we take the y derivative of the first, the X derivative of the second, y times the z derivative of the third and neglect the forcing and dissipation and arrive at

$$-\bar{U}_{yt} + y\bar{V}_y + \bar{V} - \bar{P}_{Xy} = 0, \qquad y\bar{U}_X + \bar{P}_{Xy} = 0, \qquad y\bar{\Theta}_{zt} + y\bar{W}_z = 0 \tag{C.53}$$

Adding these equations and using the incompressibility constraint yields:

$$\Omega_t^* + \bar{V} = 0 \tag{C.54}$$

First we show that this is simply the linearized version of the conservation of potential vorticity:

$$\frac{D}{Dt}\Omega^* = 0 \tag{C.55}$$

Expanding the left-hand side of this expression, we find:

$$\frac{D}{Dt}\Omega^* = \Omega^*_t + \bar{U}\Omega^*_X + \bar{V}\Omega^*_y + \bar{W}\Omega^*_z = \Omega^*_t + \bar{V} + \bar{U}\Omega'_X + \bar{V}\Omega'_y + \bar{W}\Omega'_z \tag{C.56}$$

and upon linearizing the terms proportional to Ω' are neglected. Therefore, the expressions (C.54) and (C.55) are equivalent in the linear theory.

Now let us relate the perturbation potential vorticity Ω' from Eq. (C.52) to the definition of Ω^j in Eq. (C.40). Therefore, using the hydrostatic constraint, the equation for the perturbation potential vorticity is

$$\Omega' = -\bar{U}_y + yP_{zz} = -U^0_y - \sqrt{2}\sum_{j=1}(U^j_y + j^2 P^j)\cos(jz) \tag{C.57}$$

Whereas, using the definition of Ω^j in terms of $L^j_\pm$ and the definitions of Q^j and R^j from Eq. (C.29) we find for $j > 0$

$$\begin{aligned}\Omega^j = L^j_+ Q^j - L^j_- R^j \quad &= \frac{L^j_+}{\sqrt{2}}\left(P^j + \frac{U^j}{j}\right) - \frac{L^j_-}{\sqrt{2}}\left(P^j - \frac{U^j}{j}\right)\\ &= \frac{\sqrt{2}}{j}(U^j_y + j^2 yP^j)\end{aligned} \tag{C.58}$$

and comparing the last expression in Eqs. (C.57) and (C.58) we find:

$$\Omega' = -U^0_y - \sum_{j=1} j\Omega^j \cos(jz) \Longrightarrow (\Omega')^j = -\frac{j\Omega^j}{\sqrt{2}} \tag{C.59}$$

Therefore, the quantities Ω^j are simply the components of the potential vorticity projected on the vertical baroclinic modes scaled by j and $\sqrt{2}$. Finally note that the unforced version of Eq. (C.41) is equivalent to the conservation of potential vorticity in Eq. (C.54).

References

Biello, J.A., Majda, A.J., 2004. Geophys. Astro. Fluid 98, 85–127.

Biello, J.A., Majda, A.J., 2005. A new multi-scale model for the Madden–Julian oscillation. J. Atmos. Sci. 62, 1694–1721.

Bretherton, C.S., Sobel, A.H., 2003. The Gill model and the weak temperature gradient approximation. J. Atmos. Sci. 60, 451–460.

Chao, W.C., 1987. On the origin of the tropical intraseasonal oscillation. J. Atmos. Sci. 44, 1940–1949.

Emanuel, K.A., 1987. An air–sea interaction model of intraseasonal oscillations in the tropics. J. Atmos. Sci. 44, 2324–2340.

Emanuel, K.A., Raymond, D.J. (Eds.), 1993. The Representation of Cumulus Convection in Numerical Models, Meteorological Monographs, vol. 24, Am. Met. Soc., December 1993.

Gill, A.E., 1980. Some simple solutions for heat induced tropical circulation. Quart. J. R. Meteor. Soc. 106, 447–462.

Grabowski, W.W., 2001. Coupling cloud processes with large-scale dynamics using the cloud-resolving convection parametrization (CRCP). J. Atmos. Sci. 58, 978–997.

Grabowski, W.W., 2003. MJO-like coherent structures: sensitivity simulations using the cloud-resolving convection parameterization (CRCP). J. Atmos. Sci. 60, 847–864.

Haertel, P.T., Kiladis, G., 2004. Dynamics of two day equatorial disturbances. J. Atmos. Sci. 61, 2707–2721.

Hendon, H., Leibmann, B., 1994. Organization of convection within the Madden–Julian oscillation. J. Geophys. Res. 99, 8073–8083.

Hendon, H., Salby, M., 1994. The life cycle of the Madden–Julian oscillation. J. Atmos. Sci. 51, 2225–2237.

Houze, R.A., Chen, S.S., Kingsmill, D.E., Serra, Y., Yuter, S.E., 2000. Convection over the Pacific convective envelope in relation to the atmospheric Kelvin–Rossby wave. J. Atmos. Sci. 57, 3058–3089.

Johnson, R.H., Lin, X., 1997. Episodic trade wind regimes over the western Pacific convective envelope. J. Atmos. Sci. 54, 2020–2034.

Kiladis, G., Straub, K.H., Haertl, P.T., 2004. Zonal and vertical structure of the Madden–Julian oscillation. J. Atmos. Sci. 62, 2790–2809.

Lin, X., Johnson, R.H., 1996. Kinematic and thermodynamic characteristics of the flow over the western Pacific warm pool during TOGA COARE. J. Atmos. Sci. 53, 695–715.

Lin, J.-L., Zhang, M., Mapes, B., 2005. Zonal momentum budget of the Madden–Julian oscillation: the Source and strength of equivalent linear damping. J. Atmos. Sci. 62, 2172–2188.

Madden, R., Julian, P., 1972. Description of global scale circulation cells in tropics with a 40–50 day period. J. Atmos. Sci. 29, 1109–1123.

Madden, R.A., Julian, P., 1994. Observations of the 40–50-day tropical oscillation—a review. Mon. Weather Rev. 122, 814–837.

Majda, A.J., 2003. Introduction to PDEs and waves for the atmosphere and ocean, Courant Institute Lecture Series 9, Amer. Math. Soc.

Majda, A.J., Biello, J.A., 2004. A multi-scale model for tropical intraseasonal oscillations. Proc. Natl. Acad. Sci. 101, 4736–4741.

Majda, A.J., Khouider, B., Kiladis, G., Straub, K., Shefter, M., 2004. A model for convectively coupled tropical waves: nonlinearity, rotation and comparison with observations. J. Atmos. Sci. 61, 2188–2205.

Majda, A.J., Klein, R., 2003. Systematic multi-scale models for the tropics. J. Atmos. Sci. 60, 393–408.

Majda, A.J., Shefter, M.G., 2001. Models for stratiform instability and convectively coupled waves. J. Atmos. Sci. 58, 1567–1584.

Maloney, E., Hartmann, D., 1998. Frictional moisture convergence in a composite life cycle of the Madden–Julian oscillation. J. Climate 11, 2387–2403.

Mapes, B.E., Houze, R.A., 1995. Diabatic divergence profiles in western Pacific mesoscale convective systems. J. Atmos. Sci. 52, 1807–1828.

Matsuno, T., 1966. Quasi-geostrophic motions in the equatorial area. J. Meteor. Soc. Jpn. 44B, 25–43.

Moncrieff, M., 2004. Analytic representation of the large-scale organization of tropical convection. J. Atmos. Sci. 61, 1521–1538.

Moncrieff, M., Klinker, E., 1997. Organized convective systems in the tropical western Pacific as a process in general circulation models. A TOGA COARE case study. Quart. J. R. Met. Soc. 123, 805–827.

Nakazawa, T., 1988. Tropical super clusters within intraseasonal variations over the western Pacific. J. Meteor. Soc. Jpn. 66, 823–839.

Neelin, J.D., Held, I.M., Cook, K.H., 1987. Evaporation-wind feedback and low-frequency variability in the tropical atmosphere. J. Atmos. Sci. 44, 2341–2348.

Raymond, D.J., 2001. A new model of the Madden–Julian oscillation. J. Atmos. Sci. 58, 2807–2819.

Salby, M., Garcia, R., Hendon, H., 1994. Planetary-scale circulations in the presence of climatological and wave-induced heating. J. Atmos. Sci. 51, 2344–2367.

Sperber, K.R., Slingo, J.M., Inness, P.K., Lau, W.K.-M., 1997. On the maintenance and initiation of the intraseasonal oscillation in the NCEP/NCAR reanalysis and in the GLA and UKMO AMIP simulations. Climate Dyn. 13, 769–795.

Stevens, D.E., Kuo, H.-C., Schubert, W.H., Ciesielski, P.E., 1990. Quasi-balanced dynamics in the tropics. J. Atmos. Sci. 47, 2262–2273.

Vecchi, G., Harrison, D.E., 2000. Tropical Pacific sea surface temperature anomalies, El Nino, and equatorial westerly wind events. J. Climate 13, 1814–1830.

Wang, B., Rui, H., 1990. Dynamics of the coupled moist Kelvin–Rossby wave on an equatorial beta-plane. J. Atmos. Sci. 47, 397–413.

Wheeler, M., Kiladis, G.N., 1999. Convectively coupled equatorial waves: analysis of clouds and temperature in the wavenumber–frequency domain. J. Atmos. Sci. 56, 374–399.

Wheeler, M., Kiladis, G.N., Webster, P.J., 2000. Large scale dynamical fields associated with convectively coupled equatorial waves. J. Atmos. Sci. 57, 613–639.

Yanai, M., Chen, B., Tung, W.-W., 2000. The Madden–Julian oscillation observed during the TOGA COARE IOP. Global view. J. Atmos. Sci. 57, 2374–2396.

Zhang, C., Anderson, S., 2003. Sensitivity of intraseasonal perturbations in SST to the structure of the MJO. J. Atmos. Sci. 60, 2196–2207.